Optimisation of a Fully Autogenous Comminution Circuit

CW Steyn

Optimisation of a Fully Autogenous Comminution Circuit

by

CW Steyn

A dissertation submitted in partial fulfillment
of the requirements for the degree

Master of Engineering (Control Engineering)

in the

Department of Chemical Engineering
Faculty of Engineering, the Built Environment and Information Technology

University of Pretoria
Pretoria

December 2011

Synopsis

Autogenous (AG) milling is utilised around the world for first stage particle size reduction. The system exhibits highly non-linear behaviour in addition to being subject to unmeasured variability associated with most ore bodies. Anglo American Platinum aimed at improving online optimisation of the circuit by implementing industrial model predictive control to reduce system variability and continuously drive towards the optimal operating point within system constraints.

A dimensional analysis of the circuit was conducted to explain the relationships between the various milling parameters discussed in the literature survey. The measured variables used in the analysis satisfied Buckingham's theorem, indicating that a complete subset of dimensionless groups were present and suitably able to describe process movement. These relationships were used as a reference point in determining the dynamic step response models between these variables necessary for model based control.

The industrial dynamic matrix controller commissioned on the AG mill resulted in a 66 % reduction in power and a 40 % reduction in load. These are the main controlled variables of the mill. The controller also managed to reduce its objective function, effective power utilisation, by 11 %. This stability improvement enabled a test campaign where the mill was controlled at various operating regions in order to establish the conditions conducive to the finest product size at a given mill feed rate.

Moving the mill's operating region from the benchmarked plant to this optimal grind environment (at benchmarked variability) provided an estimated potential recovery increase of 0.27 % (absolute) due to better precious metal liberation. Stabilising the mill at this point with the model predictive controller resulted in a further 0.04 % potential recovery increase (absolute). The 0.31 % potential recovery increase is estimated at a monetary value of $93.1 million per annum.

KEYWORDS: platinum, autogenous, milling, optimisation, response surface analysis, dimensional analysis, model based control, benefit analysis

CONTENTS

LIST OF FIGURES

LIST OF TABLES

CHAPTER 1

Introduction

A large portion of the total operating cost in the mining beneficiation process is associated with comminution circuits - the highest costs in these operations are normally grinding media and energy. Since the global economic downturn at the end of 2008, the control of these cost elements, together with optimised performance especially on the milling component of these circuits has become increasingly important.

The challenges that industry faces when controlling a comminution circuit are the lack of specialised skills and the non-linear nature of the process. The milling process is also influenced by various unmeasured disturbances such as ore characteristics, that is, mineralogy, size and ore hardness. The control of comminution processes is further complicated by the presence of dead-time and interaction between variables. The process characteristics also introduce unmeasured dynamics due to the high amount of mechanical wear in the system, for example, liner wear leads to an increase in mill volume.

Anglo American Platinum currently has approximately 50 tumbling mills functioning in primary, secondary and tertiary comminution circuits. The primary circuits are predominantly Run-of-Mine (ROM) mills and variations of autogenous grind (AG) milling. All of these milling circuits are currently under Neuro-Fuzzy control which is applied in a manner suitably robust to perform in the non-linear, highly unmeasured environment of primary milling. The controller also includes a non-specific optimisation drive to increase product quality while maintaining the desired throughput (Steyn et al. 2010). Note that no real-time optimisation is performed by the controller.

A need existed to refine the optimisation algorithm and to target a better defined financial benefit function on a continuous basis. It was decided that a model predictive controller would be a suitable control technology to achieve this objective. This was piloted on one of Anglo American Platinum's ROM mills, Mototolo JV. The success of the controller was immediately evident, demonstrating a stability increase of between 15 % to 20 % on the primary milling parameters (stability measured by the Anglo American Platinum stability index see figure 1.1) as well as an increase in energy efficiency based on effective power consumption (kWh per ton desired product produced). The plot indicates

a reduction in controller input variance with a clear bias towards the local optimum in the top left corner of the feasible region.

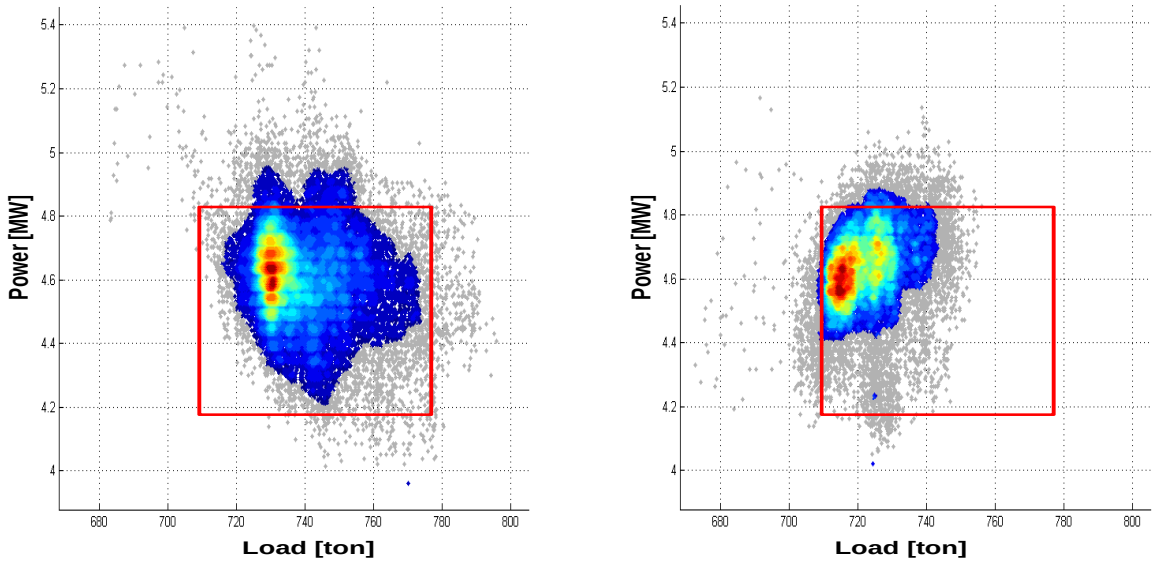

Figure 1.1: A 2d density plot of the power and load for Mototolo (JV) ROM primary mill on data a) two weeks prior and b) two weeks post MPC implementation (Steyn et al. 2010).. The red block represents the feasible region of the controller as defined by the controller limits

The next step in Anglo American Platinum's optimisation initiative was to deploy this technology on a traditionally more non-linear AG milling application. The primary AG mill at Rustenburg Platinum Mines Amandelbult UG2 No2 (RPMA2) plant was selected for this application due to the additional potential of its variable speed facility. The objectives of this project were:

1. Develop and incorporate a model predictive controller into the existing control infrastructure. The aim would be to repeat the stability improvement obtained at Mototolo JV;

2. Develop a model with sufficient accuracy to characterise the profitability of a mill;

3. Find the optimal operating point and to utilise this in the MPC algorithm to control the mill according to most favourable financial benefit;

4. Quantify the real benefits of reducing the variability in the mill and stabilising the circuit at the optimum operating conditions.

To achieve these objectives, the following goals were established:

Literature study Conduct a thorough literature review on comminution and the various performance metrics associated with tumbling mills

Benchmark the system based on the key performance indicators that have been established for comminution circuits.

Modelling Conduct a dimensional analysis to describe the behaviour of the milling circuit in terms of the parameters identified in the literature study. Obtain a dynamic empirical model of the relationship between the identified variables suitable for use in an online controller. The aim of this controller will be to:

- Obtain the optimal grind and throughput relationship.
- Establish a platform for higher order cost optimisation in order to minimise energy consumption while maintaining optimal recovery.
- Incorporate circuit flow rate and density stabilisation control, for example, discharge sump to screen and surge tank to flotation. The empirical model will be obtained by means of step tests with the use of industrial software – AspenTech SmartStep.

Optimisation Utilise the improved circuit stability in a trial to determine the optimal operating region.

Benefits Analysis Determine the potential benefit that the advanced controller introduces to the system. This comparison will be compared to the benchmarked plant performance.

Part I

Literature Study

CHAPTER 2

Comminution

2.1 Platinum in South Africa

The largest resource of the Platinum Group Metals (PGMs) in the world is found in South Africa in the largest sub-volcanic, layered intrusion called the Bushveld Complex. The PGM deposits are found in three different layers, or reefs called the Merensky, the Upper Group 2 (UG2) and the Platreef (Cawthorn, 1999; Barnes and Newall, 2006; Mainza and Powell, 2006). The PGMs include platinum, palladium, rhodium, iridium, ruthenium and osmium, with the first two being the most abundant in all deposits, except alluvial occurrences (mostly in Russia). In 2008, 5.97 million ounces of platinum were produced, of which 4.8 million ounces were consumed by the automotive industry in auto catalysts (figure 2.1) (Jollie, 2009). Note that one million platinum ounces were recycled from spent auto catalysts. Other major applications are jewellery, investments and various other industrial uses (chemical, petroleum refining and glass). The highest demand for palladium at 4.38 million ounces in 2008 was also in the form of auto catalysts (1.17 million ounces recovered from spent auto catalyst). Other major palladium applications are jewellery and electronics.

The global supply of platinum is dominated by South Africa which produced the majority of the world's platinum in 2008 (Jollie, 2009) (figure 2.2). Other minor players are Russia and North America. South Africa also had the highest supply of palladium to the world. Russia however, had the highest primary production of palladium but only sold 35 % (960 thousand ounces) thereof via Swiss markets.

The South African platinum industry is dominated by three major companies, which together account for 68 % of the world's platinum (figure 2.3). They are:

- Anglo American Platinum Limited, which produced 2.39 million ounces of platinum in 2008, equating to 52 % of South African and 40 % of the world's total production,
- Impala Platinum (Implats) with a Platinum production of 984 thousand ounces in 2008 and,

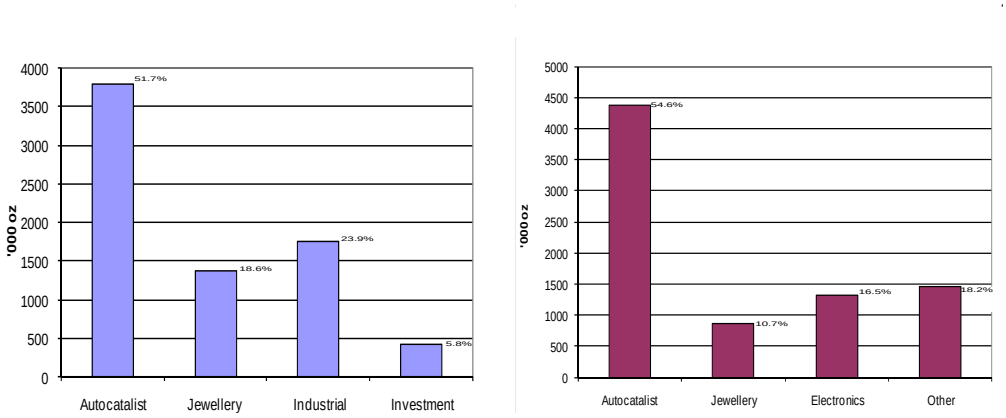

Figure 2.1: World wide demand for a) platinum and b) palladium for 2008 (Jollie, 2009).

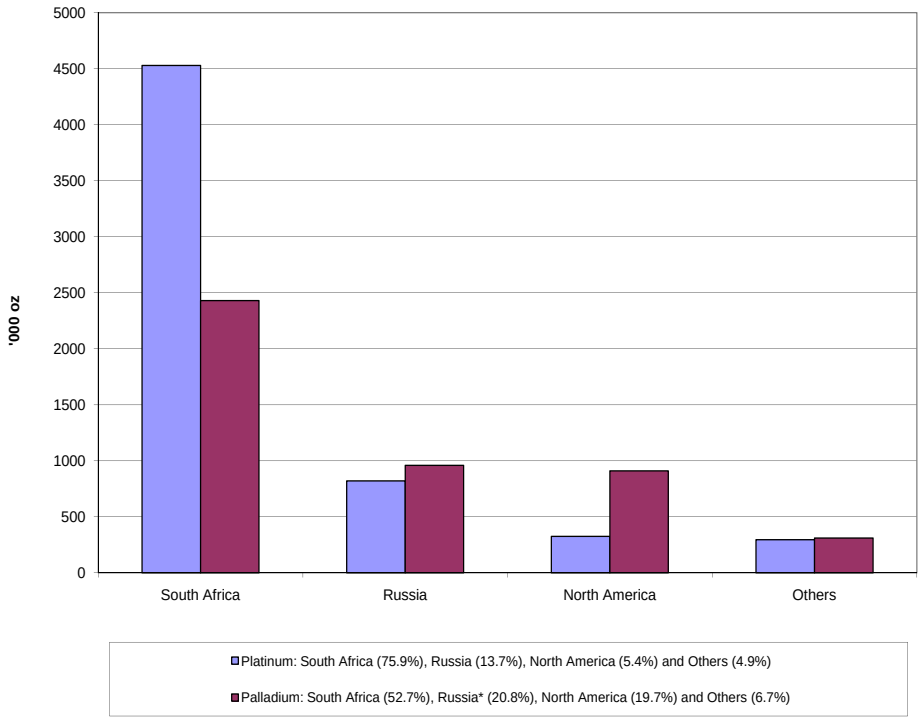

Figure 2.2: World wide supply of a) platinum and b) palladium in 2008 (Jollie, 2009).

- Lonmin Plc, which produced 716 thousand ounces of Platinum in 2008.

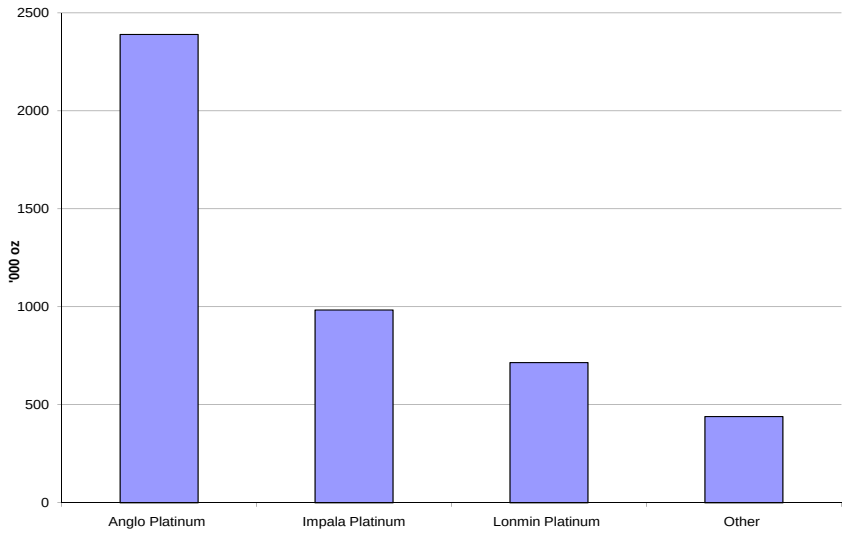

Figure 2.3: Breakdown of the South African platinum supply in 2008 (Jollie, 2009).

2.2 Anglo American Platinum Limited

Anglo American Platinum Limited (AAP) is listed on the JSE and also the London Stock Exchange (secondary listing) with operations all over South Africa – specifically, the Bushveld Complex (Platinum, 2006). The AAP value chain comprises of various metallurgical technologies and is presented in the literature in the form of an operational flow diagram. The AAP beneficiation process includes (see illustration in figure 2.4):

- Ore extraction by means of various mining methods
- Concentration which includes milling and flotation
- Smelting which occurs in electric arc furnaces
- Refining of both the precious—and base metals

The focus of this dissertation will be on the comminution stage of the AAP beneficiation process.

2.3 Comminution Circuits

The word “comminution” originates from the Latin word *comminuere* which means “to make small” (Napier-Munn *et al.*, 1999). The reduction in size of large rocks into a smaller

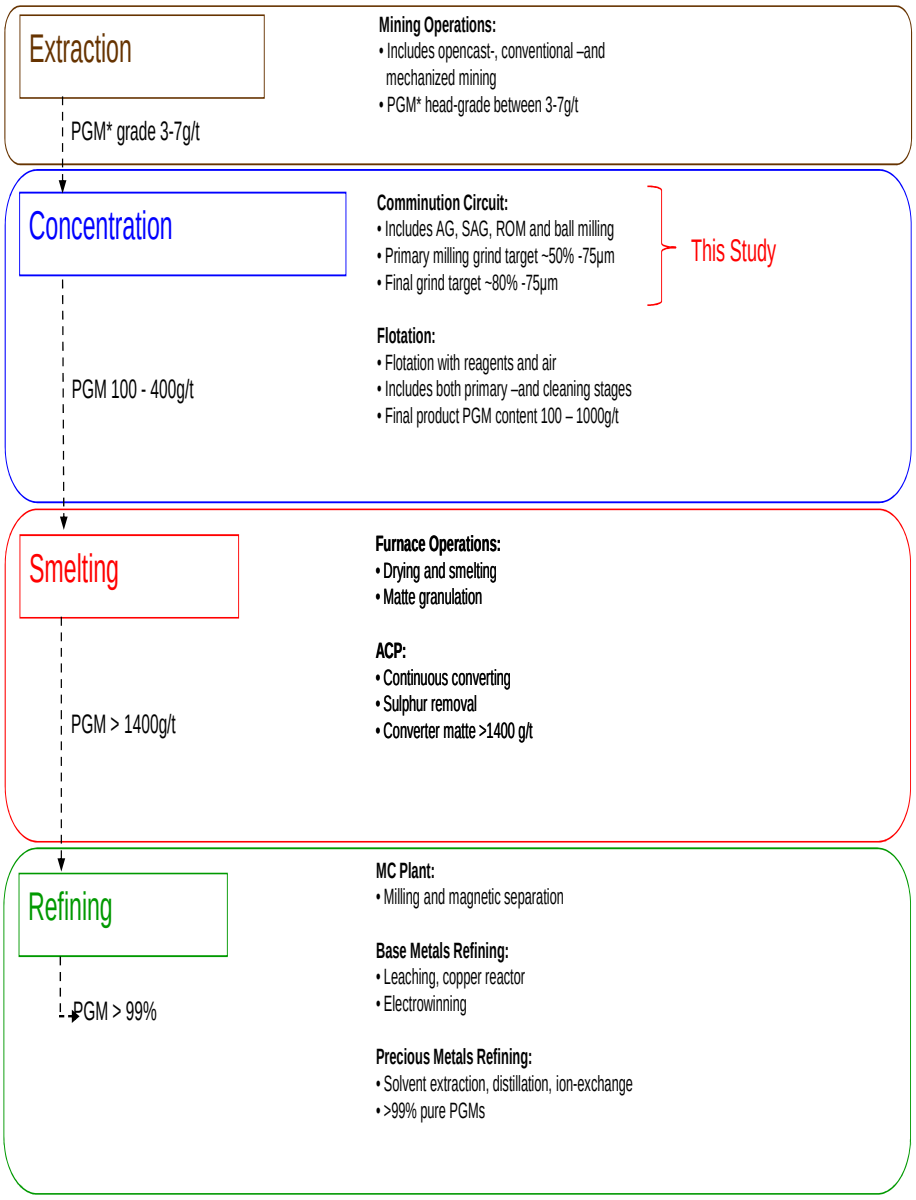

Figure 2.4: The Anglo American Platinum value chain (Platinum, 2006).

treatable form is a pervasive field of study stretching almost as far back as recorded history itself - breaking rocks for the building of temples and roads. In modern industrial civilisations, the magnitude and hence the importance of optimising comminution circuits was confirmed in a report by the US National Materials Advisory Board which estimated that 1.5 % of the USA's generated electrical energy was used in comminution processes (Napier-Munn *et al.*, 1999). The report also estimates a 20 TWh/a energy saving if realistic improvements on comminution circuits could be made with a special focus on classification and control.

Comminution circuits can be separated in two groups (Hayes, 2003):

1. Size reduction units, eg.:
    - Crushers (jaw, gyrator, cone crushers)
    - Tumbling mills (autogenous, semi-autogenous, ball and rod mills)
    - Stirred mills (tower, vertical pin and horizontal mills)

2. Classification units eg.:
    - Screens
    - Hydro-cyclones

2.4 Mineral Liberation

The main purpose of a mineral processing plant is to separate the valuable compounds from the other less valuable material, or gangue (Napier-Munn *et al.*, 1999). This beneficiation process or concentration of valuable species is continued until a saleable product is manufactured. To be able to separate the sellable mineral selectively from the gangue, either a physical or chemical property of the mineral must be targeted (Hayes, 2003). The purpose of any comminution circuit is therefore to liberate or "expose" these valuable minerals in the ore body by reducing the particle size of the ore received from mining operations (Napier-Munn *et al.*, 1999). Proper liberation is necessary for downstream processes to recover the freed-up mineral into a concentrate. The ideal product size needed for proper liberation is one of the main design criteria of any comminution circuit. Under-grinding the host rock will lead to insufficient recovery while over-grinding can be very costly in terms of energy and media consumption.

It is important to note that comminution processes do not change the chemical properties of the mineral but aim at separating the various mineral phases (Hayes, 2003). If the size of the particles is reduced to the size of the mineral grains, some particles will only contain one mineral phase (figure 2.5).

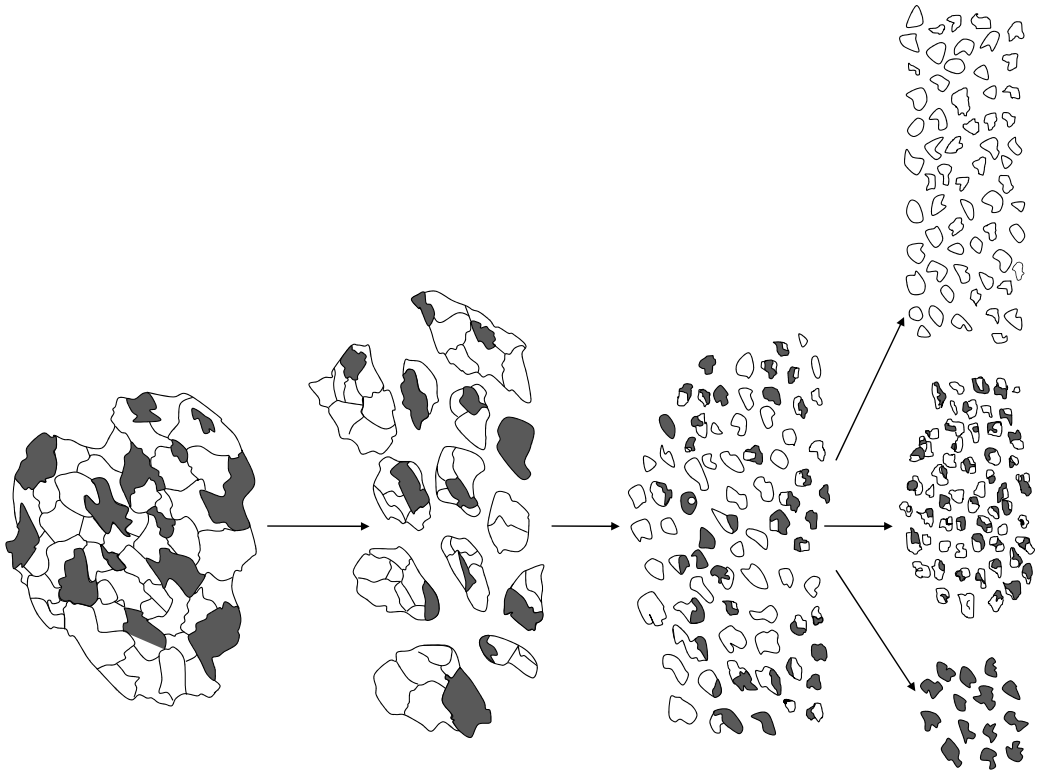

Figure 2.5: The size reduction of a two-phase material (Hayes, 2003).

2.5 Particle size distribution

An important performance measurement of any comminution circuit is the particle size distribution of the solids in a stream (Napier-Munn *et al.*, 1999). This is normally described by an analytical procedure that expresses the range of particles in the sample as a mass percentage reporting to a certain size class. The most common way of determining the size distribution of a product stream is by sieving. A sample is manually sieved on screens with apertures ranging from 9.5 mm down to 38 µm in size increments of $\sqrt{2}$ (9.8 mm, 6.7 mm, 4.75 mm, ..., 53 µm, 38 µm). Sieve results for smaller size fractions (20 µm) can be obtained but is a difficult and time consuming process. The sieves used in this procedure have a square aperture. The size classification is therefore defined as the projected diameter in the plane of greatest stability, $d_i = \sqrt{\frac{4A}{\pi}}$. The particle is hence described as a sphere with diameter ϕ and with a surface area equal to area A of the particle. There are several ways in which to present the results of a size analysis (Wills, 1992):

1. The mass of the material in each individual size class

2. The mass percentage in each size class

3. The cumulative mass percentage material retained on the screen. This result includes

all material retained on sieves with larger apertures. Cumulative percentage retained is indicated by adding a "+" before the value and unit, for example +75 µm.

4. The cumulative mass percentage passing a certain size. This includes all particles smaller than that particular sieve size. Cumulative percentage passing a certain sieve size is noted by a "-" before the value and unit.

2.6 UG2 Ore Mineralogy

The UG2 ore found on the Western Limb of the Bushveld Complex was investigated by Nel *et al.* (2005) focusing on ore treated by Impala. It was found that UG2 ore contains about 20 % to 30 % chromite [$(Cr,Fe,Mg,Al)_3O_4$] with aluminum silicates making up the rest - these include feldspars, pyroxenes, chlorite and hydro-thermally altered silicates (amphiboles and talc). Wesseldijk *et al.* (1999) reported the concentration of chromite in UG2 ore to be as high as 60 % by mass. The ore also contains base-metal sulphide elements of between 0.1 % and 0.2 % composed of pyrrhotite (50 %), pentlandite (30 %) and chalcopyrite (10 %). The Nel *et al.* (2005) study divided the PGM grains and association into four categories, from highest to lowest floatability:

- Completely liberated PGMs. The size of the PGM grains was found to be approximately 10 µm and smaller. Shackleton *et al.* (2007) however, described the behaviour of these particles as difficult to predict due to the small grain size with slower floatability characteristics than base-metal sulphides.

- Base-metal and iron sulphide associated PGMs – 70 % of the PGM in Western Limb UG2 ore occurs as this association.

- PGMs appearing of the surface or grain boundary of the host mineral - mainly silicates

- PGM completely enveloped by the host mineral. These grains are considered to be unrecoverable by conventional flotation techniques.

The PGM content of an open-circuit mill product as shown in figure 2.6 indicates that most (60 %) of the valuable mineral can be found in grains < 38 µm. PGMs in the UG2 ore body are made up of 45 % platinum, 25 % palladium, 10 % rhodium and 15 % ruthenium.

The high amount of chromite in UG2 ore is worth mentioning due to the downstream process issues associated with high chrome in the concentrate. Chromite is a spinel species that remains stable at temperatures up to 2000 °C (Wesseldijk *et al.*, 1999). The higher melting point, relative to operating temperatures of conventional PGM furnaces, leads to the formation of a partly solid spinel layer (Barnes and Newall, 2006). The higher density

of this layer causes it to form at the slag/matte interface and due to its high viscosity prevents the transport of PGMs to the matte. Chromite is however, not easily recovered by flotation as it is considered to be hydrophilic, but the smaller particles will report to the final product by means of entrainment in floatable minerals as well as entrainment associated with water recovery (Wesseldijk *et al.*, 1999; Nel *et al.*, 2005).

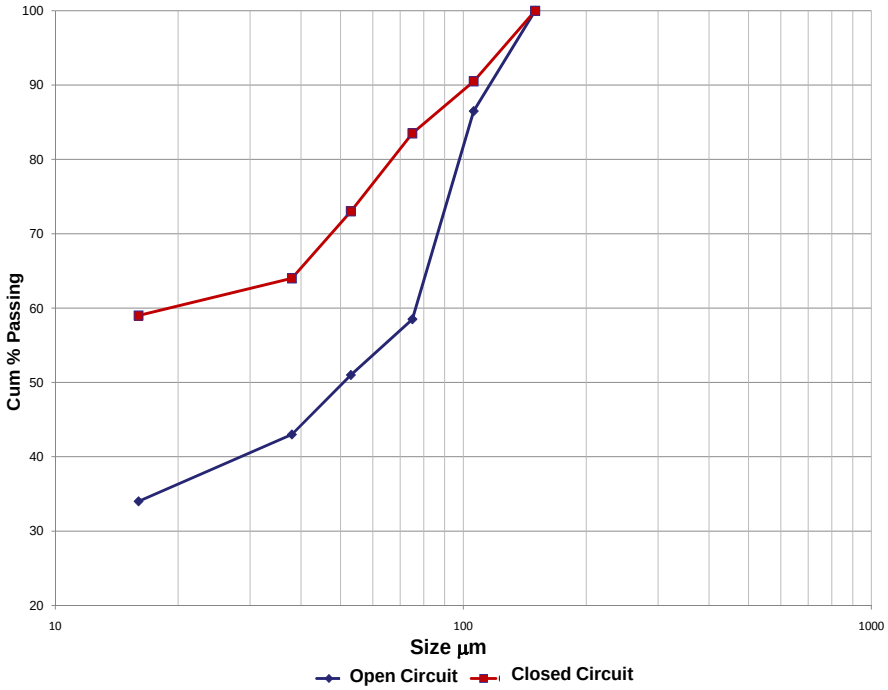

Figure 2.6: PGM distribution by size at an Impala concentrator on the Western Limb of the Bushveld Complex (Nel *et al.*, 2005):788.

2.7 Breakage Mechanisms

Due to the higher throughput that commercial size comminution circuits treat, it is often necessary to reduce the size of irregular-shaped particles (Hayes, 2003). The mechanisms applied for this size reduction or fracturing of the ore are the following stress applications (figure 2.7):

Slow compression The stress is realised throughout the material and increased until the shear and tensile stresses are enough to spread in the existing cracks. Since the fracturing propagates in the larger rocks first, this technique will lead to the formation of larger particles when compared to the other techniques

Fast compression Also known as impact grinding, fast compression can be compared to the stress incurred from a hammer hitting a rock (Hayes, 2003). The stress

levels are severe and propagated through the material by means of compressive stress waves. The particle will however not fracture immediately but only when the stress waves are internally reflected from the surface of the particle, extending the existing cracks in the structure. This leads to the formation of new cracks and fracturing occurs resulting in greater product size reduction than with slow compression samples. This grinding mechanism gives way to a coarser product at higher throughput (Napier-Munn *et al.*, 1999).

Abrasion This grinding technique involves the generation of high shear stresses that occur when particles are rubbed against each other or against hard surfaces such as the mill shell and grinding media. Localised fracturing of the original particle's surface occurs and yields a bi-modal product – one size close to the original particle and the other a small size fraction (Hayes, 2003). Napier-Munn *et al.* (1999) regards *attrition* grinding as a technique similar to abrasion grinding except that a small particle gets fractured while trapped between two bigger particles. Abrasive grinding techniques result in finer product grind but lower throughput.

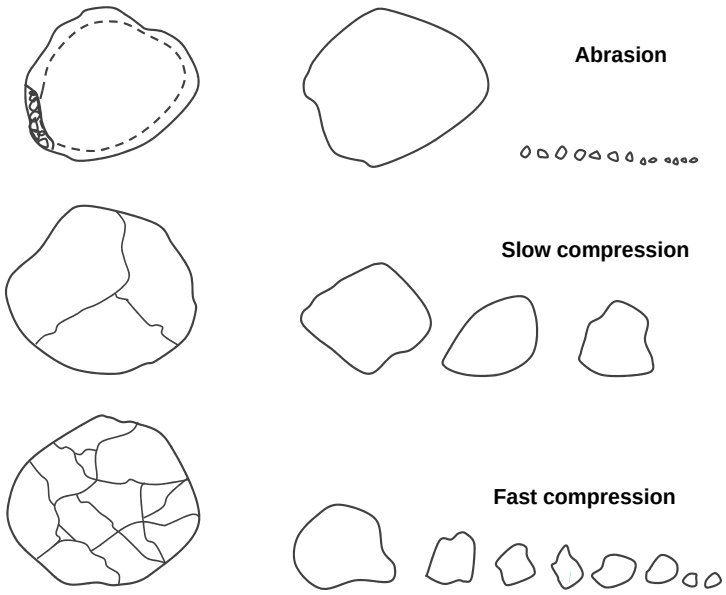

Figure 2.7: Mechanisms of particle breakage and fracturing (Hayes, 2003).

The grinding mechanisms present in a mill are mostly impact, abrasion and attrition grinding (Napier-Munn *et al.*, 1999). These are essentially localised to two regions in the mill:

1. The impact region situated on the surface of the toe of the mill and,
2. within the main body of the charge (figure 2.8).

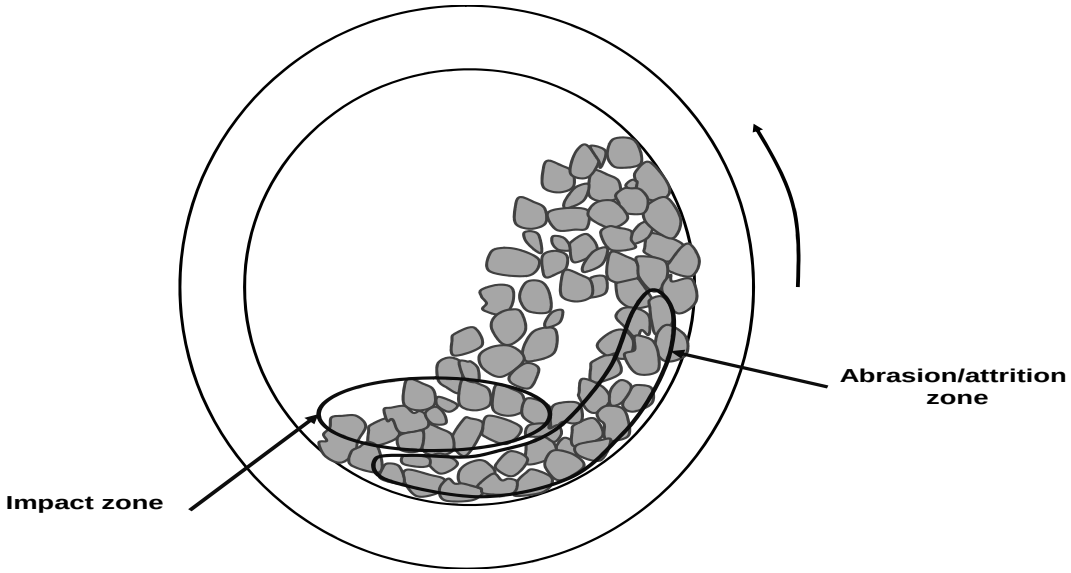

Figure 2.8: The two main grinding zones inside a tumbling mill (Napier-Munn *et al.*, 1999).

2.8 Bond Work Index

To assist in the determination of the energy requirements of a comminution process, Fred Bond developed an approach in 1952 that equipment manufacturers are using as a design tool to the present day (Napier-Munn *et al.*, 1999). The method is known as Bond's third theory that also provides a method for evaluation and optimisation of these circuits. The method assumes that the energy required is proportional to the new crack tip length generated from particle breakage (Wills, 1992). The work input is then equal to the work represented by the product minus the work represented by the feed. Assuming particles are of similar shape, the diameter of these particles is inversely proportional to the surface area of unit volume ($\phi = k\frac{V}{A}$). Wills (1992) then claims that the length of a crack (in unit volume) is proportional to the one side of the area and therefore inversely proportional to the square root of the diameter. In calculating the work input (W), the theory uses F_{80} and P_{80} to describe the size fractions that 80 % of the particles in the feed and product will pass (note that any percentage passing a certain size class may be used). The equation that describes Bond's third theory is:

$$W = \left(\frac{10}{\sqrt{P}} - \frac{10}{\sqrt{F}}\right) WI \tag{2.1}$$

Where WI denotes the work index (kWh/t) and expresses a material's resistance to grinding and crushing (Napier-Munn *et al.*, 1999).

Numerically the work input describes the energy (kWh/t) that is necessary to reduce the size of an ore that is theoretically infinitely large to a certain percentage passing a

certain size class, for example, 80 % passing 100 micron. The Bond work index is also considered by Wills (1992) and Napier-Munn *et al.* (1999) as the most widely used metric to determine an ore's grindability, where grindability is the ease with which materials are comminuted. Examples of the work index of various ore bodies are given by Wills (1992):

Table 2.1: The Bond Work Indices of various mineral bodies

Material	WI	Material	WI
Barite	4.73	Ferro-Silicon	10.01
Bauxite	8.78	Fluorspar	8.91
Coal	13.00	Granite	15.13
Dolomite	11.27	Limestone	12.74
Emery	56.70	Quartz	13.57

The method of obtaining the WI is not that straightforward and defined for each individual application (Napier-Munn *et al.*, 1999):

Crushability test Particles of size class +50 mm but -75 mm are subjected to impact breakage of a known force. Two weights (mass known) that swing on wheels are used to impact the rock simultaneously on opposing sides of the smallest dimension of the rock. The height from where the weights are released is increased until the rock breaks. The WI in kWh/t can then be calculated:

$$WI = 53.49\frac{ICS}{SG} \tag{2.2}$$

Where ICS equals the impact crushing strength in J/mm of rock thickness and SG refers to the specific gravity of the rock.

Ball mill grindability test The test involves a series of laboratory mill, grind tests where the WI is then calculated by using equation 2.3. The method is extensive and does not fall within the scope of this literature study but from this test, the ball mill WI is calculated using the following equation:

$$WI = \frac{49.1}{P_1^{0.23} \cdot GBP^{0.82} \cdot \left(\frac{10}{\sqrt{P_{80}}} - \frac{10}{\sqrt{F_{80}}}\right)} \tag{2.3}$$

Where P_1 is the sieve size of the product that the WI should be correlated to. GBP is defined as the ball mill grindability and obtained from the experimental procedure by calculating the amount of final product (of size $< P_1$) produced per revolution of the laboratory mill.

AG/SAG work index The determination of the WI for AG/SAG mills via the standard grindability described for ball mills cannot be used. This is due to the fact that the

Bond method hinges on two assumptions that are generally reasonable for ball mills but not for AG/SAG mills (Napier-Munn *et al.*, 1999):

- The energy consumption in grinding should be dominated by the production of new surface areas
- The feed and product can be classified by a single size. In order to achieve this, the plots of size distribution presented as cumulative percent passing vs. the log size class should be parallel lines.

Using the Bond method in the design of AG/SAG mills in terms of size and power draw, requires the use of operating data from either an existing application or a pilot scale mill.

2.9 Milling

The introduction of milling or grinding circuits to South Africa occurred in 1883 with the discovery of gold in the Transvaal (Gauteng) in the form of a Gates crusher followed by a series of 340 kg stamps (SAIMM, 1987). The first use of tumbling (or tube) mills in South Africa was recorded in 1921, phasing out the stamps as the need for higher production rates and finer product increased. These mills were mostly operated as AG mills. It was not until the 1930's that ball mills were used in the gold industry. Applications of rod-milling came into being in North America after the 2nd world war in 1949, which provided a cheaper, more efficient option at the time. Run-of-mine (ROM) milling was the next (and most recent) major development with the first industrial scale mill commissioned in Evander (South Africa) in 1958. Although tumbling mills have enjoyed a fair amount of focus with regards to improving efficiency and reliability, it is still regarded as extremely wasteful in terms of energy consumption (Wills, 1992). Mills are generally categorised by the shell's aspect ratio, the type and amount of grinding media as well as the method used to discharge the slurry product. The aspect ratio of a mill is defined as the diameter over the length of the mill. Three groups are defined:

- "Pancake" or "flying saucer" mills with higher aspects at 1.5 to 3, the design normally supported by North America
- Square mills with diameter similar to the length of the mill
- Low aspect mills at ratio 0.3 to 0.6 and mostly favoured by the South African industry.

2.9.1 Autogenous Milling

The word "autogenous" is derived from the Greek word meaning self generated or self produced (Napier-Munn *et al.*, 1999). The main characteristic of this form of milling is that the grinding medium comprises of the ore being ground and therefore the absence of a secondary media, normally steel. In semi-autogenous (SAG) applications, steel balls are added to supplement the ore grinding media. The SAIMM (1987) suggests that ferrous media in SAG mills are only up to 10 % (by volume) of the mill load. The main advantages of autogenous mills are

- Lower capital costs
- Ability to treat a larger variety of ore types than traditional mills
- Lower operating costs due to the reduction in steel consumption

AG and SAG mills make use of discharge grates (normally steel or rubber) to hold the media inside the mill. Only particles of a certain size can pass through these grates as product. The most common discharge mechanism is the diaphragm style grate with two main designs that differ in the way the slurry is removed from the mill once it flows through the grate (see figure 2.9):

- End discharge - slurry exits the mill via gravity as the end of the mill is completely open
- Pan lifter discharge - makes use of a trunnion and lifters arrangement to transport slurry out of the mill. As the mill rotates, the lifters (acting like a paddle wheel) pick up the slurry and direct it towards the trunnion and out of the mill.

2.9.2 Ball Mills

Ball mills are considered to be the most common tumbling mills with applications ranging from laboratory units to larger industrial mills with operational power consumption of 10 MW to 12 MW (Napier-Munn *et al.*, 1999). Ball mills are most commonly used for secondary, tertiary or regrinding applications, but can also be applied in primary milling circuits with feed sizes up to 20 mm. Pure ball mills operate at a higher steel ball charge of > 35 %. Napier-Munn *et al.* (1999) do however suggest that a ball mill feed should be < 20 mm whereas SAIMM (1987) regards the typical feed of pure ball mills to be 80 % passing 10 mm. Ball mills are known to be energy intensive units due the larger effort needed to move the heavier inert steel grinding media in the mill. The steel charge alone accounts for up to 85 % of the total mass inside the mill and therefore dictates the power draw and grinding capability.

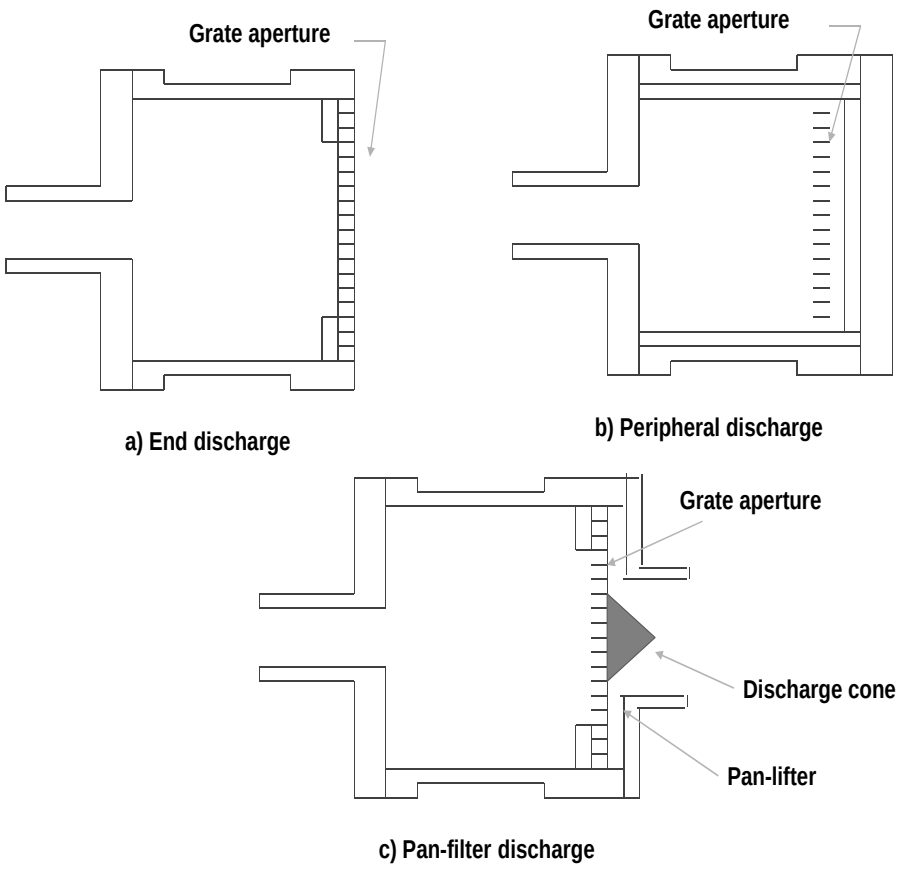

Figure 2.9: Schematics of various discharging mechanisms (Napier-Munn *et al.*, 1999).

Optimisation of these mills' performance has great cost savings implications. Ball mills are cylindrical mills with aspect ratios normally between 1 to 1.5 (square to low aspect ratio). The discharge mechanisms of these mills are mostly either grate discharge similar to that discussed in the AG/SAG section or overflow mills with no diaphragm and only an exit hole with a larger diameter than the inlet hole.

2.9.3 Run-of-Mine (ROM) Milling

Run-of-mine refers to the type of feed the mill is treating, and according to the definition it means "not graded according to size or quality". This indicates that the ore is fed to the mill in the "as-hoisted" condition with no intermediate treatment apart from a top-size reduction stage to ease transportation (SAIMM, 1987). No ore classification occurs prior to milling. ROM circuits therefore operate at fewer degrees of freedom due to the lack of control over the feed type it receives (Craig *et al.*, 1992; Hulbert, 2002). This type of milling was introduced as a pebble mill (autogenous) due to its lower operational cost implications relative to conventional comminution circuits (Powell *et al.*, 2001; SAIMM, 1987). The two types of milling used on ROM milling applications are normally either

autogenous/semi-autogenous or ball milling. Economically, ball milling can not compete with autogenous milling. Balls are therefore only added to the ROM autogenous mill to supplement the grinding media if the pebbles in the feed are insufficient (SAIMM, 1987). The lack of competent grinding media, as is the case with UG2 platinum ore, is often cited for the reason that ROM ball mills are used rather than the conventional AG/SAG mills (Mainza and Powell, 2006).

Despite the coarser feed to the mill, the additional steel charge leads to ROM ball mills producing a finer product than the traditional AG/SAG mills but at considerably higher energy cost (Mainza and Powell, 2006).

Table 2.2: Comparison of ROM mills with traditional SAG mills (Powell *et al.*, 2001)

	AG/SAG (Aus, NA)	ROM (SA)	Unit
Speed	70 - 80	75 - 90	% Critical
Charge filling	20 - 30	35 - 45	% Mill Volume
Ball filling	4 - 15	15 - 35	% Mill Volume
Internal length	3 - 5	5 - 12	metre
Aspect ratio D/L	0.7 - 2	0.5 - 0.8	
Recycle stream	Trommel oversize/ Pebble crusher	Cyclone/Vibrating screen	

2.10 Circuit Configurations

Using a classifier in the circuit is referred to as closing the circuit and presents a very effective way to bias the grinding energy towards the larger particle sizes (SAIMM, 1987). Breakage inside a tumbling mill is considered a first order rate process. This means that the rate at which a certain size fraction is reduced in size is proportional to the amount (in mass) of particles in that size fraction. The coarser particles in the mill will therefore receive more breakage energy if they occur more often inside the mill (at higher concentrations) than the smaller size particles. Fines classifiers in the form of hydro cyclones or classification screens are often used to achieve this. Separating the fines from the stream after the first pass through the mill and recycling the coarse material allows the operation to feed the mill at considerably higher rates than single pass circuits in order to achieve similar product quality. Vibrating screens are normally used in applications with a feed to classifier + 200 µm while hydrocyclones are used for the finer end of the scale (Napier-Munn *et al.*, 1999).

CHAPTER 3

Mill Performance Metrics

3.1 Mill Filling

Throughout the literature it is clear that milling performance is sensitive to the volumetric fill of the mill (Napier-Munn *et al.*, 1999; Powell and Mainza, 2006; van der Westhuizen and Powell, 2006). The main performance outputs of milling circuits, throughput, power draw and product size (or grind), are all described as a function of the mill filling. The relationship between the mill filling and all these parameters is well documented and described as the "grindcurve" of the mill (Powell and Mainza, 2006). Since the above mentioned parameters all peak at various filling degrees (figure 3.1) it is essential to establish a good understanding of the grindcurves as a guide for optimisation. It is of particular interest to note that the throughput peaks at a lower filling than the power draw.

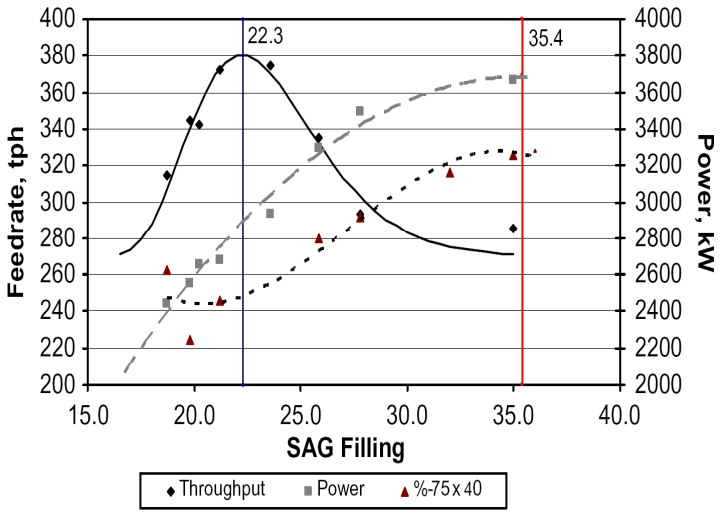

Figure 3.1: The grindcurves of a typical SAG mill (van der Westhuizen and Powell, 2006).

Mill filling is normally derived from a relationship with the measured load of the mill (van der Westhuizen and Powell, 2006). The relationship is normally established by a

series of mill stops to determine the filling at a certain mill load. van der Westhuizen and Powell (2006) describe the relationship between load cell reading and filling as a straight line (also see figure 3.2).

$$J = m \cdot M_{lc} + c \tag{3.1}$$

The y-intercept (c) in equation 1 describes the curve displacement, associated with the longer term changes such as liner wear or changes to the media charge. The gradient m, in equation 3.1 relates a change in volume filling to a change in mass and can therefore be determined using the bulk density of the ore charge and the volume of the mill, where:

$$m = \frac{1}{(\rho_{b,ore} \cdot V_{mill})} \tag{3.2}$$

The bulk density of the charge is a function of the ore density ρ_{ore} as well as the slurry that fills the voidage φ. Note that this should exclude the steel fraction since steel changes are regarded as long term load changes and should not affect the filling indication over a short period. The bulk density is then determined as follows:

$$\rho_{b,ore} = (1 - \varphi) \cdot \rho_{b,ore} + \varphi \cdot \rho_{slurry} \tag{3.3}$$

Note: Powell and Mainza (2006) established that this relationship tends not to be linear when the load indication is obtained from the mill bearing's lubrication oil back-pressure. The load/volumetric filling relationship should then be established experimentally.

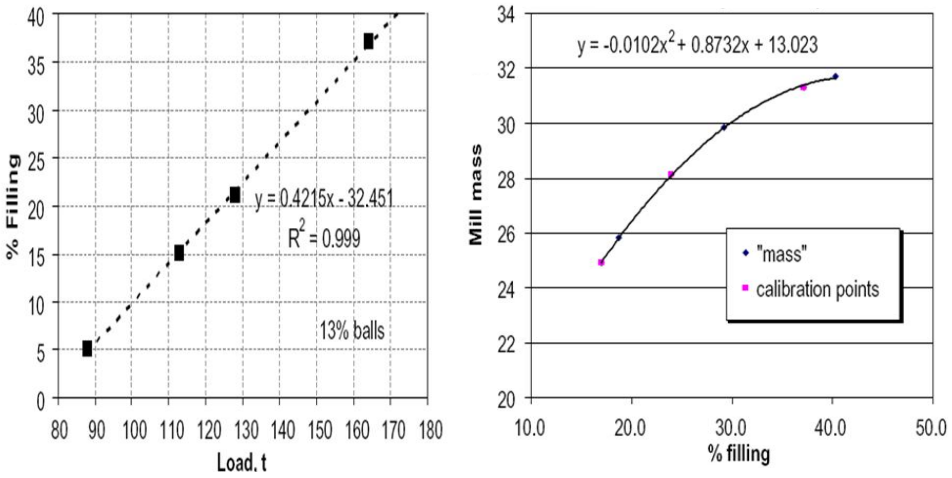

Figure 3.2: Mill volumetric filling to load relationship with load a) measured by a load cell or b) inferred from bearing pressures (Powell and Mainza, 2006).

With trunnion discharge mills, common to North-America and Australia, a maximum volume filling of 35 % is common, while the South-African end-discharge mills, fillings of 40 % to 50 % are not unusual (Napier-Munn *et al.*, 1999).

3.2 Speed

The speed of the mill is expressed as a fraction of the speed at which the centrifugal force would equal gravitational force g and the mill charge starts to spin against the mill shell surface without falling (Napier-Munn *et al.*, 1999). Under these conditions, the maximum vertical force of a particle travelling inside the mill is equated to the centrifugal force (Hayes, 2003):

$$mg = \frac{2mv^2}{\phi} \tag{3.4}$$

Since the velocity of the mill shell $v = \pi\phi N$, the critical speed of the mill N_c, is derived (in rpm):

$$N_c = \frac{42.3}{\sqrt{\phi}} \tag{3.5}$$

Increasing the rotational speed of the mill increases the power draw of the mill due to an increase in kinetic and potential energy, (figure 3.3a) thus leading to a higher shoulder in the mill's trajectory (van der Westhuizen and Powell, 2006). Additional rotational speed will also increase the throughput of the mill over the normal mill filling range of 20 % to 40 %. Larger increases in throughput were observed (figure 3.3b) when the mill speed increased from 65 % to 75 % critical speed. The throughput and power peaks also became more pronounced at higher values when the speed of the mill was increased and closer together. The steeper, more pronounced power and throughput peaks give rise to an increased difficulty in controlling the mill at higher speeds.

Although increased speed results in increased throughput and power draw, van der Westhuizen and Powell (2006) found that higher speeds resulted in coarser product grinds (figure 3.3c). The mill's performance parameters with regards to speed presents a trade off scenario where throughput is favoured by an increase in mill speed while fineness of grind is improved at lower speeds. Although the overall grind suffered (coarsened) as a result of the increase in speed, the total amount of desired product increased at higher speeds (figure 3.3d). In addition, the grind peak became flatter and less pronounced at higher mill speeds, as opposed to those of the throughput and power trends.

3.3 Power

As far as SAG milling performance is concerned, the power utilisation of a mill is probably the most investigated and modelled parameter (van der Westhuizen and Powell, 2006). Hodouin *et al.* (2001) describes the power to load (or filling) of a mill as an increasing and then decreasing function with the highest efficiency close to the peak on the ascending side of the curve. van der Westhuizen and Powell (2006) also state that the power draw of a

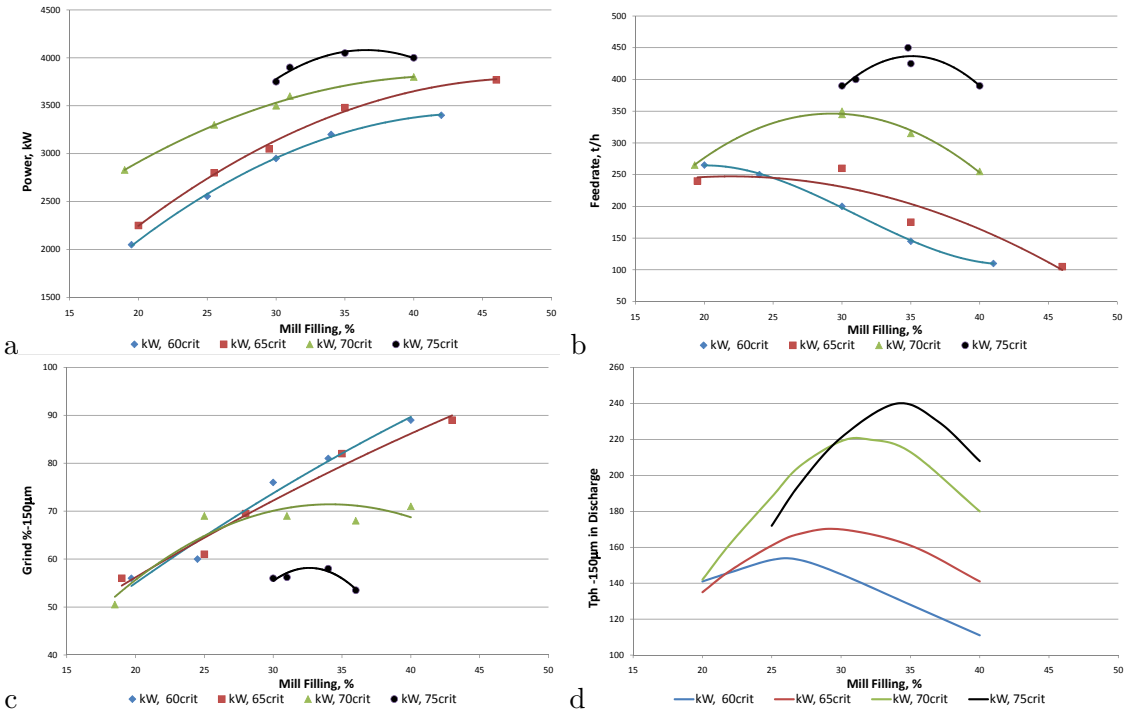

Figure 3.3: a) Power draw, b) throughput, c) grind and d) fines production (tph) of a SAG mill at the South Deep Gold Plant for various mill fillings and speeds (van der Westhuizen and Powell, 2006).

mill is expected to increase when the mill filling is increased – this statement is observed in figure 3.3a. The optimal operating point on this curve is discussed in subsequent sections. The increase in power is due to the additional charge at higher filling that is available to absorb the energy from the mill. There is however a point where the power draw of the mill starts to decrease with the increase in charge. This power peak normally occurs at fillings of 45 % to 50 % and is due to the following reasons:

- As the filling increases, the mill's centre of gravity shifts towards the middle of the mill (cross sectional), but the additional weight of the charge increases the power draw. At some point the shift towards the centre of the mill starts to outweigh the increase in mass causing the torque of the mill to decrease.

- The increase in charge volume causes the position of the toe of the mill to lift to a point where the potential energy conveyed to mill is reduced.

The mill power consumption is also one of the most important physical performance metrics, as the efficiency of the mill is often reported in the form of specific power consumption (SPC) of the form (Napier-Munn *et al.*, 1999):

$$\text{SPC} = \frac{energy\ consumed}{throughtput}[kWh/t] \tag{3.6}$$

Note that the denominator of equation 3.6 is often changed to the mass of a certain size class in the product stream. The SPC then refers to the power consumed to produce

a certain desired product. A more efficient mill will thus have a lower SPC. The SPC is highly influenced by the ball load, volumetric filling of the charge (balls and ore), mill speed and feed size (Napier-Munn *et al.*, 1999). Fuerstenau *et al.* (1990) mentions that the mill's torque or power draw is uniquely correlated to the mill's grinding rate and hence the degree of size reduction achieved. This can also be observed in figure 3.1.

3.4 Throughput

In a milling operation, throughput is generally limited by the power and capacity inside the mill (Napier-Munn *et al.*, 1999). Any increase in the ore throughput of a mill will result in an increase in the volume of the charge inside the mill. It is important to note that this is only true if the speed of the mill is kept constant. The throughput can be increased up to the point where the mill contents spill. In order to increase the throughput of a mill it is therefore essential to conduct a capacity study with regards to the charge inside the mill. It is also important to consider the power capacity of the mill when investigating the available volume and possible throughput increases. The throughput of a mill displays similar characteristics to the power vs. filling curve (Craig *et al.*, 1992; van der Westhuizen and Powell, 2006). It increases as the filling increases with a definite peak observed to occur at generally a lower filling level (20 % to 40 %) than the power curve (45 % to 50 %), as seen in figures 3.1 and 3.3b. It was noticed that the throughput of the mill is primarily driven by the rate of breakage of the coarser size particles to sizes below the discharge aperture - this is true if no discharge constraints are present. Due to the decrease in the distance from the shoulder to the toe of the mill, the amount of impact breakage is reduced resulting in a reduction of the coarser ore's breakage rate constant. However, due to the increased mass of the coarser particles, the amount of coarse particle breakage increases, thus increasing the throughput. This trend will continue up to the point were the mill is so full that the rate of breakage reduces dramatically due to the lack effective impact, resulting in the throughput drop-off at higher mill fillings.

3.5 Grind

Grind as a performance metric of milling performance is often more difficult to predict than power and throughput (van der Westhuizen and Powell, 2006). The product grind is also difficult to manipulate in open circuit milling (Napier-Munn *et al.*, 1999). The size of the product in open circuit SAG milling is mainly a function of the ore but can be manipulated by changes in the ball load, mill speed (figure 3.3c), grate and ball size. The rule-of-thumb regarding the optimisation of grind is that the fineness of the product will increase as the power draw, or mill filling increases (Craig *et al.*, 1992; van der Westhuizen and Powell, 2006). The breakage rate of the coarser particles decreases when the filling

increases, the breakage rate of the fines (+ 1 mm) is increased. The reason for this is an increase in abrasion grinding while less impact occurs. The fineness of the product is dictated by the fines breakage rate and the solids content of the mill. The fineness of the product will always increase at higher filling since both these parameters increase with an increase in mill filling.

3.6 Rheology

Rheology is defined by Napier-Munn *et al.* (1999) as the study of deformation and flow. This is characterised by the in-mill slurry *viscosity* as well as the slurry's particle size distribution, particle shape, solid concentration and physico-chemical conditions. Fuerstenau *et al.* (1990) observed that a slurry undergoes a qualitative change at higher solids concentration which leads to increased viscosity. Klimpel (1983) explained that particles undergo a first order rate of breakage when milling occurs at solids volume concentrations of 40 % to 45 % where distinct dilatant characteristics are observed. Increased slurry solids concentration leads to increased absolute, first order grinding rates but with more pseudoplastic behaviour (Klimpel, 1983; Napier-Munn *et al.*, 1999). At an even higher solids concentration, a shift to non-linear grinding kinetics can be observed which leads to lowered breakage rates (see figure 3.4).

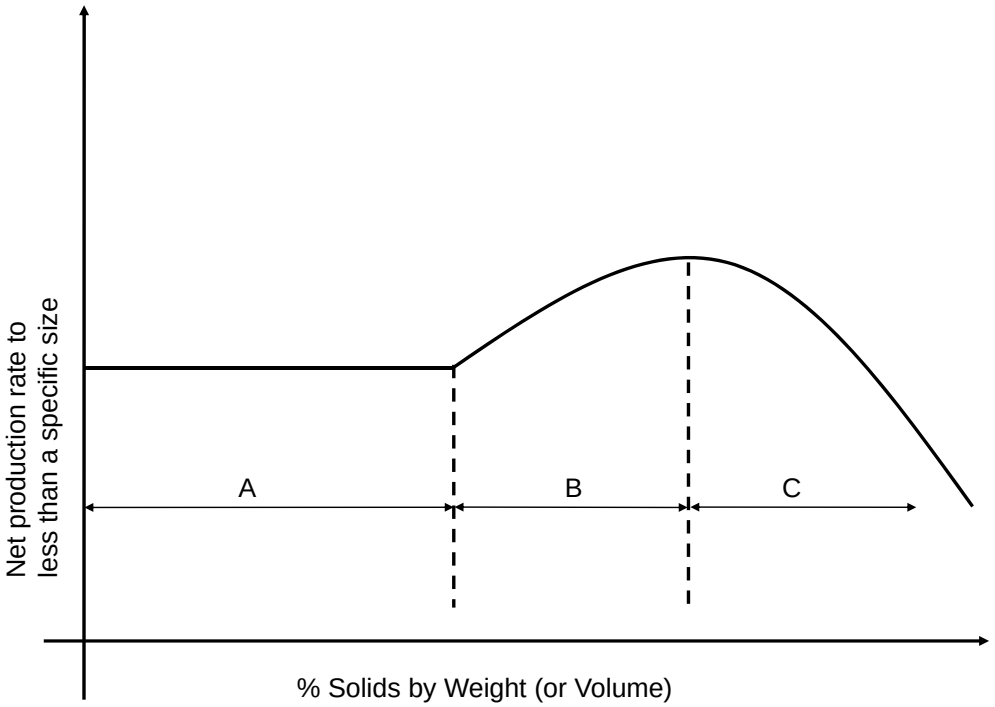

Figure 3.4: Production rate as a function of percentage solids in the mill (Napier-Munn *et al.*, 1999)

Morell and Kojovic (1996) investigated the effect of flow through a grate discharge mill on its power draw. The flow through the mill was assigned to two distinct zones which are dependent on the magnitude of the flow. At lower flowrates, transport out of the mill occurs at the areas where the grates are in contact with the charge (see figure 3.5). More

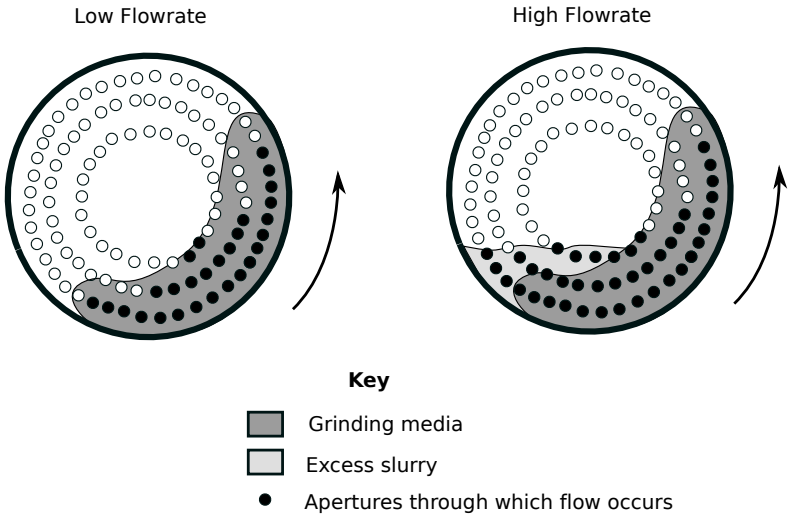

Figure 3.5: Transport regions out of a grate discharge tumbling mill, Morell and Kojovic (1996)

of the charge interstices are occupied as the flow through the mill increases. A slurry pool starts to form when flow increases to a point when all available interstices are occupied by slurry. They also found significantly different effects on power for the two methods of transport out of a grate-discharge tumbling mill. An increase in power draw was observed for increases in flowrate when the grinding interstices were not fully occupied. When flowrates increased to a point where a slurry pool began to form, a decrease in power was observed with further increases in flowrate. Results of this are shown in figure 3.6. They described the power draw of a grate-discharge mill using empirical functions for each of the two transportation zones:

1. Power as a result of flow via the charge J_{pm} and
2. Power as a result of flow via the slurry pool J_{pt},

$$J_{pm} = 0.013 Q_m^{0.5} \phi^{0.67} \gamma^{-1.25} A^{-0.5} D^{-0.25} \tag{3.7}$$

$$J_{pt} = 0.001 Q_t \gamma^{-2} A^{-1} D^{-0.5} \tag{3.8}$$

with,
Q_m, Q_t = Volumetric flowrate via grinding media and mill toe respectively
ϕ = fraction of the mill speed (to critical speed)
γ = grate design parameter related to the position of apertures
A = grate open area

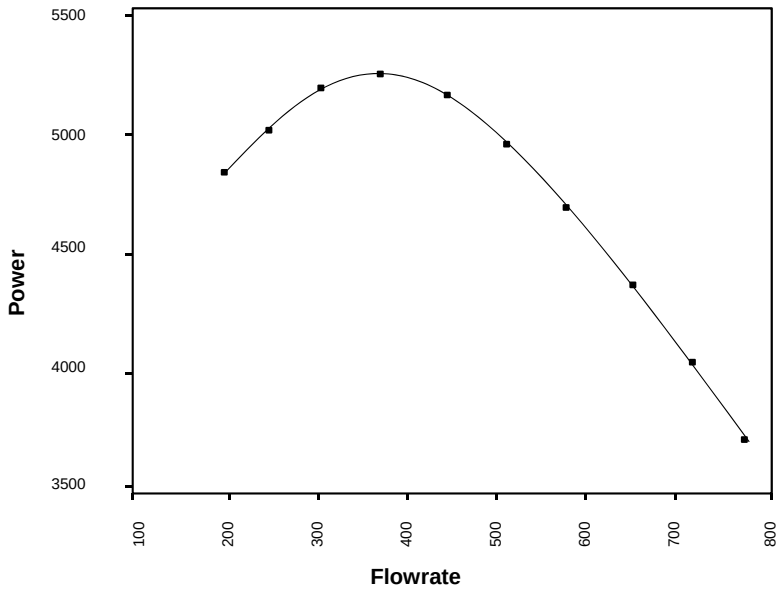

Figure 3.6: The impact of increased flow rate on the power of a grate-discharge tumbling mill, Morell and Kojovic (1996)

D = Mill diameter

3.7 Wear

The wear of a mill is associated with the consumption of steel in the form of liner and steel ball deterioration (Napier-Munn *et al.*, 1999). These are normally dependant on the ore type and the quality/material of construct of the liners and media, but certain operating conditions can give rise to increased wear:

- Lower charge filling creates an opportunity for steel balls to collide with each other and the liners, therefore increasing the amount of wear.
- Higher ball level will increase steel consumption for the same reason. The minimum ball charge that will maintain production targets should be targeted.
- Increased mill speeds will also give rise to more collisions and therefore higher steel consumption.

3.8 Recovery

When referring to mineral processing plants, *recovery* is the amount of valuable mineral present in the end product, or final concentrate relative to what was fed to the plant (Wills, 1992). Determining the recovery on process plants from mass flow instrument readings is

often considered inadequate for such an important performance indicator (Hayes, 2003). This is due to the errors associated with these measurements. It is therefore preferred to calculate plant recovery from chemical analysis of the process streams that tend to be more accurate. These analyses represent the *grade* or concentration of the valuable mineral in the stream. The recovery calculation based on the grades alone, is called the two product formula and is derived as follows:
If a mass balance with its boundary across the entire plant is conducted, total throughput at steady-state will be,

$$F = C + T \tag{3.9}$$

With F, C and T the mass flow, in ton/h, of the feed, final concentrate and tails, respectively. A component balance at steady-state will provide the formula,

$$Ff = Cc + Tt \tag{3.10}$$

Manipulating these two independent equations and considering that the definition of recovery states that,

$$R = \frac{Cc}{Ff} \tag{3.11}$$

It can then be shown that recovery can be calculated using only the grades of the respective streams:

$$R = \frac{c.(f-t)}{f.(c-t)} \tag{3.12}$$

Equation 3.12 indicates that there exists a relationship between the grade of a particular stream and the recovery described. This is often referred to as the *grade-recovery* family of curves that takes on the form $\text{Grade} = a \cdot \ln(100 - \text{Recovery})$ (figure 10.1 in the appendix). This curve presents a feasible region for flotation optimisation that is unique for any given set of operating conditions (Hodouin *et al.*, 2001). The amount of mass produced in the circuit relative to the plant's fresh feed $\frac{C}{F}$ is referred to as the *mass pull* of the process (note that the term also appears in the recovery calculation, equation 3.11).

The grade-recovery curve presents a trade-off situation where increased recovery might lead to a more dilute product while a high quality product will cause a loss in valuable mineral. Hayes (2003) therefore suggests the point of operation should be to maximise recovery whilst maintaining the minimum concentrate grade specification. Hodouin *et al.* (2001) mentions that despite recovery being a steady-state concept, there exists an upper bound on the grade-recovery curve within the feasible region of operating conditions and constraints, where revenue is maximised. The upper bound mentioned will unfortunately change continuously as market price for the metal as well as the available ore and feed characteristics change.

CHAPTER 4

Modelling and Control

4.1 Modelling

4.1.1 Dimensional Analysis

Identifying the influence that variables have on each other by means of a mathematical model can be laborious and complex. Giordano *et al.* (2009) explains that obtaining a model that predicts a physical phenomenon often requires extensive experiments, curve fitting and interpolation. Dimensional analysis is a method that can significantly reduce the amount of data necessary by describing a dimensionally correct equation among variables. It is a very effective method to determine the relationships between variables in a process. All variables related to the milling process are measured in combinations or simple products of unit length L, mass M and time T and expressed in the form $L^n M^p T^q$. For example, the dimensional formula of the feed to the mill in t/h is expressed as $L^0 M^1 T^{-1}$. The dimensional formula of dimensionless quantities is $L^0 M^0 T^0$. The systematic method of dimensional analysis is based on two arguments:

1. Equations that describe the relationship between physical quantities involve the sum of terms with each term of the form $m_1^{p1} m_2^{p2} \cdots m_k^{pk}$.

2. A homogeneous expression can by constructed by taking a product of dimensionless quantities. Expressions where the sum of the products have the same dimension are considered a homogenous equation. Buckingham's Theorem states that the relationship among quantities can be manipulated, if a complete set of dimensionless products $(\Pi_1, \cdots, \Pi_n)$ are present, to form a function f such that,

$$f(\Pi_1, \ldots, \Pi_n) = 0 \tag{4.1}$$

Example: To describe the combinations of powers p_1, p_2 and p_3 which yield dimensionless products in a system with three variables $m_1^{p1}, m_2^{p2}$and m_3^{p3}, one first needs

to consider the following equation:

$$(L^{n1}M^{v1}T^{q1})^{p_1}(L^{n2}M^{v2}T^{q2})^{p_2}(L^{n3}M^{v3}T^{q3})^{p_3} = L^0M^0T^0 \tag{4.2}$$

Three equations, one for L, M and T, can thus be derived and solved by means of Gaussian reduction and parametrisation to produce the relevant dimensionless products.

4.1.2 Empirical Process Modelling Techniques

According to Camacho and Bordons (2007), the most common methods used to describe the dynamic behaviour of a process are:

Impulse response models, also known as convolution models, relate the inputs and outputs in the following manner (also refer to figure 4.1):

$$y(t) = \sum_{i=1}^{N} h_i u(t-i) = H(z^{-1})u(t) \tag{4.3}$$

where $H(z^{-1}) = h_1z^{-1} + h_2z^{-2} + \ldots + h_Nz^{-N}$ and z^{-1} refers to the backward shift operator. The output calculation has an imposed practical limitation of N coefficients. This limitation implies that only stable processes can be represented. The predicted output parameters $\hat{y}(t)$ can then be calculated as follows:

$$\hat{y}(t+k|t) = \sum_{i=1}^{N} h_i u(t+k-i|t) = H(z^{-1})u(t+k|t) \tag{4.4}$$

For multiple inputs to the process, any output can be described by the sum of the responses imposed by inputs m:

$$y_j(t) = \sum_{k=1}^{m}\sum_{i=1}^{N} h_i^{kj} u^k(t-i) \tag{4.5}$$

Impulse response models are most commonly used in Model Algorithmic Control (MAC) and also (less often) in Generalised Predictive Control (GPC) and Extended Prediction Self-Adaptive Control (EPSAC). The impulse response method has the following advantages:

1. it requires no prior process information
2. it presents the relationship between inputs and outputs in an intuitive manner
3. non-minimum phase or delays and other complex dynamics are easy to describe

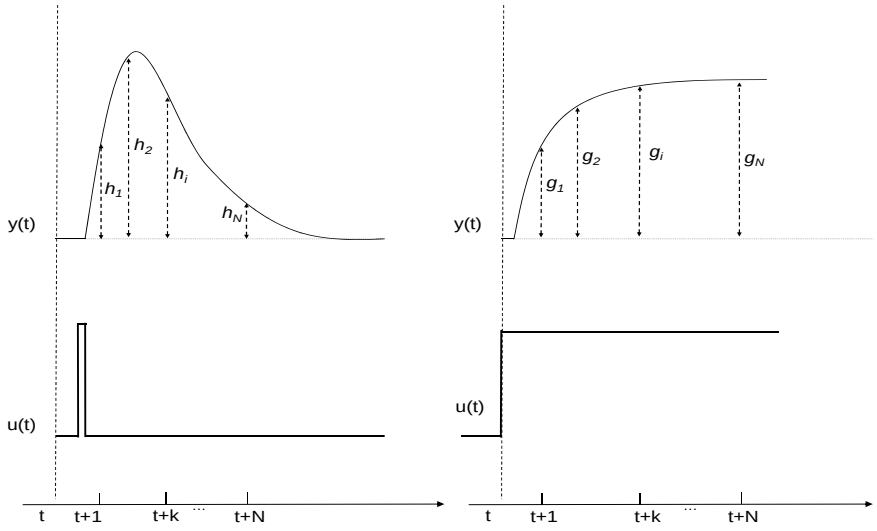

Figure 4.1: Examples of a) impulse response and b) step response

Step response models are similar to impulse models and most commonly applied to Dynamic Matrix Control (DMC) and its variants. The truncated input-output relationship is given by:

$$y(t) = y_0 + \sum_{i=1}^{N} g_i \Delta u(t-i) = y_0 + G(z^{-1})(1-z^{-1})u(t) \tag{4.6}$$

With g_i representing the unit step responses of the system at time $t + k = i$ (shown in figure 4.1). The predicted output is than calculated (y_0 can be set to 0 without loss of generality):

$$\hat{y}(t+k|t) = \sum_{i=1}^{N} g_i \Delta u(t+k-i|t) \tag{4.7}$$

The step response method has the same pros and cons as the impulse response method.

Transfer function model. This method makes use of the transfer function concept where the output is given by:

$$A(z^{-1})y(t) = B(z^{-1})u(t) \tag{4.8}$$

with,

$$A(z^{-1}) = 1 + a_1 z^{-1} + a_2 z^{-2} + \ldots + a_{na} z^{-na}$$
$$B(z^{-1}) = b_1 z^{-1} + b_2 z^{-2} + \ldots + b_{nb} z^{-nb}$$

The predicted outputs are then calculated as follows:

$$\hat{y}(t+k|t) = \frac{B(z^{-1})}{A(z^{-1})}u(t+k|t) \tag{4.9}$$

Notation $t+k|t$ specifies the value of the parameter at time $t+k$ calculated at time t. The future outputs are calculated using a dynamic model of the process. The transfer function method is probably the most widely used method discussed and applied to GPC, EPSAC, unified predictive control (UPC) and extended horizon adaptive control (EHAC). Although this method requires prior fundamental knowledge of the process, it is valid for unstable processes.

State space models are most often used in Predictive Functional Control(PFC) and are represented as follows:

$$\begin{aligned} x(t) &= Ax(t-1) + Bu(t-1) \\ y(t) &= Cx(t) \end{aligned}$$

with A,B and C being the system matrices and x the state. The predicted output is given as follows:

$$\begin{aligned} \hat{y}(t+k|t) &= C\hat{x}(t+k|t) \\ &= C[A^k x(t) + \sum_{i=1}^{k} A^{i-1}Bu(t+k-i|t)] \end{aligned} \tag{4.10}$$

If the states are not accessible, an observer should be included which can make the calculations complicated. The advantage of the state space method is that it deals with the multi-variable problems in a straight forward manner. Although the state x does not necessarily have physical meaning, the control is simply the feedback of a linear combination of the state vector.

Other Neural Networks, Fuzzy Logic etc. are forms of non-linear models that can also be used. These do however give rise to more complicated optimisation problems.

4.2 Regulatory Control

4.2.1 Description

A typical industrial plant is controlled in a hierarchical structure divided into the supervisory/advanced control layer and the regulatory/base control layer (Skogestad and Postlethwaite, 2005). The supervisory layer contains the optimisation algorithm that provides a setpoint (SP) to the regulatory control which is then tasked to have the process variable (PV) track this value by actuating a control output (OP). The proportional-integral-derivative PID is the most commonly used regulatory control algorithm in industry since its inception in 1940 (Luyben, 1990; Marlin, 2000). Regulatory control is discussed in more detail in appendix A..

4.3 Fuzzy Logic/Expert System Control

4.3.1 Description

Fuzzy logic was introduced in the 1960's by Lofti Zadeh as a way to translate non-statistical, linguistic statements into precise mathematical language (v Lith, 2002; Johnston, 1998; Scheffer, 2001). The objective of this technology is to distill and translate the human operator's experience into deterministic control rules. The fuzzy logic method provides a framework for the characterisation and capture of human expert knowledge and decision making. The controller consists of a sequence of statements that connect a set of process beliefs to a crisp control action. The process beliefs are called the antecedent while the action is known as the consequent. The statements that connect them are rules usually of the form IF-THEN, for example,

IF Mill-load is High **AND** Mill-power is Low **THEN** Increase Water Ratio

Fuzzy-logic control is not the main focus of this thesis, but as the algorithm is currently being used on the primary mill in question, a more detailed description of this algorithm is available in appendix A.

4.4 Model Predictive Control

4.4.1 Description

Model Predictive Control (MPC) represents a range of control algorithms that utilise a model of the process to implement a control signal in order to minimise an objective function (Camacho and Bordons, 2007). MPC was developed in the late seventies and has expanded considerably with various applications in the process industry and other

industries like robotics and clinical anaesthesia. MPC on these applications reported high efficiency and utilisation with long periods without operator intervention.

Algorithms belonging to the MPC family are characterised by a strategy of predicting future process outputs by means of past and future inputs (or control signals). This strategy is presented in figure 4.2:

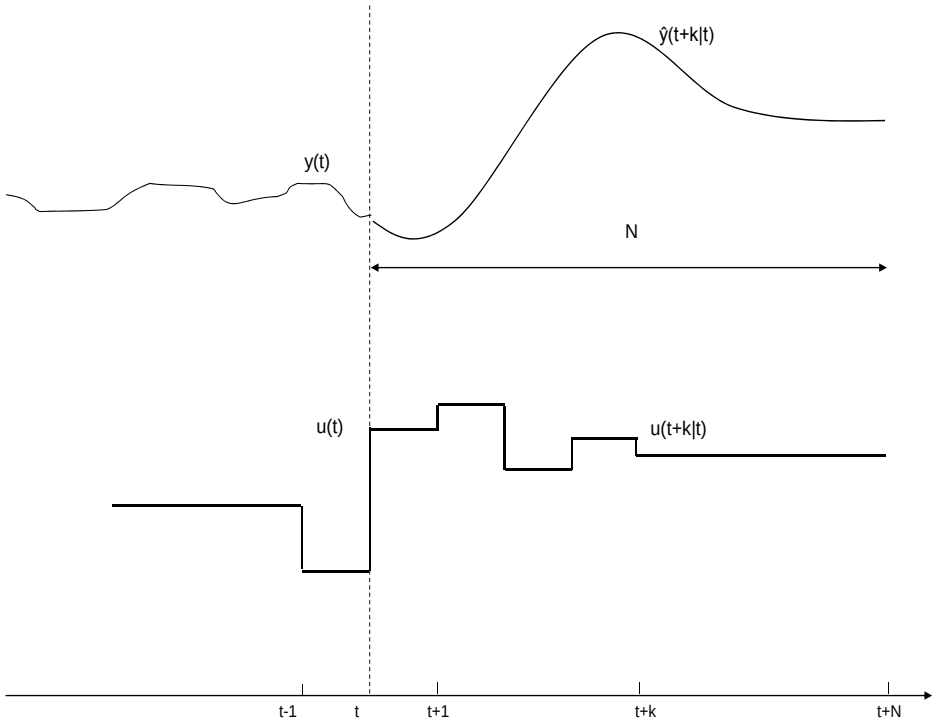

Figure 4.2: The Model Predictive Control strategy

The nomenclature in figure 4.2 are explained as follows:

1. The predicted future outputs $\hat{y}(t+k|t)$ from time t until the end of the prediction horizon are calculated at time t based on past inputs $u(t-i)$ as well as future control signals $u(t+k|t)\ k = 0 \ldots N-1$.

2. The predicted future outputs are calculated by optimising a criterion or objective function in order to minimise the error between the process variable and a reference trajectory $\omega(t+k)$. An explicit solution can be obtained if this criterion is quadratic, the model is linear and no constraints are imposed, otherwise an iterative optimisation method has to be used.

3. Only the calculated control signal $u(t|t)$ is applied to the process while all subsequent $u(t+k|t), k \neq 0$ gets rejected. Step 1 is thus repeated at the next sampling instant $t+1$ with the newly implemented control signal. It is important to note that at the

control signal at the next sampling instance $u(t+1|t+1)$ will differ from $u(t+1|t)$ due to new available information that will include unmeasured disturbances and model error ($\hat{y}(t+1|t) \neq y_m(t+1)$)[1].

Three elements that are common to all model predictive algorithms are:

Prediction Model The success of an MPC lies with its model which presents the cornerstone of this control method (Seborg *et al.*, 2004; Camacho and Bordons, 2007). The model should include the dynamic behaviour of the process and be accurate enough to permit future prediction and theoretical analysis. Process behaviour that is not reflected in the models is referred to as unmeasured disturbances or model error. These disturbances (or error) can also be included in the algorithm as a disturbance model. MPC utilises every possible form of modelling to describe the future movements of the process. Examples of these modelling techniques are discussed in section 4.1.2.

Objective Function The aim of the objective function is to ensure that the future prediction $\hat{y}$ remains as close to a reference trajectory ω within the allocated horizon N, while at the same time penalising control movement $\Delta u(t)$. The objective function expression follows:

$$J(N_1, N_2, N_u) = \sum_{j=N_1}^{N_2} \delta(j)[\hat{y}(t+j|t) - \omega(t+j)]^2 + \sum_{j=1}^{N_u} \lambda(j)[\Delta u(t+j-1)]^2 \quad (4.11)$$

with coefficients δ and λ representing the weights that dictate the importance of future behaviour. These coefficients are usually constants but can also be presented as an exponential $\delta(j) = \alpha^{N_2-j}$. This enables the controller to weight errors further from t more if $0 < \alpha < 1$ and errors closer to t if $\alpha > 1$. Parameters N_1, N_2 and N_u are the minimum and maximum prediction horizons and the control horizon respectively (control horizon explained below). N_1 and N_2 are chosen intuitively to mark the range in which the future prediction should follow the reference. A higher N_1 indicates that errors in the first instances are of little importance. Note that N_1 is usually chosen greater that the system's dead-time d since the controller will not be able to affect the process before $t + d$.

The fact that the *reference trajectory* or future movement of the outputs are known in predictive control grants this technology an advantage in avoiding undesirable process responses and negate the effect of process delay. The reference trajectory $\omega(t+k)$ is mostly used to determine a smooth path that the process can follow

[1] y_m indicates the actual measured process parameter

towards the known reference $r(t+k)$.

$$w(t+k) = \alpha\omega(t+k-1) + (1-\alpha)r(t+k) \qquad k = 1 \ldots N \tag{4.12}$$

For systems with variable setpoints:

$$\omega(t+k) = r(t+k) - \alpha^k(y(t) - r(t)) \tag{4.13}$$

Constraints are imposed on all physical processes due to a number of reasons ranging from physical, engineering to environmental. These constraints usually add a degree of complexity to the minimisation of the objective function. Constraints are considered as follows:

$$\begin{aligned} u_{min} \leq \quad & u(t) \leq u_{max} \quad \forall t \\ du_{min} \leq \quad & u(t) - u(t-1) \leq du_{max} \quad \forall t \\ y_{min} \leq \quad & y(t) \leq y_{max} \quad \forall t \end{aligned} \tag{4.14}$$

Obtaining the Control Law The entire MPC algorithm is based on the selection of future inputs $u(t+k|t)$ in order to minimise an objection function [4.11]. If no analytical solution can be obtained as is generally the case due to constraints being present, an iterative method of optimisation is used. Iterative methods are usually very complex and resource intensive as the solution contains $N_2 - N_1 + 1$ independent solutions. The methodology or structure followed to reduce the amount of degrees of freedom is called the control law. The control law is normally structured to improve robustness and performance by disallowing the free evolution of the control signal which would result in undesirable high frequency control movement that can lead to instability. One such law implemented by most MPC methods is the concept of a control horizon $N_u < N_2$. The control horizon presents a future instance after which zero control movements are allowed $\Delta u(t+j-1) = 0 \quad \forall j > N_u$. Representing the control signals as a linear combination of a certain predetermined base function is another example of the control law:

$$u(t+k) + \sum_{i=1} n\mu_i(t)B_i(k) \tag{4.15}$$

with B usually chosen according to the nature of the process; $B_0 = 1 \quad B_1 = k \quad B_2 = k^2$

4.4.2 Dynamic Matrix Control

One of the most commonly used MPC methods is the Dynamic Matrix Controller DMC (Camacho and Bordons, 2007). DMC was developed by Cutler and Ramaker of the Shell Oil Company in the late seventies and has since been accepted in various industries and applications. For an asymptotically stable system, the Single-Input Single-Output SISO system can be computed along the prediction horizon $(k+1,\ldots,p)$, for m number of control actions (m representing the control horizon).

$$\hat{y}(t+p|t) = \sum_{i=p-m+1}^{p} g_i \Delta u(t+p-i) + f(t+p) \tag{4.16}$$

where f is the system's response that is not dependant on the future control actions, also known as the free response of the system, given by:

$$f(t+k) = y_m(t) + \sum_{i=1}^{\infty} (g_{k+i} - g_i)\Delta u(t-i) \tag{4.17}$$

If a dynamic matrix $\mathbf{G}$ can be defined by the response coefficient g_i,

$$\mathbf{G} = \begin{bmatrix} g_1 & 0 & \ldots & 0 \\ g_2 & g_1 & \ldots & 0 \\ \vdots & \vdots & \ddots & \vdots \\ g_m & gm-1 & \ldots & g1 \\ \vdots & \vdots & \ddots & \vdots \\ g_p & g_{p-1} & \cdots & g_{p-m+1} \end{bmatrix} \tag{4.18}$$

the predicted output can be calculated as follows:

$$\hat{\mathbf{y}} = \mathbf{G}\mathbf{u} + \mathbf{f} \tag{4.19}$$

where $\hat{\mathbf{y}}$ is a vector of future system responses, $\mathbf{G}_{pxm}$ represents the response matrix with p rows (prediction horizon) and m columns (control horizon), $\mathbf{u}$ the calculated future control signal and the free response of the system $\mathbf{f}$.

4.4.3 Multi-Variable DMC

Equation 4.19 can easily be extended for the multi-variable problem by expanding the response matrix,

$$\mathbf{G} = \begin{bmatrix} G_{11} & G_{12} & \dots & G_{1n_u} \\ G_{21} & G_{22} & \dots & 0 \\ \vdots & \vdots & \ddots & \vdots \\ G_{n_y1} & G_{n_y2} & \dots & G_{n_yn_u} \end{bmatrix} \tag{4.20}$$

where $G_{n_yn_u}$ represents the coefficient matrix given in [4.18] for output n_y. The prediction, output and free response vectors then become:

$$\hat{\mathbf{y}} = [\overbrace{y_1(t+1|t), \dots, y_1(t+p_1|t)}^{\text{first output } y_1}, \dots, \overbrace{y_{n_y}(t+1|t), \dots, y_{n_y}(t+p_{n_y}|t)}^{\text{last output } y_{n_y}}]^T \tag{4.21}$$

$$\mathbf{u} = [\overbrace{\Delta u_1(t), \dots, \Delta u_1(t+m_1-1)}^{\text{first input } u_1}, \dots, \overbrace{\Delta u_{n_u}(t), \dots, \Delta u_{n_u}(t+m_{n_u}-1)}^{\text{last input } u_{n_u}}]^T \tag{4.22}$$

$$\mathbf{f} = [\overbrace{f_1(t+1|t), \dots, f_1(t+p_1|t)}^{\text{free response } f_1}, \dots, \overbrace{f_{n_y}(t+1|t), \dots, f_{n_y}(t+p_{n_y}|t)}^{\text{last free response } f_{n_y}}]^T \tag{4.23}$$

4.4.4 Control Law for DMCplus^{TM}

The solution of the QP in equation 4.11 is computationally intensive and difficult to ensure feasibility before solving. In an attempt to industrialise the algorithm, AspenTech developed a staged procedure where feasibility is ensured upfront (possibly by relaxing constraints). This enables an analytic solution of the MV trajectory. This four staged procedure is explained as follows with each cycle abiding to the routine (AspenTech, 2000) course notes:

Open Loop Prediction

The open-loop prediction or free response of the system can be extended as the sum of four effects; $\mathbf{f}_u$ the response of the system due to past control movement, $\mathbf{Dd} + \mathbf{f}_d$ the response to known disturbances and $\mathbf{f}_n$ unmeasured system disturbances or model error.

$$\mathbf{f} = \mathbf{f}_u + \mathbf{Dd} + \mathbf{f}_d + \mathbf{f}_n \tag{4.24}$$

Obtaining a Feasible Solution

The next step in the DMCplus^{TM} control law is to determine whether a feasible solution is possible for any combination of inputs. A feasible solution is possible when the allowed MV movement within the MV constraints can bring all the CVs within limits, see equation 4.14 (figure 4.3). If no solution is available, the algorithm will relax its CV limits as follows:

1. CVs are ranked in order of importance with the lower value rank indicating the highest importance. The limits of variables with a higher rank value will be relaxed in order of importance until a feasible solution is established

2. The limits of CVs with the same rank will be relaxed according to a predetermined steady-state equal-concern-error SS-ECE using either a QP or a LP

As soon as a solution is available, the algorithm proceeds to the next step with an updated set of CV limits required for a feasible solution.

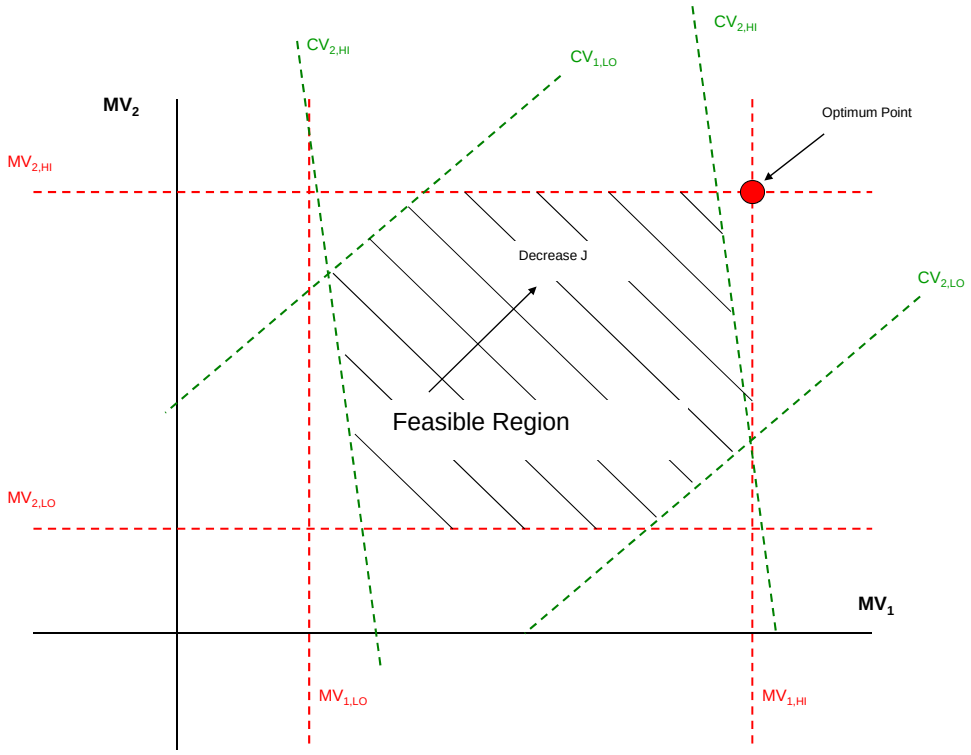

Figure 4.3: Graphical representation of the feasible region defined by MV and CV constraints

Steady-State Optimisation

The aim of optimisation is to minimise the objective function for a given system within the allowable process constraints (Snyman, 2005). The mathematical form of this constrained problem is given as follows:

$$\min f(x), \quad x = [x_1, x_2, \ldots, x_n]^T \in \mathbf{R} \tag{4.25}$$

Subject to constraints usually of the form:

$$g_j(x) \leq 0, \qquad j = 1, 2, \ldots, m$$
$$h_j(x) = 0, \qquad j = 1, 2, \ldots, r$$

The AspenTech framework (DMCplus^{TM}) allows for the usage of either linear or quadratic programming (AspenTech DMCplus^{TM} course notes):

- *Linear Programming* A special case of general optimisation arises when both the objective function and the constraints are linear functions (Snyman, 2005). Such an instance is called linear programming, stated in the following form:

$$\begin{aligned} &\min_x f(x) = \mathbf{c^T x} \\ &\textit{such that}, \\ &\mathbf{Ax} \leq \mathbf{b} \end{aligned} \tag{4.26}$$

  Within DMCplus^{TM} the vector $\mathbf{c}$ in equation 4.26 is an n-vector containing the steady-state cost parameter $SSCost$ allocated to each manipulated variable. The $SSCost$ vector represents the direction of minimising the linear programming objective function. Δu_{ss} represents the steady state MV step conducive to the lowest J:

$$\min J = \sum_{i=1} n(SSCost_i \times \Delta u_{ss}) \tag{4.27}$$

- *Quadratic Programming* The objective function is defined as a positive-definite quadratic function subject to these linear constraints (Snyman, 2005). The minimisation function in DMCplus^{TM} is given by:

$$\min J = (\sum_{i=1} n(SSCost_i \times \Delta u_{ss}) - Maximum\ Profit)^2 \tag{4.28}$$

  Maximum defined as the point on a plane only subject to MV constraints (represented as "Optimum Point" in figure 4.3)

Future MV movement

The next step in the DMC control law is to calculate the future input movement in order to get the outputs to the steady-state end values.

1. *Minimise CV Error*
   CV error e in this instance is defined as the difference between the open loop response

and the steady state value (or SP). MV movement to achieve minimum CV error is given as:

$$\Delta u = [G^T G]^{-1} G^T e \tag{4.29}$$

with vector e being defined similarly to equations [4.21] - [4.23].

2. *Minimise MV movement*
   Minimising CV error in the most aggressive manner might provide the best control solution. Model error, circuit constraints etc. can however, induce cycling and other unwanted control effects if aggressive MV movement is allowed. An MV movement suppression parameter K is added to equation 4.29 where:

$$K \cdot \Delta u = 0 \tag{4.30}$$

   The components in equation 4.29 changes as a result of MV minimisation (equation 4.30) to:

$$\mathbf{G}' = \begin{bmatrix} G \\ KI \end{bmatrix} \tag{4.31}$$

3. *CV Importance*
   To distinguish between the importance of various CVs, a weight W_i is assigned to the error of each CV.

$$\Delta u = [G'^T G']^{-1} G'^T e W \tag{4.32}$$

Note that only the first step at $t = 0$ is implemented at the end of each control cycle.

4.4.5 Advantages

1. Most of the MPC methods require limited process knowledge as the concepts are rather intuitive
2. Tuning is relatively easy
3. MPC deals effectively with complex dynamics, non-minimum and unstable phases plus it compensates intrinsically with dead-time
4. MPC adapts easily to the multi-variable environment
5. Feed-forward control can be used to effectively reject measured disturbances
6. Process constraints are treated in a conceptually simple manner
7. Knowing the future movement of the process provides a very useful optimisation tool.

4.4.6 Disadvantages

1. The control law can be computationally intensive
2. Most MPCs assume linearity, which can result in model error and hence incorrect control movement
3. Although constraint handling is effective it does impose further computational weight
4. Acquiring the process model (other than a fundamental model) can be difficult and unsettling to the process
5. Discrepancies between the process and the model, present in most industrial plants, will affect the controllability

CHAPTER 5

Economics

5.1 Project Framework

The importance of justifying the cost associated with advanced control implementations in terms of the financial benefit is found throughout the literature (Hodouin *et al.*, 2001; Bauer and Craig, 2008; Wei and Craig, 2009b). Bauer and Craig (2008) devised a framework for the successful and continued economic evaluation of control implementations for the duration of a project. The framework is grouped into three main segments each representing the various life cycles of the project (figure 5.1):

1. Estimation of both the cost and benefits of the control project *prior to implementation*. During this phase of the project the base-case review of the current control system is identified by means of analysing historical plant data. During this analysis it is important to identify critical product qualities, manipulated variables, possible constraints and most important a steady-state economic model. From the base-case identification the choice of an APC system follows and consequently, an initial economic benefit can be derived.

2. Economic assessment *after implementation* of the control system. Comparing two control systems is more complex since process and equipment conditions change continually. These changes include raw material characteristics, sensor drift, equipment wear etc. Improved confidence in the comparison can be achieved by switching between the two controllers (if the old system is still available). The method is explained in more detail in section 5.1.1.

3. Continued system maintenance subsequent to the project can ultimately lead to the success or failure of the controller. Bauer and Craig (2008) mentions that the performance of almost all control solutions will deteriorate if left unsupervised.

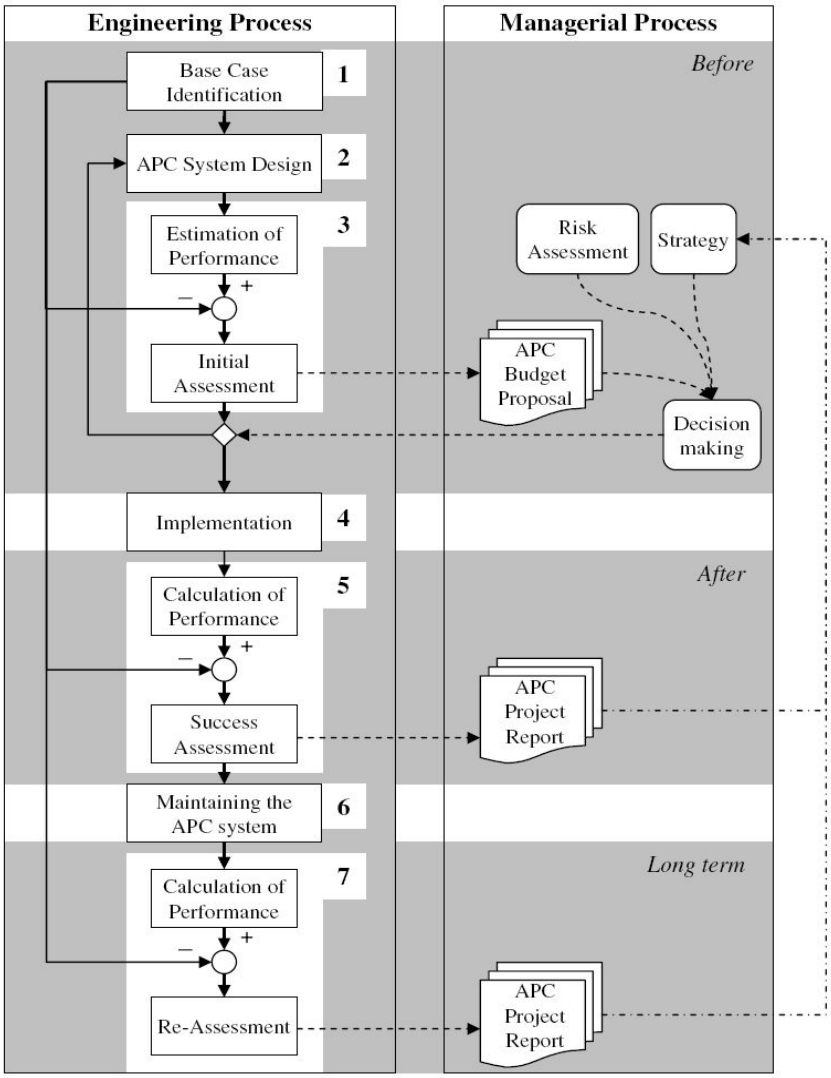

Figure 5.1: Project framework as suggested by Bauer and Craig (2008)

5.1.1 Experimental Design

Hulbert (2002) and Craig and Koch (2003) describes the experimental method by which to objectively measure the benefits of a control system in order to obtain results that are statistically significant and correct. The method is divided into four tasks:

Eliminating external effects Hulbert warns that evaluating the performance before and after controller implementation, although popular, can be misleading. Changing conditions external to the experiment are cited and can have an indeterminate effect on the results. Examples of such factors;

- Calibration of process instruments
- Unaccounted equipment and utility wear, for example, mill liners, ball charge reduction
- Unmeasured changes to raw materials feeding the system, for example, ore hardness, mineralogical disturbances
- Upstream process changes can also lead to biased results

The key in negating external factors is to switch between the test participants in relatively short periods over a longer period of time. In doing so, the effects of slower external factors are spread out more evenly across the test. These short test units should span at least one cycle of periodic external effects and should be longer than the characteristic response of the plant. A good experimental strategy is to alternate between tests α and β of the same duration in a manner $\alpha\beta\alpha\beta\alpha\beta$. The ideal length of the test units will be about one to three days for the milling circuit alone but extended to about a week if the downstream process is included in the test. Using the nominal average of successive pairs $\alpha\beta$ will ensure that long-term bias is removed. A two sided t-test is recommended in order to confirm a statistically significant difference between the two test modes $\alpha\beta$.

Reference conditions It is inadvisable to use the conditions prior to the control system installation as the "normal" or reference scenario when trying to obtain control system benefits. Due to changing conditions within the control architecture such as renewed base-layer control tuning, a more optimised operation is achieved during controller commissioning. The most commonly used reference condition is to run the old control system with the new improvements as the auxiliary control. Another reference condition is to run the new controller at various strategies. This method is often used in optimisation test work because various well defined operating conditions can be tested. Hulbert (2002) also mentions that using a parallel unit as a reference is not recommended due to the many individual characteristic differences, for example, bias in the feedstock is likely to occur.

Sampling and measurement Accurate measurement and representative sampling are of great importance in comparative testing. Calibration of instruments should be done beforehand and never during a test. It is also advised to refrain from using hand sampling methods during a test due to the bias that human conduct introduces.

Accounting for human intervention Hulbert (2002) advises to take cognisance of the human intervention effect on the test. Ulterior motives or ignorance can lead to major bias in the results.

5.2 Economic Performance

Hulbert (2002) states that the economic benefit that control solutions introduce to milling circuits is not satisfactorily quantified. This statement was confirmed in an industrial survey conducted by Wei and Craig (2009a), where almost half of the respondents declared that they were not satisfied with the economic analysis techniques used during the implementation of a grinding circuit control system. The difficulty in relating the key performance variables in a milling circuit to the economic consequence of the overall metallurgical plant is often cited as the reason for this project shortcoming (Sosa-Blanco *et al.*, 2000; Hodouin *et al.*, 2001). In addition to this, the determination of the financial benefits that a milling circuit has on the overall operation is also described as difficult since no concentration of the valuable mineral is achieved (Hodouin *et al.*, 2001; Wei and Craig, 2009b). Not only is the financial benefit associated with milling of importance, but also the impact that inadequate milling may have on the downstream recovery and product quality (Hulbert, 2002).

The economic benefit of milling circuits is therefore usually expressed in the form of particle size reduction or mineral liberation. Distinguishing between grinding and flotation as separate units that are optimised individually can however lead to sub-optimal overall plant performance (Wei and Craig, 2009a). Sosa-Blanco *et al.* (2000) states that the reason for this lack in performance is that such an approach neglects the interaction between the various units that are usually closely correlated. The true economic benefit to the operation due to the milling circuit performance should therefore be evaluated in the downstream process, that is, recovery benefit seen on the flotation circuit. Hodouin *et al.* (2001) confirms this by stating that the fundamental objective of comminution circuits is the liberation of valuable minerals (not just size reduction) in such a way that succeeding processes can operate at maximum efficiency.

5.2.1 Global Economic Performance

The concept of optimising a profitability function that will marry grinding and flotation by relating profit, recovery, tonnage and grind was initially proposed by Bascur (1991)

where the total profit TP ($ per ton) of the entire metallurgical operation is estimated by a performance criterion of the form:

$$TP = \sum \text{Valuable}_i \cdot \text{Sales}_i - \text{Variable Costs} - \text{Fixed Costs} \tag{5.1}$$

Sosa-Blanco *et al.* (2000) expanded this performance criterion by using the smelter return per ton of ore R_o and defining a global performance index for a plant in terms of the net revenue per unit time R:

$$R = FR_o - C_{Mn} - C_{Ml} \tag{5.2}$$

The parameters C_{Mn} and C_{Ml} in equation 5.2 represent the costs per unit time associated with mining and milling respectively. These cost are further separated into fixed costs C_{Fi} (capital etc.) and variable costs C_{Vi} (utilities) that normally vary with the feed F to the system.

Since precious metal smelters rarely treat ore, the net smelter return per ton of *concentrate* R_c is substituted into equation 5.2 by making use of the mass pull ρ of the circuit.

$$R_o = R_c\rho \tag{5.3}$$

Sosa-Blanco *et al.* (2000) continues by expanding on R_c in terms of the payment for the metal per ton of concentrate υ and cost associated with its treatment post mining and milling. These costs include transportation C_T, smelting C_S, refining cost per individual metal $\sum C_{Ri}$ and penalties associated with metal i impurities $\sum P_i$ (all costs relative to a ton of concentrate).

$$R_c = \sum \upsilon_i - C_T - C_S - \sum C_{Ri} - \sum P_i \tag{5.4}$$

If the costs are assumed to be constant within the nominal operating range of the process then $\sum \upsilon_i = \sum \alpha_i C c_i$ becomes the dominant term in $FR_c\rho$ and hence in equation 5.2. The variables α_i refer to the price of metal i and c_i the concentration of metal i in concentrate stream C.

It is obvious to see that the R_c is maximised by increasing metal recoveries (more C) while maintaining the grade c_i at a level as not to incur penalties, achieving metallurgical efficiency while moving along the optimum grade-recovery curve. Such an economic strategy of maximising the concentrator's net revenue while maintaining the product quality defined by the buyer-seller agreement is illustrated by Hodouin *et al.* (2001) in figure 5.2.

It can however be that maximum economic benefit is achieved when capacity is increased while accepting a decrease in recovery and/or grade and a possible loss of

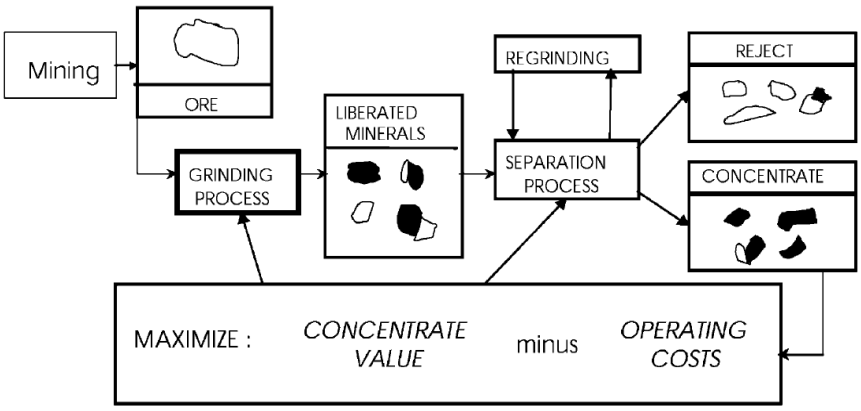

Figure 5.2: A strategy to optimise the economic potential of a milling/flotation concentrator (Hodouin *et al.*, 2001) :996

valuable metals to the process effluent. These strategies often have ethical implications due to resource and environmental conservation. This gives rise to a compromise between economical and metallurgical performances where the latter is often affected negatively by the former. Maximising the net smelter profit per ton of ore as presented in equation 5.2 might not always be acceptable. In order to emphasise metallurgical efficiency, Sosa-Blanco *et al.* (2000) devised a criterion that depicts the operation's ability to exploit the potential value within the feed ore. This operating efficiency E_q is presented as a dimensionless number that characterises the plant's performance in terms of the potential value of the feed:

$$E_q = \frac{FR_c\rho}{(FR_c\rho)_{ref}} \tag{5.5}$$

The denominator in equation 5.5 presents a reference to the ideal plant performance at $F_{ref} = F_{max}$ and $(R_c\rho)_{ref}$ associated with the ideal concentrate.

5.2.2 Performance Functions Method

Wei and Craig (2009b) also state that the objective of any milling circuit is to produce a certain quality product at an acceptable throughput whilst reducing operating costs. The overall economic performance of the circuit Ψ was hence derived as the sum of the economic performance of a series of individual process parameters Ψ_{y_i}:

$$\Psi = \sum \Psi_{y_i} \tag{5.6}$$

The economic performance of each individual parameter is obtained by integrating over the product of the relative parameter's performance function $v(y_i)$ and a probability density function $f(y_i)$, the latter being derived from operating data:

$$\Psi_{y_i} = \int_{-\infty}^{\infty} \upsilon(y_i) f(y_i) dy_i \tag{5.7}$$

The performance functions (PF) of the system form the fundamental basis for comparing the new system to the base-case featuring in steps 1, 5 and 7 of the framework (Bauer and Craig, 2008). Defining the PFs best suited for the system usually requires in depth knowledge of the process since the economic model is usually unique. The most commonly used PFs were determined in the industrial survey by Bauer and Craig (2008) and presented in figure 5.3.

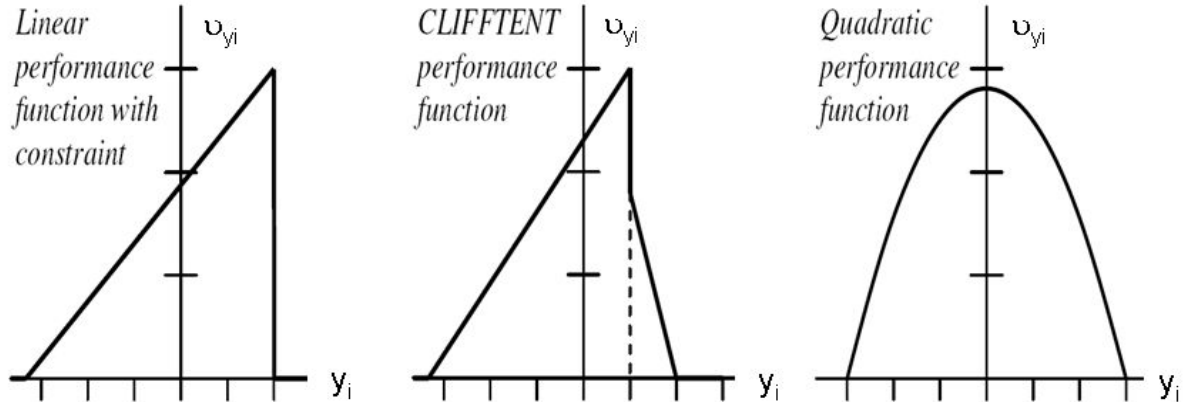

Figure 5.3: Frequently used performance functions: a) linear with constraints, b) CLIFFTENT and c) quadratic (Wei and Craig, 2009b)

The purpose of the PFs is to describe the economic consequence of the relevant parameter in terms of profit ΔP or cost ΔC (Wei and Craig, 2009b). It is therefore vital that the process parameter represented by the PF can be linked to a monetary value and that loss is incurred when it moves away from the optimum. The PFs should also be independent of the control technology and should rather be based on system dynamics, economics and market conditions. The performance function of any individual parameter is therefore mathematically defined in terms of milling $\upsilon_m(y_i)$ and flotation $\upsilon_f(y_i)$ benefit as:

$$\begin{aligned} \upsilon_{y_i} &= \Delta P(y_i) - \Delta C(y_i) \\ &= \Delta P_m(y_i) + \Delta P_f(y_i) - \Delta C_m(y_i) - \Delta C_f(y_i) \end{aligned} \tag{5.8}$$

Wei and Craig (2009b) described the economic evaluation of a milling circuit by defining PFs for the product grind, mill load and the discharge sump level. To achieve this, despite the complex economic relations on a milling circuit, the following assumptions were made:

1. The impact that the various controlled variables have on the economic performance

of the system is assumed to be independent.

2. Mineral recoveries will vary with changes in product grind.

3. A separation unit (flotation) receives the milling product.

4. The operating costs of both milling and flotation will not be affected significantly with the foreseen magnitude of the change in grind and hence the possible recovery benefit.

5. Head-grade and throughput is assumed to be constant over the assessment period.

Product Grind The derivation of a performance function for the mill product relies on the steady state relationship between the product size of the milling section and the recovery of the downstream flotation unit. This link is known as the grind-recovery relationship and arises from two fundamental consistencies (Bascur, 1991; Edwards and Vien, 1999; Sosa-Blanco *et al.*, 2000; Wei and Craig, 2009b):

1. *The consistent recovery vs. the particle size fraction of the flotation feed relation.* This relationship is usually obtained from test work in a metallurgical laboratory where ore samples at different size ranges undergo flotation in order to determine a relationship between recovery and size fraction. It is then possible to devise a recovery to particle size fraction profile which has been found to be highly consistent. The shape of the curve is generally regarded to be independent within reasonable changes in PSD, mineralogy and pulp density to flotation.

2. *The consistency between the PSD of the mineral and the ore PSD of the milling product.* The size distribution of the mineral in all probability falls into the various size fractions described in the test above, recovery vs. mineral PSD can therefore be described. The mineral PSD and ore PSD consistency provides the key to obtaining recovery in terms of the distribution of particles which is often the way that the feed to the flotation circuit is measured. Note that the recovery-PSD relationship is quadratic and remains constant for various minerals in both laboratory tests and industrial applications.

The significance of the recovery-PSD relationship is emphasised by the fact that it describes the economic influence of the milling circuit without any additional analysis of the flotation circuit. The PF for product grind υ_{PSD} is therefore based on a recovery-PSD curve and hence also quadratic, as shown in figure 5.4.

Mill Load Wei and Craig (2009b) describe the PF of the mill load as a piece-wise function (figure 5.5a). This form of PF is based on the assumption that the economic impact

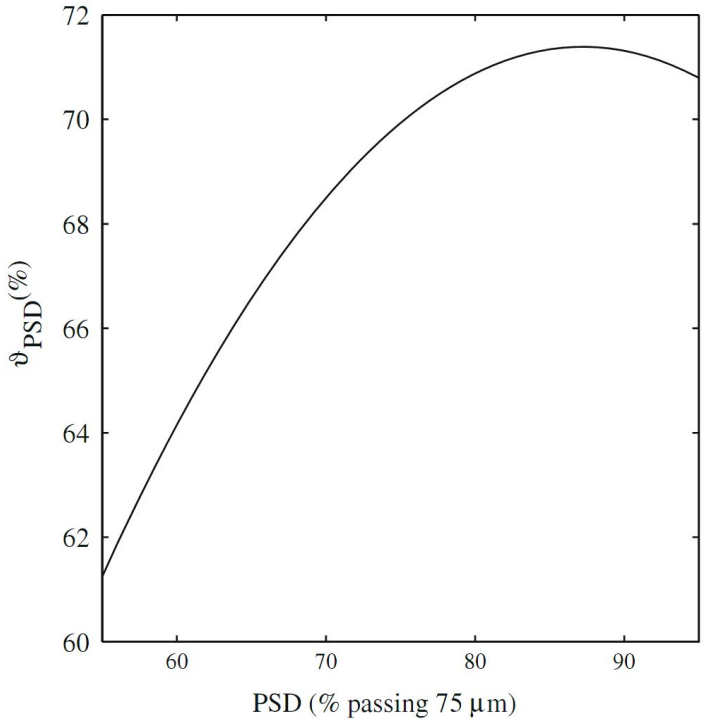

Figure 5.4: A typical product grind PF based on the relationship between recovery and PSD (Wei and Craig, 2009b):830

of the load remains constant as long as it is kept within limits. Exceeding these limits will however impact the process as evasive actions are needed to restore the mill to its usual operating region. Penalties are therefore implemented in the PF when the controller allows the load to violate its limits. The asymmetrical PF for the load is due to the more severe financial impact incurred when the mill is overloaded rather than unloaded.

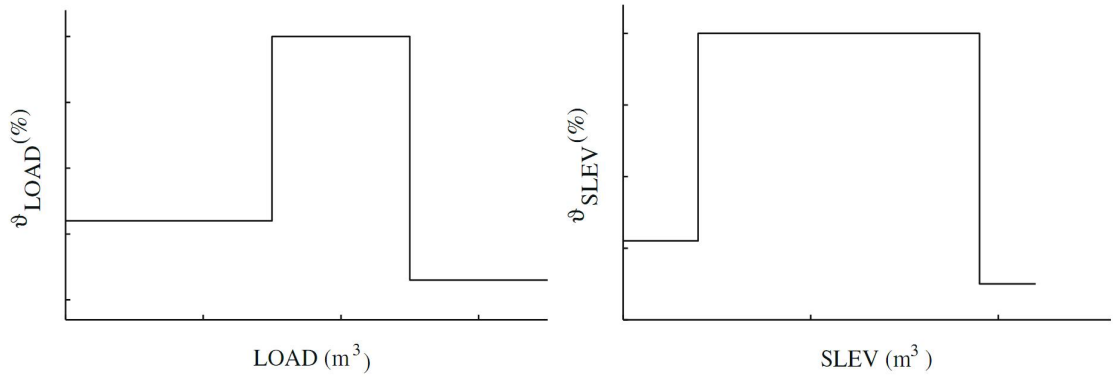

Figure 5.5: The piece-wise performance functions for a)mill load and b)sump level (Wei and Craig, 2009b):831

Sump Level The same argument used for the mill load applies to the discharge sump level as illustrated in figure 5.5b. Economic consequences occur when the sump level defies one of the predetermined limits.

5.3 Stability Metrics

Up to this point, the only economic consequences discussed have been those at steady-state conditions. Since these circuits are seldom operated at steady-state, the transient conditions have a large impact on the downstream processes and hence the controller's economic performance (Hulbert, 2002). Losses of more than 1% in recovery can be imposed on flotation circuits due to its sensitivity to feed fluctuations. Martin *et al.* (1991) presented an estimation of the control benefits by reducing the variability of an output and then shifting the average in a profitable direction. This analysis can be conducted on before control data and assuming similar limit violation for optimum control as was the case before control (see figure 5.6). Reducing process variability can thus improve the economics of a system by moving an output closer to a constraint as well as reducing irreversible losses due to process variation such as mechanical wear (Martin *et al.*, 1991; Hugo, 2003). It is therefore important to first improve milling control in terms of stability before the trade-off between throughput and grind is optimised.

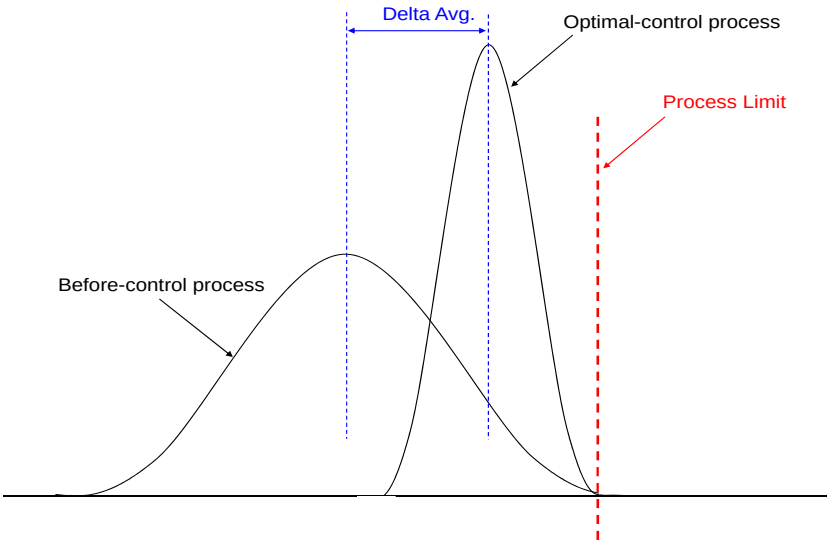

Figure 5.6: Moving the process output closer to a constraint by reducing process variance (Martin *et al.*, 1991)

5.3.1 Minimum Variance

Minimum variance presents the theoretically best achievable variance for any system output (Vishnubhotla *et al.*, 1997). This technique can be used as a benchmark for existing controllers and is estimated from historical closed loop time series data. Vishnubhotla *et al.* (1997) derives the minimum variance for a feedback control system (shown in figure 10.2) as follows:

$$\sigma_{mv}^2 = \left(\varphi_0^2 + \varphi_1^2 + \varphi_2^2 + \ldots + \varphi_{\theta-1}^2\right)\sigma_a^2 \tag{5.9}$$

Where σ_a^2 represents a constant variance of the system's disturbance a_t and θ the process lag. The sequence $(\varphi_0^2 + \ldots + \varphi_{\theta-1}^2)$ is derived as follows:

For a feedback control system (figure 10.2) with process transfer function $G_p = \overline{G}_p.\, q^{-\theta}$, the closed loop relation between the process output y and disturbance a_t is given as:

$$y = \frac{G_d}{1 + q^{-\theta}\overline{G}_p K} \tag{5.10}$$

Using a diophantine identity, the disturbance transfer function G_d can be expanded as follows:

$$G_d = \underbrace{\varphi_0 + \varphi_1 q^{-1} + \varphi_2 q^{-2} + \ldots + \varphi_{\theta-1} q^{-(\theta-1)}}_{\mathrm{F}} + R q^{-\theta} \tag{5.11}$$

R being a proper rational transfer function. Substituting equation 5.11 into equation 5.10, it is possible to reduce y:

$$\begin{aligned} y &= \frac{F + q^{-\theta} R}{1 + q^{-\theta}\overline{G}_p K} a_t \\ &= \left[F + \frac{R - F\overline{G}_p K}{1 + q^{-\theta}\overline{G}_p K} q^{-\theta} \right] a_t \\ &= F a_t + L a_{t-\theta} \end{aligned} \tag{5.12}$$

F is thus independent of controller K and therefore the minimum variance process output (Vishnubhotla *et al.*, 1997). Since G_d (for measured and unmeasured disturbances) and the transfer function R is often unavailable, the φ_i sequence is obtained by replacing y with the output error $\epsilon = y - r$. The minimum variance performance assessment is then carried out with ϵ which can be written as an infinite order moving average:

$$\epsilon = (\varphi_0 + \varphi_1 q^{-1} + \varphi_2 q^{-2} + \ldots + \varphi_{\theta-1} q^{-(\theta-1)} + \varphi_\theta q^{-\theta} + \ldots) a_t \tag{5.13}$$

The closed loop response of a minimum variance controller can thus be determined using only the closed-loop data and the process dead-time (Hugo, 2003; Vishnubhotla *et al.*, 1997). A minimum variance performance index for the controller can then be defined as the ratio between the minimum variance and the actual process error:

$$\eta \triangle \frac{\sigma_{mv}^2}{\sigma_\epsilon^2} \tag{5.14}$$

In the multi-variable optimisation problem, the setpoint of a particular process variable is often the output of the controller (as opposed to the actuator in the SISO case). Establishing ϵ and hence the minimum variance criterion is often unachievable. Hugo (2003) suggested that in the constrained optimisation problem for linear multi-variable

systems, the difference between the output's current setpoint and its optimum constraint should be used as ϵ. Note that the controller will probably not display acceptable control if any of its inputs are saturated.

The main disadvantages of the minimum variance benchmarking are (Hugo, 2003):

1. It is important to note that targeting the minimum variance benchmark may not necessarily represent optimal control. Minimum variance control is often associated with excessive input movement and poor robustness properties

2. Perfect process and disturbance models, which are often unachievable in industry are required

3. The minimum variance performance index presents an often unachievable high standard

5.3.2 Spectral Density

The analysis of stability and process performance within the time domain is usually considered to be the norm (Vishnubhotla *et al.*, 1997). Analysis in the frequency domain however, is analogous to the time domain and provides additional insights into the process parameters (Fourier transforms discussed in Appendix A). Spectral analysis of a signal can detect periodicities which may otherwise remain undetected in the time domain due to noise. The spectral density of a signal describes how much of a sinusoidal wave, in terms of its amplitude, is present per unit of bandwidth (Smith, 2002). The reasons why spectral analysis is so important in the study of random stochastic processes are (Priestley, 1971; Smith, 2002):

1. An immediate interpretation of the power-frequency spectrum is provided

2. Statistical information of stochastic processes is provided by the spectrum

3. The spectrum of a system can be described using a fairly small sample record and simple digital techniques

Optimal Control The same minimum variance criterion discussed for the time domain can be extended to the frequency domain as a performance metric (Vishnubhotla *et al.*, 1997). This is realised by comparing the power spectral density of the minimum variance output $\Phi_{mv}(\omega)$ to the actual achieved output spectrum $\Phi_y(\omega)$. If the closed loop output can be represented as an infinite order moving average series:

$$y = [1 + \varphi_1 q^{-1} + \ldots + \varphi_{\theta-1} q^{-(\theta-1)} + \ldots]a_t = G_y(q^{-1})a_t \tag{5.15}$$

If the process lag θ is known, the minimum variance output consists of the first $\theta - 1$ terms in equation 5.15:

$$y_{mv} = [1 + \varphi_1 q^{-1} + \ldots + \varphi_{\theta-1} q^{-(\theta-1)}]a_t = G_{mv}(q^{-1})a_t \tag{5.16}$$

The power spectrum of the outputs is then given as:

$$\Phi_y(\omega) = |G_y(\omega)|^2 \sigma_a^2 \tag{5.17}$$

$$\Phi_{mv}(\omega) = |G_{mv}(\omega)|^2 \sigma_a^2 \tag{5.18}$$

Integrating the power spectrum across the entire range $[-\pi, \pi]$ presents the variance of the signal:

$$\sigma_i^2 = \int_{-\pi}^{\pi} \Phi_i(\omega) d\omega \tag{5.19}$$

The difference between the actual output and the minimum variance output is thus the difference between the areas under the power spectral curves.

$$\sigma_{mv}^2 \leq \sigma_y^2 \quad OR \quad (\sigma_{mv}^2 - \sigma_y^2) \leq 0 \tag{5.20}$$

It is important to note that the actual output spectrum can be less at some frequencies. The total area under the actual output spectrum curve however must always remain more than the minimum variance spectrum. This means that if the actual output spectrum is less at certain frequencies, it should be substantially more at other frequencies. In optimal control this is known as the water bed effect (Vishnubhotla *et al.*, 1997; Skogestad and Postlethwaite, 2005). As mentioned before, minimum variance control usually induces excessive input movement and can also lead to poor robustness. Instead of a minimum variance criterion, a desired closed loop spectrum based on the system's needs at various frequencies can be specified.

Part II

Application

CHAPTER 6

Circuit Benchmark

6.1 Process Description

Rustenburg Platinum Mines Amandelbult UG2 No.2 (RPMA2) is one of Anglo American Platinum's mineral ore processing plants situated in the North West province of South Africa. The plant targets an ore throughput of 210 kton/month at a PGM head-grade of about 3 g/t. Ore from the mine undergoes one stage of top size reduction in a primary jaw-crusher before it is classified by a 100 mm grizzly screen and conveyed to the fines and coarse ore silos. The fine and coarse ore are fed to a 6.1 m ϕ × 8.5 m effective grinding length (EGL) primary mill that operates fully autogenous (see figure 6.1). The circuit is operated in a closed loop with a horizontal vibrating screen fitted with 630 μm polyurethane classification panels. The oversize from the screen is recycled to the feed of the mill while the undersize particles are gravity fed to an agitated 200 m^3 flotation feed surge vessel (rougher feed tank). The mill discharges directly on another vibrating screen that removes the critical size material (scats ∼25 mm particles) from the circuit. This stream serves as the circuit's bleed stream.

The primary mill is fitted with two bearing lubrication recirculation pumps that feed the trunnion and pinion bearings. The lubrication oil temperature is regulated by means of a heating coil and cooling fans.

Once the ore enters the mill, the main transport media for the comminution circuit is water. Water enters the system at the mill inlet, the mill discharge sump and the rougher feed vessel. The circuit was also designed with two continuous spillage streams that make up part of the dilution water supply to both the mill discharge and rougher feed vessels. Additional dilution water is added to the satellite spillage sumps (408-TK-01 and 408-SU-28) whenever spillage is not available.

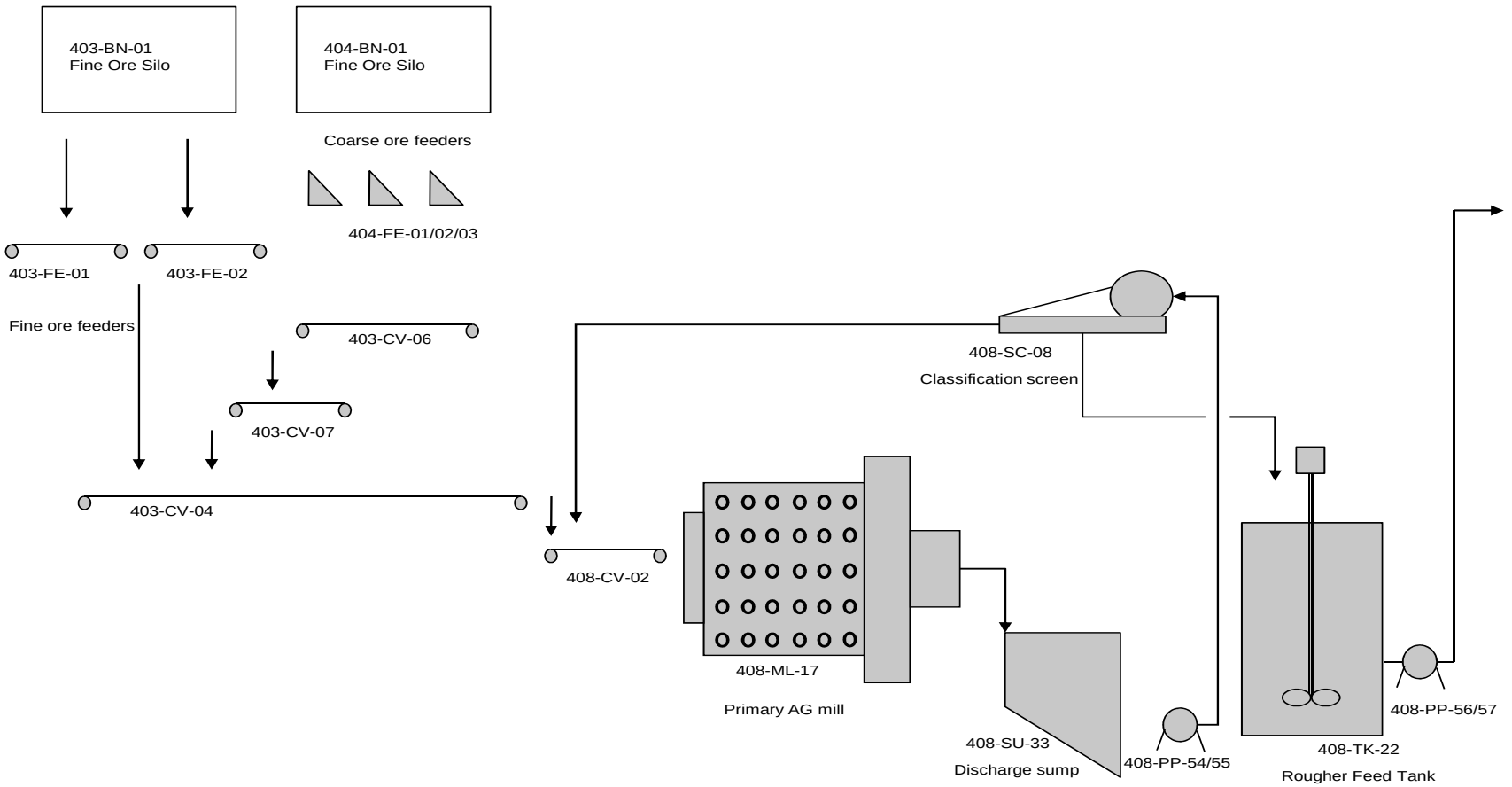

Figure 6.1: The RPMA2 primary milling process flow diagram (RPMA2 Control Narrative 2008)

6.2 Control Infrastructure

Anglo American Platinum follows a two tiered approach when controlling its primary mills. It consists of an in-house developed supervisory advanced control system called the multi-component controller (MCC) which is tightly integrated into the base layer control schema (Steyn *et al.*, 2010), see figure 6.2. The supervisory system is a Fuzzy-logic Rules based control system that runs on the Anglo Platinum Expert Toolkit (APET) that was developed in the Gensym (G2) environment. APET not only runs the advanced layer engine but it also monitors and represents the base-layer PID environment.

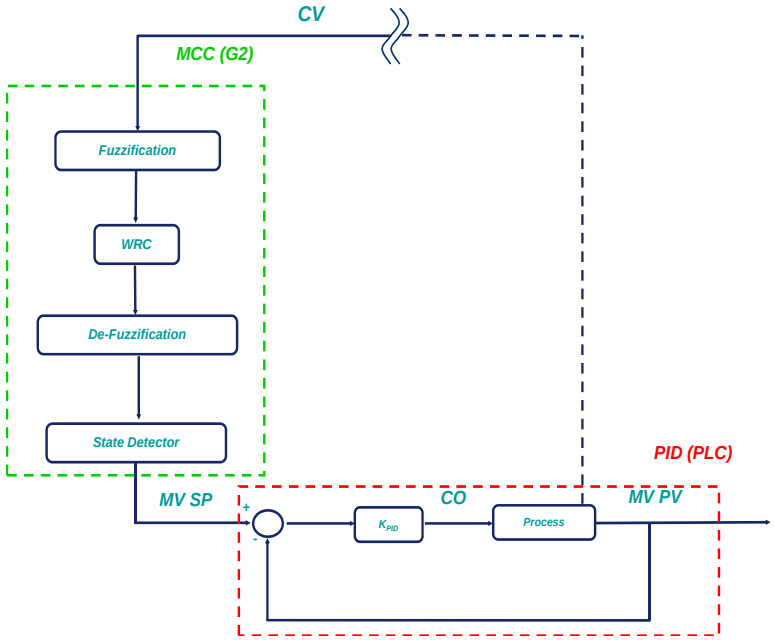

Figure 6.2: Anglo Platinum's primary milling control infrastructure (Steyn *et al.*, 2010)

6.2.1 Base Layer

The base-layer control of the circuit is situated on the PLC domain which accounts for the PID control algorithms, interlocks and sequences (Steyn *et al.*, 2010). To control the mill from the foundation layer (with circuit boundary before the rougher feed tank) the operator needs to provide four setpoints via the human-machine interface (HMI) for the following variables (use figure 6.3 as reference):

Total ore feed-rate Controlled by a PID controller that cascades down to a coarse ore ratio controller. The total ore process variable PV is obtained from a weightometer situated on the combined ore (fine + coarse) feed belt.

Coarse ore ratio The HMI SP is received by the coarse ratio controller mentioned above. The coarse ore ratio variable is the ratio of coarse ore mass flow to total amount of raw ore mass flow that enters the mill (excluding the recycle ore). This ratio controller cascades to two ore feed rate PID controllers; one for coarse ore and the other for fine ore. Both of these PID controllers receive their PVs from weightometers situated on the coarse and fine ore feed conveyor belts and actuate the respective ore feeders.

Inlet water ratio The PV of this controller is the calculated ratio of inlet water flow to total raw ore fed to the mill. The SP is assigned to a ratio controller that cascades down to a flow PID controller that actuates the inlet water auto valve.

Discharge sump level The SP is received by two level PID controllers that cascade down to the discharge slurry flow PID and the dilution water flow PID. These inner loop PID controllers than cascade to a variable speed drive VSD pump and modulating auto water valve respectively. The process variable is obtained from a level probe situated on the discharge sump. Note that the level PID that cascades to the dilution water does not take part in active level control but only serves as pump protection, hence receiving a $SP = \text{HMI-SP} - DB$ with $DB < \text{HMI-SP} - \text{Low}$.

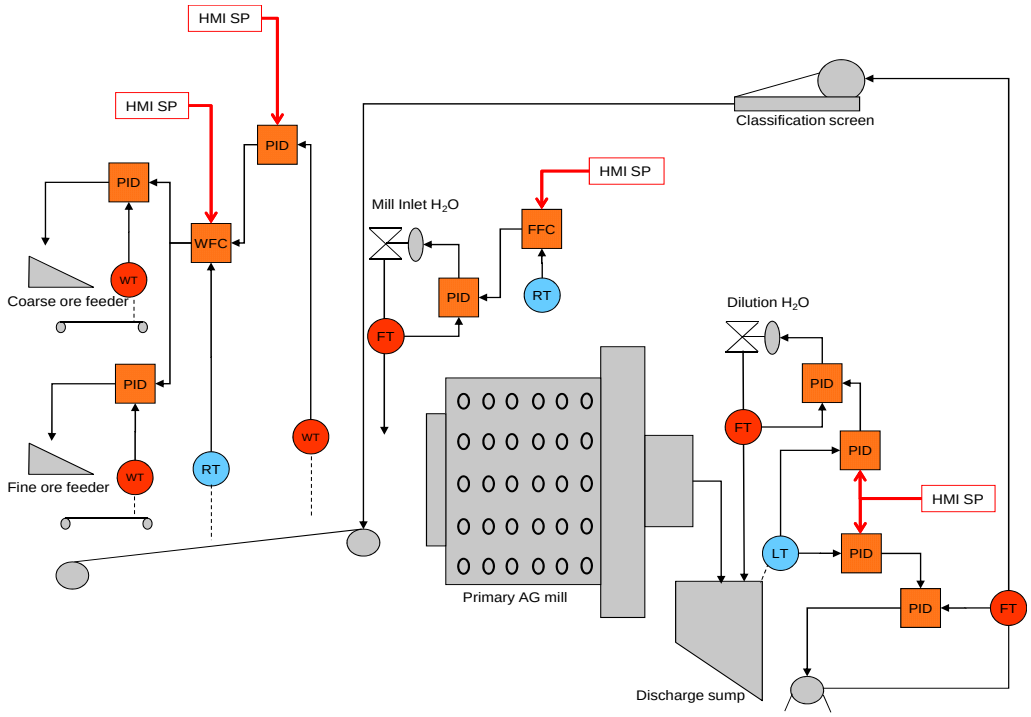

Figure 6.3: Anglo American Platinum's primary milling base-later control infrastructure

It can be concluded that the control of the mill on a base-layer level is fairly manual. None of the main milling parameters described during the literature study (apart from

throughput) is under active control. RPMA2 is constrained by ore supply from the mines. The mill feed (or throughput) and coarse ore ratio are therefore fixed according to an operational mining plan. The inlet water HMI SP is adjusted by metallurgical staff to control milling performance. Operational staff will also adjust the inlet water during abnormal situations to control excessive power and/or load. The discharge sump level HMI SP is fixed within the normal operating region of the sump. This region is defined by the overflow point (high) and the pump cavitation level (low).

6.2.2 Advanced Layer – Mill

The advanced layer is defined as a supervisory algorithm that supplies the base-layer of setpoints instead of an operator. The advanced milling controller at RPMA2 utilises a 3 × 3 Quasi-Fuzzy Rules-Based methodology with the following structure:

1. Antecedents
    - Power proximity (normalised) and velocity (slope)
    - Load proximity (norm), velocity and acceleration (second derivative)
    - Screen current proximity (indication of screen loading)
2. Consequences
    - Total ore feed rate, t/h
    - Coarse ore ratio, fraction
    - Inlet water ratio, fraction

Instead of the traditional "IF-AND-THEN" rules described in the literature study, the RPMA2 controller uses a set of logical rules or process states to link the antecedents to the consequence (hence the name *Quasi*-Fuzzy controller). These process states function in a hierarchical order where the highest state or rule dictates the degree of activation passed on to the consequences and de-fuzzies. The main process states that take part in control are:

Screen capacity limited Screen Amps high AND NOT decreasing

Power at extreme Mill power extremely high OR extremely low

Mill overload Mill load extremely high AND power decreasing AND load increasing

Load at extreme Mill load extremely high OR extremely low

Default operating region Mill load high OR low OR ok

Note that all of the process states use fuzzy members

6.2.3 Advanced Layer – Discharge Sump

The discharge sump advanced controller is decoupled from the mill controller. It is a traditional 2 × 2 Fuzzy-logic controller that utilises the standard "IF-THEN" rules controlling level and density. It is important to note that the discharge density, important to the downstream flotation circuit, is now under control. The controller however aims primarily to control the level within the defined range, thus utilising the surge capacity of the vessel allowing minimum flow rate movement in order to aid downstream stability. The following control parameters are used:

Antecedents

Level proximity, velocity and acceleration

Density proximity

Consequences

Slurry flow rate, m^3/h

Dilution water flow rate, m^3/h

The main process states that take part in the discharge sump control are:

Level at extreme Sump level high AND NOT decreasing OR Sump level low AND NOT increasing

Feed disturbance Feed pump/belt stop OR start

Pump choke Discharge pump SP-PV > 50 m^3/h AND pump output at maximum

Downstream sump constraint Downstream sump level-at-extreme process state active

Default operating region None of the above

6.3 Circuit Modelling

6.3.1 Dimensional Analysis

As described in section 4.1.1, the aim of this dimensional analysis is to confirm the relationship between all the various comminution parameters described throughout the literature (see section 3). It is therefore necessary to define these dimensionless groups in terms of parameters that are monitored and historised. The variable parameters in the system that are monitored are power, mill load, mill speed, throughput, mill inlet water, feed size distribution and coarse ore ratio. The feed size, presented as a percentage

passing 45 mm, proved to have the highest influence on milling parameters during a previous milling investigation (Mototolo JV). A fixed, physical parameter of the mill was also included to describe the system, namely, mill diameter. It was decided to exclude the grind (or product quality) from the dimensional analysis since it is not monitored continuously but only available as a shiftly composite. Other variables not measured online excluded from the dimensional analysis are Bond's work index, in-mill viscosity, and other mineralogical characteristics of the ore body like mineral components and grain size.

Table 6.1: Table of the various parameters used to describe the dimensionless groups in a milling circuit

Parameter	Symbol	Unit	n	v	q	Power parameter P_1
Mill power	q	W	2	1	-3	P_1
Mill load	L	ton	0	1	0	P_2
Mill speed	v	rpm	0	0	-1	P_3
Throughput	t	t/h	0	1	-1	P_4
Mill inlet water	Q	m^3/h	3	0	-1	P_5
Feed size	f	%	0	0	0	P_6
Coarse ore ratio	R_{CO}	%	0	0	0	P_7
Mill diameter	ϕ	m	1	0	0	P_8

With n, v and q the powers in the expression $L^n M^v T^q$

A test to determine the degree of correlation between these variables was conducted. Using correlated variables in the dimensional analysis can bias the model towards a certain relationship due to duplicity and thus dampen the influence of other variables on the system. The correlation analysis was done on actual plant data and produced the following correlation coefficients:

	P_1	P_2	P_3	P_4	P_5	P_6
P_1	1.00	0.57	0.57	0.01	0.35	-0.26
P_2	0.57	1.00	-0.02	0.05	0.40	-0.06
P_3	0.57	-0.02	1.00	0.02	0.11	-0.13
P_4	0.01	0.05	0.02	1.00	0.03	0.00
P_5	0.35	0.40	0.11	0.03	1.00	0.11
P_6	-0.26	-0.06	-0.13	0.00	0.11	1.00

Figure 6.4: Correlation coefficients of the milling variables listed in table 6.1

The highest correlation was observed between the pairing mill power and mill load (0.57) and also mill power and mill speed (0.57). Mill power was therefore not considered during this dimensional analysis as it is assumed that the influence of power can be

sufficiently described by the mill speed and load. Correlation between variables was significantly reduced without power. The correlation matrix is shown in figure 11.1 (appendix B).

The formula will thus be of the form $L^{P_2}v^{P_3}t^{P_4}Q^{P_5}f^{P_6}R_{CO}^{P_7}\phi^{P_8}$. Consider then the following equation:

$$(L^0M^1T^0)^{P_2}(L^0M^0T^{-1})^{P_3}(L^0M^1T^{-1})^{P_4}(L^3M^0T^{-1})^{P_5}\ldots \\ (L^0M^0T^0)^{P_6}(L^0M^0T^0)^{P_7}(L^1M^0T^0)^{P_8} = (L^0M^0T^0) \quad (6.1)$$

which produces the three conditions on the powers:

$$\begin{aligned} L: &\quad 3P_5 + P_8 &&= 0 \\ M: &\quad P_2 + P_4 &&= 0 \\ T: &\quad -P_3 - P_4 - P_5 &&= 0 \end{aligned}$$

Applying Gaussian reduction and parametrisation to the system gives the following reduced equations:

$$\{\begin{pmatrix} P_2 \\ P_3 \\ P_4 \\ P_5 \\ P_8 \end{pmatrix} = \begin{pmatrix} 1 \\ 0 \\ -1 \\ 1 \\ -3 \end{pmatrix} P_2 + \begin{pmatrix} 0 \\ 1 \\ 0 \\ -1 \\ 3 \end{pmatrix} P_3 \quad |P_2, P_3 \in \mathbf{R}\} \quad (6.2)$$

The set of dimensionless groups for equation 6.2 is then obtained by setting for $\Pi_1 : P_2 = 1, P_3 = 0,$, and for $\Pi_2 : P_2 = 0, P_3 = 1$. Note that feed size $\mathbf{f}$ and $\mathbf{R_{CO}}$ are also dimensionless groups on their own. The dimensionless groups are hence given as:

$$\begin{aligned} \Pi_1 &= L^1v^0t^{-1}Q^1\phi^{-3} &&= \mathbf{L^1t^{-1}Q^1\phi^{-3}} \\ \Pi_2 &= L^0v^1t^0Q^{-1}\phi^3 &&= \mathbf{v^1Q^{-1}\phi^3} \\ \Pi_3 &= &&\mathbf{f^1} \\ \Pi_4 &= &&\mathbf{R_{CO}^1} \end{aligned}$$

In order to confirm that a complete set of dimensionless groups has been established, it is necessary to obtain a function that describes the relation between the groups (Buckingham's Theorem given in equation 4.1). A linear and a pure quadratic fit of Π_1 to the rest of the dimensionless groups,that is, $\Pi_1 = f(\Pi_2, \Pi_3, \Pi_4)$ was attempted. The fit was conducted on a $2\frac{1}{2}$ month period, using only data where the circuit was running

uninterrupted for at least 24 hours (>1440 data points at data intervals of 1 min). From this data set, 40 % was classified as "good" and presented as a linear fit in figure 6.5 where Π_4 is kept constant.

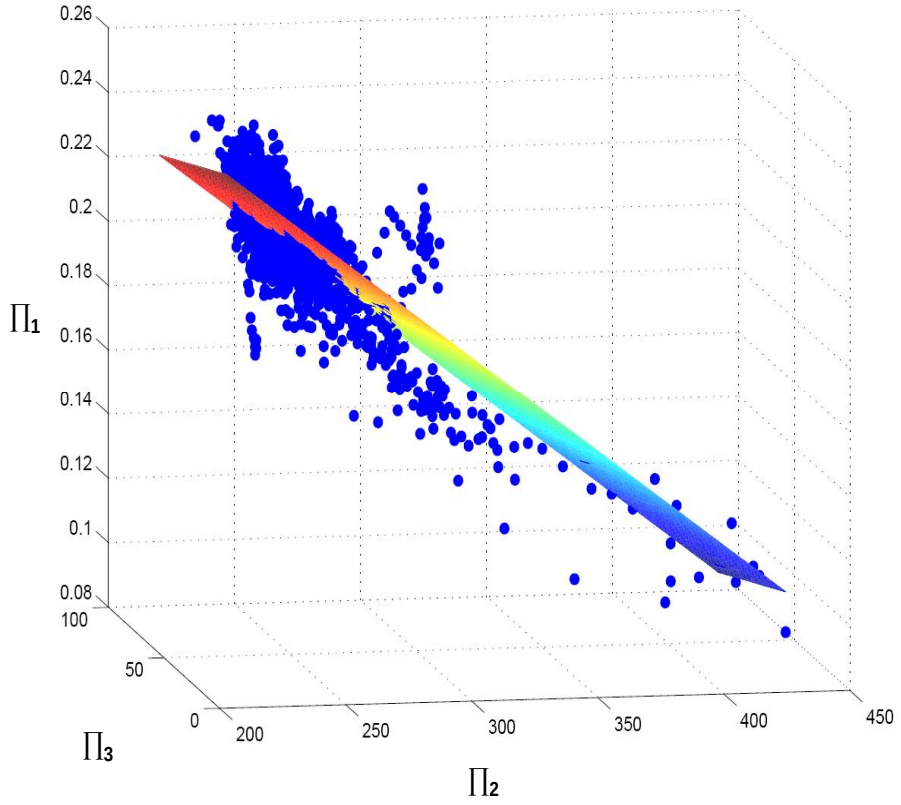

Figure 6.5: A 3D-plot of the linear fit of the dimensionless group Π_1 using Π_2 and Π_3 while Π_4 is kept constant

The linear fit resulted in an R^2-value of 82 % and is given as:

$$\Pi_1 = 0.408 - 0.0006\Pi_2 - 0.0002\Pi_3 - 0.419\Pi_4 \tag{6.3}$$

while the pure-quadratic fit (without interaction terms) resulted in a root-mean-squared-error $RMSE$ value of $8.6x10^{-3}$ which equates to 4.1 % of Π_1.

$$\Pi_1 = c_1 + c_2\Pi_2 + c_3\Pi_3 + c_4\Pi_4 + c_5\Pi_2^2 + c_6\Pi_3^2 + c_7\Pi_4^2 \tag{6.4}$$

with,

$$c = [0.353 \quad -0.0012 \quad -0.0002 \quad 2.311 \quad 9.1 \times 10^{-7} \quad -2.55 \times 10^{-7} \quad -13.1] \tag{6.5}$$

The relatively high R^2 and small $RMSE$ percentages lead to the assumption that the both the linear and quadratic fit are suitable to describe the relationship between

the dimensionless groups. More importantly, according to Buckingham's theorem, this indicates that a complete subset is present and adding any additional inputs will be superfluous. It is therefore possible to describe any of the above milling parameters using either equation 6.3 or 6.4. An example of this is given in figure 6.6 where the actual mill load is closely followed by the modelled version of the linear and quadratic fit[1]. From this plot it is noticeable that the modelled values are closely correlated the actual measured mill parameter. These closely correlated load plots are a further indication that a complete subset of dimensionless groups are indeed present.

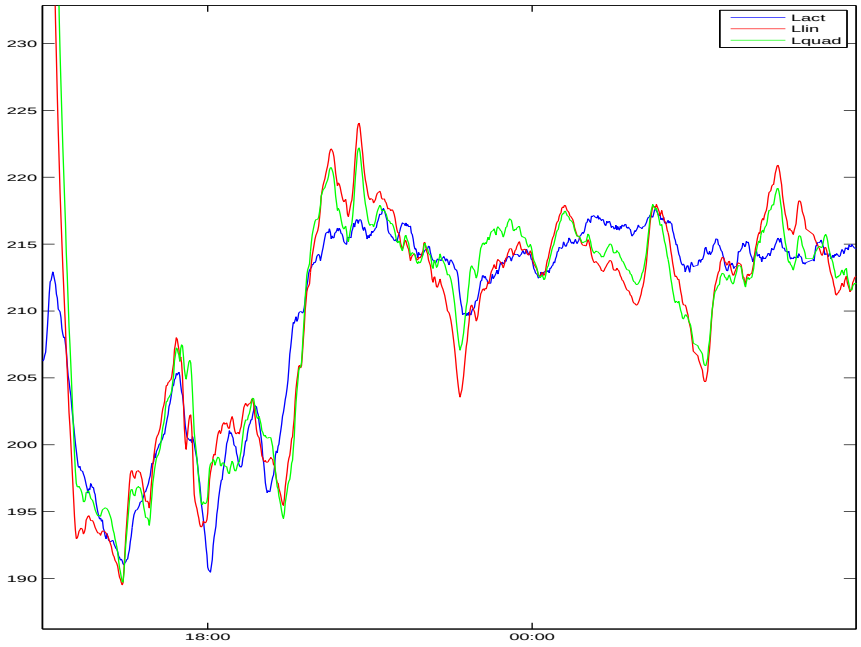

Figure 6.6: Dimensional analysis model fit for the mill load, a)actual, b)linear and c)quadratic dimensionless group fit

The following conclusion can thus be derived from the dimensional analysis:

- The mill power is highly correlated to the mill speed and load
- Buckingham's Theorem is sufficiently satisfied indicating that a complete subset of dimensionless groups is present
- The behaviour of the milling circuit can be explained by the parameters discussed in the literature study. Equations 6.3 and 6.4 show that the load of the mill can be described by a combination of the manipulated variables currently controlling the mill and discussed in section 3

[1] All plots are filtered with an exponential filter with $\alpha = 0.85$

- The relationship describing the milling parameters is highly non-linear and correlated
- No result from the dimensional analysis is claimed to be fundamental but serves as an indication that a relationship does indeed exist between the parameters chosen for the analysis. These relationships form the foundation of the model predictive controller design.

6.3.2 Modelling

Anglo American Platinum as an organisation made the decision to use AspenTech's DMCplus^{TM} as the platform to develop its model predictive control infrastructure. The decision was based on an economic and performance assessment conducted on a wide variety of control products available to the industry at the time. DMCplus^{TM} conducts their process modelling by means of a step-test campaign where all the independent parameters are moved in order to produce responses from the dependent variables. The relationship between these independent (or manipulated variables MVs) to the dependent (or controlled variables CVs) was confirmed by the dimensional analysis. Furthermore, DMCplus^{TM} utilises finite-impulse-response as well as state-space modelling (section 4.1.2), as techniques to determine the matrix of linear models describing the milling circuit relationships. The model matrix produced from the step tests, conducted during September 2010 are presented as a step response matrix as shown in the figure 6.7.

The following characteristics are observed from the response matrix:

General

1. The model horizon (or prediction horizon) of the controller that produced the most reliable models was 60 minutes. An indication of the model quality is given in the appendix.
2. One of the most significant observations is that the mill load behaviour is described as an integrator over the allocated model horizon of 60 min.
3. The inlet water ratio to mill power model presented a positive gain for the operating region of the mill. This indicates, according to figure 3.6, that the flowrate through the mill is low enough for the interstices within the charge not to be completely occupied and that no slurry pool has formed.
4. Movement of both power and load are positive to the mill feed. This indicates that the mill is operated on the left hand side of the power to volume filling/load curve. This characteristic of the mill, according to figure 3.3, occurs at volumetric fills greater than 45 %

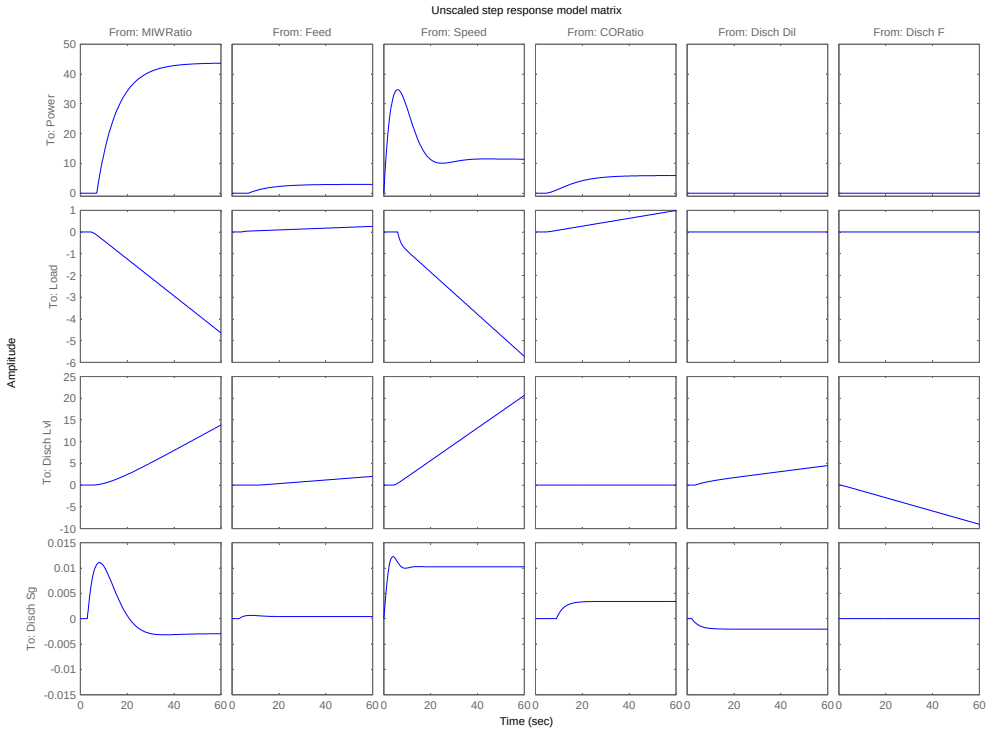

Figure 6.7: The step-response matrix for the RPMA2 mill and discharge sump obtained during the September 2010 step campaign

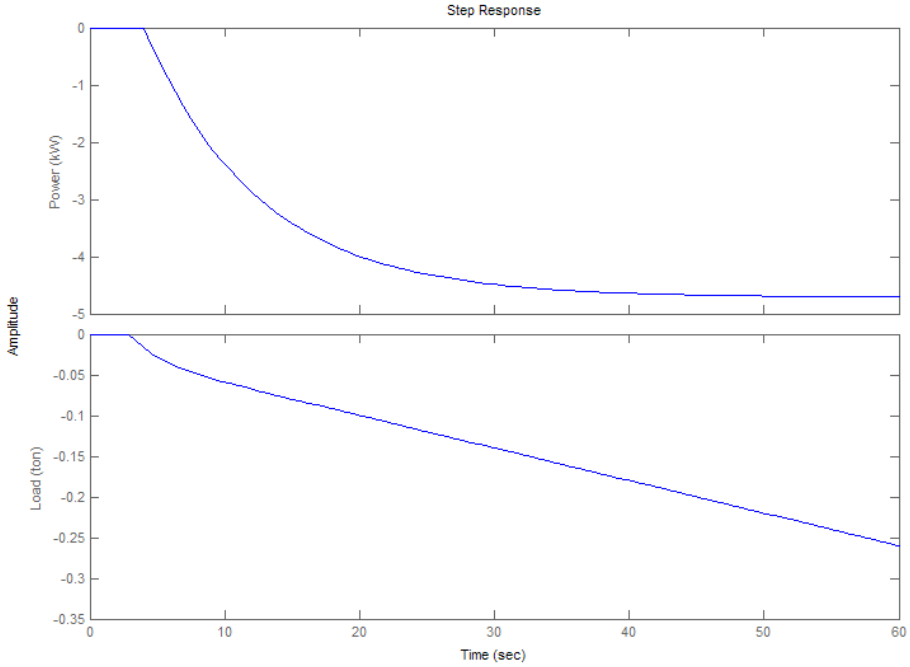

Figure 6.8: The step-response matrix for the RPMA2 measured disturbance variable feed size (September 2010 step campaign)

5. Speed increases produced a positive, higher order, underdamped response from power which concurs with the findings in figure 3.3. The increased speed leads to a decrease in load.

6. Both power and load increase with an increase in coarse ore ratio. The fact that both the power and load decrease with an increase in the feed +45 mm size fraction indicates that the 45 mm size class is probably too small to be classified as competent grinding material.

7. The effect of increased inlet water shows a sharp increase on discharge density since the transport through the mill is increased. After about 20 minutes, this transient effect expires and a new density steady state is reached lower than the initial value due to the decrease in solids density.

Model Gain The model gains of the system indicate that the mill inlet water has the largest unscaled gain on mill power with ore feed being the smallest. If the system is scaled according to input range and output error (Skogestad and Postlethwaite, 2005), the ore feed yields the largest power gain with inlet water the second highest. The scaling parameters, input movement range and output error, can be found in the appendix. Mill speed yields the largest gain on mill load for both scaled and unscaled models with inlet water ratio in second. It is noticeable that the coarse ore ratio produced the lowest scaled gain for both power and load.

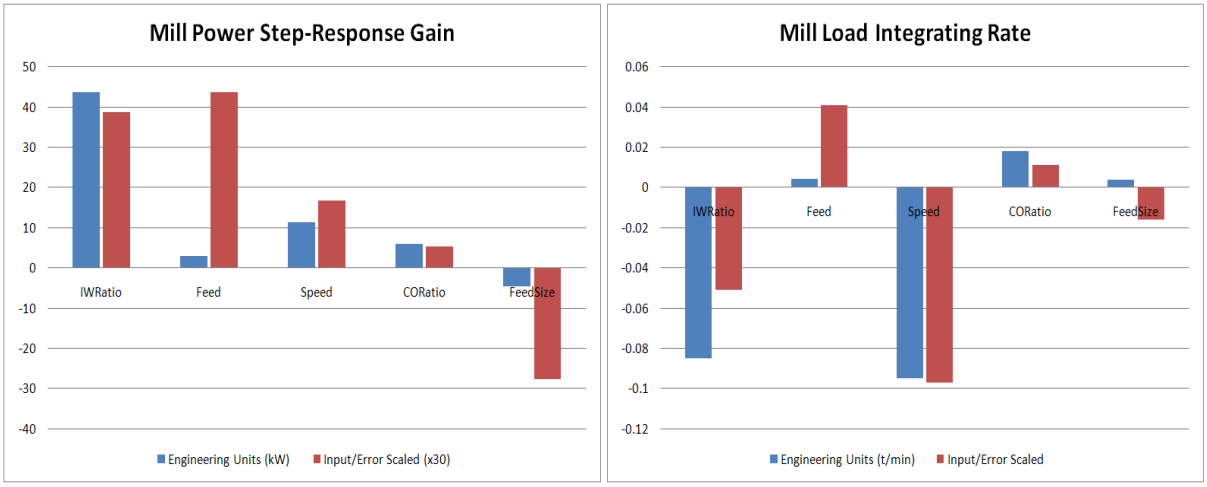

Figure 6.9: The step-response model gain and integrating rate for mill power and load respectively

Model Dynamics The system dead-time for the various models ranged between 4 min to 7 min, see figure 6.10. Most significant of the mill's dynamic responses are the large variance in time constants from 8.5 min for inlet water and feed size to 42 min for the coarse

ore ratio. A detailed list of the primary mill's dynamic constants, damping coefficient and time constants, lead constants and dead-times are provided in the appendix (figure 11.3).

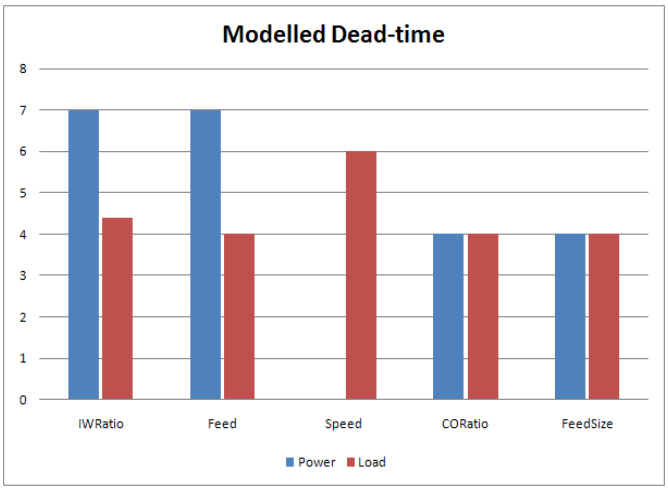

Figure 6.10: The step-response modelled dead-time for mill power and load respectively

6.4 Performance Benchmark

RPMA2 was commissioned in February 2009 with the advanced controllers active and has never run on its milling base-layer control alone. All historical data available is therefore related to fuzzy control with no data available for pure PID control. Data from one month prior to the project kick-off was used to benchmark the circuit performance. Only good quality data at a sampling rate of 1 point per minute was used. Good quality data is generated when the mill is running and ore is being added. During the period 1 August 2010 to 9 September 2010, 17180 good quality samples were collected.

6.4.1 Time Domain

Note that the time domain histogram plots can be found in appendix B. These plots presents the probability density functions of the various parameters with the upper and lower quartiles in dark red and the mean as a blue line.

Mill Controlled Variables The primary mill was predominately controlled at a power of 2688 kW and a load of 203 ton with standard deviations of 364.2 kW and 6.8 ton respectively. Relatively, these deviations equate to 13.5 % for power which is relatively high and 3.1 % for load which can be regarded as acceptable. It was reported by site that mill inlet seal failure occurs at a loads >230 ton. To prevent the fuzzy controller from violating this physical limit, the load control high limit, was set to 220 ton. Increasing the load to improve the product grind, as per figure 3.1, can therefore only be achieved if the load standard deviation is decreased further.

The load distribution plot (figure 11.4) and the power-to-load curve (figure 6.11) indicate a tendency for the load to concentrate more to the high side of its limits range. This is as a result of the fuzzy controller's optimisation drive to increase load and hence decrease product size. This is achieved by implementing a bias in the controller's rules to reduce inlet water ratio and increase feed when possible. It is important to observe that the speed of the mill was still controlled manually by the operators which is probably the reason for the higher standard deviation of power.

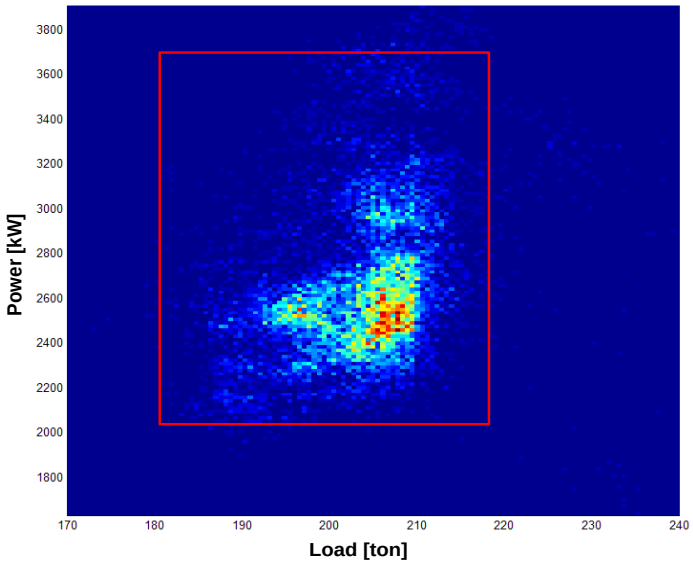

Figure 6.11: Primary mill power to load curve as a 2D histogram with controller limits (red), 1 August 2010 to 9 September 2010

Mill Manipulated Variables The distribution plots for mill feed tonnage and inlet water ratio (figures 11.5 a,b) also illustrates the fuzzy controller's optimisation initiative to always decrease inlet water and increase mill feed when possible; inlet water ratio SP concentrates to the lower end of its distribution while the feed SP is concentrated on the high end of its distribution. A difference of 29.6 ton/h in standard deviation between feed SP and PV was observed. This 88 % increase in deviation can be due to poor PID performance or physical limitations of the process and was cited as an improvement area for the project. The deviation between inlet water ratio SP and PV of 0.0023 or 14 % was deemed to be acceptable. It was assumed that the speed PV is equal to the SP since no speed feedback was obtained. It can be observed that the speed distribution is not smooth but rather irregular. This is due to the fact that the speed was operated manually at various fixed setpoints prior to this project. The distribution indicated that the mean of the speed was found at 90 % of the maximum speed with a standard deviation of 4.5. Note that the maximum speed is set at approximately 80 % of the critical speed. The highest amount of data points during this period were collected at 87 % of the

maximum speed. The coarse ore ratio, calculated as coarse-ore tonnage divided by total tonnage, illustrated very poor tracking between SP and PV. It can be seen that the coarse ore is often not available as the main part of the ratio distribution is concentrated within the zero bin.

Mill Disturbance Variable The distribution plot for the feed size produced a mean of 39 % passing 45 mm at a relatively high standard deviation of 8.8 % -45 mm (figure 11.7). This 22 % relative standard deviation illustrates the high variability in the size of the ore fed to the mill and emphasises the difficulty of tight primary milling control.

Effective Power Utilisation The effective power utilisation η_{power}, is defined as the amount of power used to produce one ton of desired product. That is, the amount of particles passing 75 μm calculated at steady-state by:

$$\eta_{power} = \frac{Power}{Feed \cdot Grind} \tag{6.6}$$

.

The 8 hour shiftly composite grind sample[2] was used to calculate this parameter due to the lack of an online grind measurement. This performance parameter is therefore calculated per shift, hence the lack of data in the distribution plot. A mean effective power usage of 25.2 kWh/t -75 μm at a standard deviation of 6.7 kWh/t -75 μm was observed. The primary aim of the project will be to reduce this parameter.

6.4.2 Frequency Domain

In order to convert time domain data to the frequency domain using Fourier transforms, section 10.3 (in appendix A) describes that the data should be continuous. Since the mill feed is the final interlock to the mill's running condition, it serves as an indication of good quality data. Periods within the data, where mill feed was $>$ 100 t/h for longer than 1440 samples (1 day) were considered good data. Seven such periods, totalling 17106 samples, or 11.9 days, within the period 1 August 2010 to 9 September 2010 were considered good enough running data on which to perform a frequency analysis on. The power spectral density PSD plots for the entire 11 days of good running data can be found in appendix B. The first observation applicable to all these plots is the increase in PSD at frequencies $< 1 \times 10^{-3}$ Hz. These are sinusoids with periods $<$ 16 minutes. The step response models indicated that all the process time constants for the stable models (power models) are $\geq$ 8.5 minutes. Any sinusoid at periods smaller than this, or frequencies $<$ 0.002 Hz is therefore considered process noise.

[2]Taken at regular intervals of between 10 min to 15 min

Controlled Variables The amplitude for both power and load increases as the frequency decreases. The highest amplitude for both power and load was obtained at a frequency of 9.5×10^{-5} Hz or at a period of 3 hours.

Manipulated Variables Primary mill feed amplitude decreased from the noise frequencies and appears to stabilise towards the lower frequencies. Both mill inlet water and mill speed increase towards the lower frequencies. The coarse ore ratio SP showed similar behaviour to that of the total mill feed by stabilising towards the lower frequencies.

Disturbance Variable The frequency spectrum of the mill feed size (% -45 mm) shows a similarity to that of the controlled variables i.e:

- high amplitudes within the noise frequency band,
- lower amplitudes between the 10^{-3} Hz to 10^{-4} Hz frequencies and,
- increasing amplitudes towards the lower frequencies.

Since the mill feed size was the only disturbance variable identified in the process, a theoretical minimum variance for the controlled variables, power and load, could be formulated from the Laplace Domain step response models (table 11.1) as described in section 5.3.1. Discrete approximations of the feed size to power G_{fP} and feed size to load step model G_{fL}, with 1 minute sampling intervals are presented as the following z-transfer functions:

$$G_{fP}(z) = \frac{-4.71z}{9.5z - 8.5} \tag{6.7}$$

$$G_{fL}(z) = \frac{-0.044z^2 + 0.04z}{3z^2 - 5z + 2} \tag{6.8}$$

These discrete models can be expanded using deconvolution or long division:

$$G_{fP} = -0.496 - 0.444z^{-1} - 0.397z^{-2} - 0.355z^{-3} - 0.318z^{-4} + \ldots \tag{6.9}$$

$$G_{fL} = -0.0147 - 0.0111z^{-1} - 0.0087z^{-2} - 0.0072z^{-3} - 0.0061z^{-4} + \ldots \tag{6.10}$$

Since a 5 min process lag was obtained for both these models, the minimum variance approximations for the process outputs power and load are therefore defined by the first 5 terms of equations 6.9 and 6.10. This is in accordance to equations 5.11 and 5.12:

$$y_{mv,power} = (0.496 - 0.444z^{-1} - 0.397z^{-2} - 0.355z^{-3} - 0.318z^{-4})a_t \tag{6.11}$$

$$y_{mv,load} = (-0.0147 - 0.0111z^{-1} - 0.0087z^{-2} - 0.0072z^{-3} - 0.0061z^{-4})a_t \tag{6.12}$$

The step response of the minimum variance approximation model and the actual step response model are presented in figure 11.9 (appendix B). The frequency spectrum of mill power and load versus the theoretical minimum variance response to mill feed size are presented in figure 6.12. The following conclusions can be drawn:

1. A relatively constant difference between the minimum variance and the process variables is observed which leads to the conclusion that the feed size does indeed affect power and load.
2. The amplitude of the process signals appear to be 5 and 2 times greater than the minimum variance approximation for power and load respectively. It is therefore assumed that the movement of power and load can not only be characterised by the mill feed size. Other unmeasured disturbances that influence power and load are also present.
3. The opportunity exists to further stabilise power and load should the extra MV movement necessary for this be accepted.

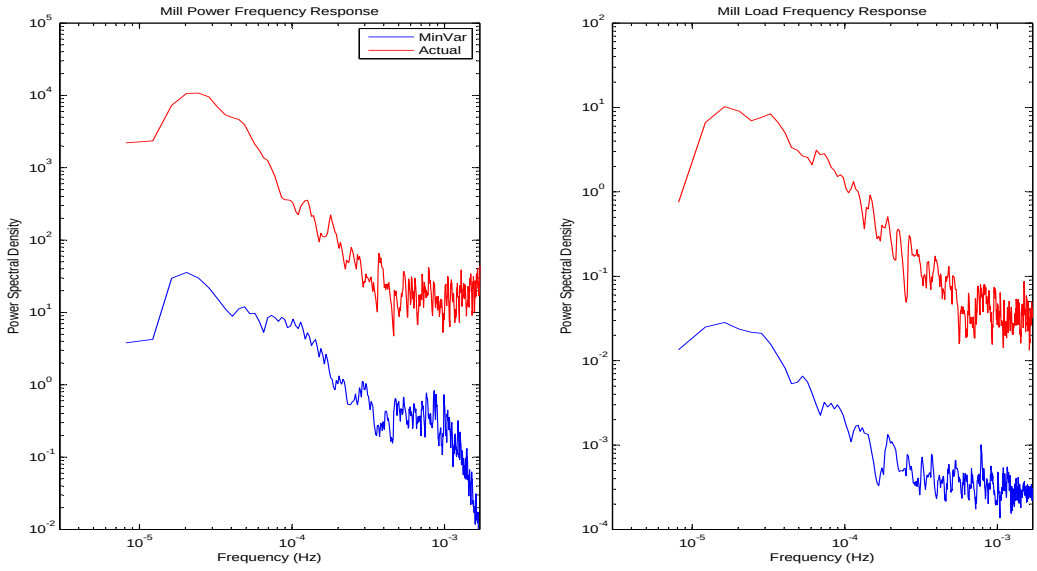

Figure 6.12: The frequency signature of actual power and load versus the theoretical minimum variance response for measured disturbances

6.5 Controller Design and Implementation

6.5.1 Controllability Analysis

The scaled model matrix as explained in section 6.3.2 was considered for the controllability analysis.

Functional Controllability Skogestad and Postlethwaite (2005) mention that the requirement for minimal functional controllability is that the amount of inputs u should be at least equal to the amount of outputs y. The mill is a 4 by 2 system. With regards to the inputs of the mill controller, consider the following:

1. The mill feed rate should be controlled at the business plan during normal operation which in this case implies the high limit of the input. This input constraint may only be violated during abnormal situations. Mill feed will therefore not be considered for the controllability analysis.
2. The mill's coarse ore feed was shown to be an unreliable input due to its setpoint tracking performance and availability. This input will also not be considered for this analysis.

The controller considered for this analysis can therefore be reduced to a 2×2 controller with inlet water ratio and mill speed as inputs and power and load as outputs. The reduced controller does meet the required minimum functional controllability requirement. A process is however functionally uncontrollable if and only if the minimum singular value $\sigma_l(G(j\omega)) = 0, \forall\omega$. The frequency characteristics of the square process (shown in figure 6.13) indicate that the minimum gain, or minimum singular value is 0.95 $\forall\ \omega > 1 \times 10^{-2}$, after which the minimum gain is reduced dramatically. This implies that the controller should be able to influence the system at frequencies lower than 0.01 Hz. This frequency is an order of magnitude greater than what was previously classified as noise. This implies that the controller should be able to exercise control within the noise band, $0.01\text{Hz} > \omega_{noise} > 0.001$ Hz. It is important to note that the maximum singular value or controller gain increases towards the lower frequencies.

Relative Gain Array RGA A method of measuring the interaction between a controller's inputs and outputs is presented by Skogestad and Postlethwaite (2005) as the RGA. The RGA of a square process is calculated as follows:

$$RGA(G) = \Lambda(G) \triangleq Gx(G^{-1})^T \tag{6.13}$$

The RGA also presents a method of finding the best decoupled input-output pairings. In the 2 by 2 mill model, only two pairings P_1 and P_2 are possible:

$$G_{P_1} = \begin{bmatrix} g_{11} & g_{12} \\ g_{21} & g_{22} \end{bmatrix} \qquad G_{P_2} = \begin{bmatrix} g_{12} & g_{11} \\ g_{22} & g_{21} \end{bmatrix}$$

The RGA-number is a measure of the diagonal dominance for the pairings. The higher the RGA-number, the higher the degree of correlation between outputs per

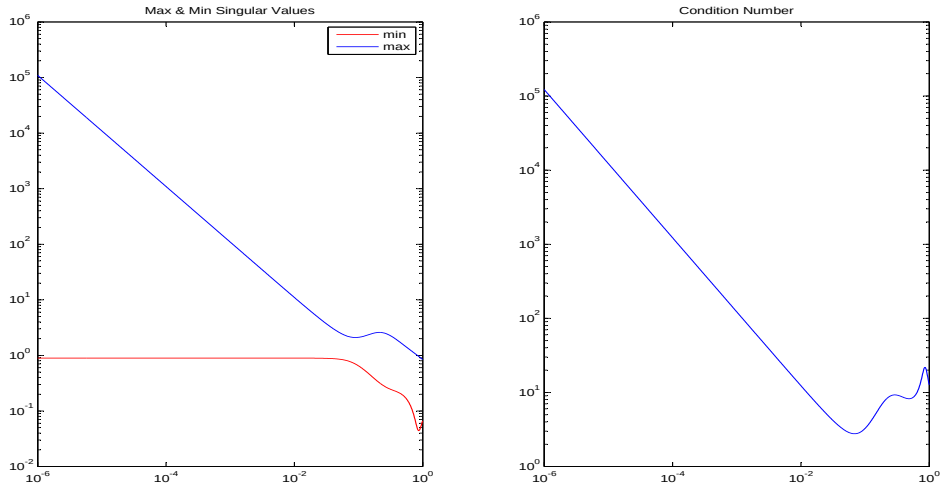

Figure 6.13: The frequency characteristics of the square process a) max and min singular values and b) condition number

input. The RGA-numbers for the two pairings are presented in figure 6.14. The pairing P_1 presented the lowest RGA-number and hence the lowest input/output correlation. If decoupling of the system is required, the pairings that provide the highest decentralisation are: g_{11} – inlet-water ratio to power and g_{22} – speed to load.

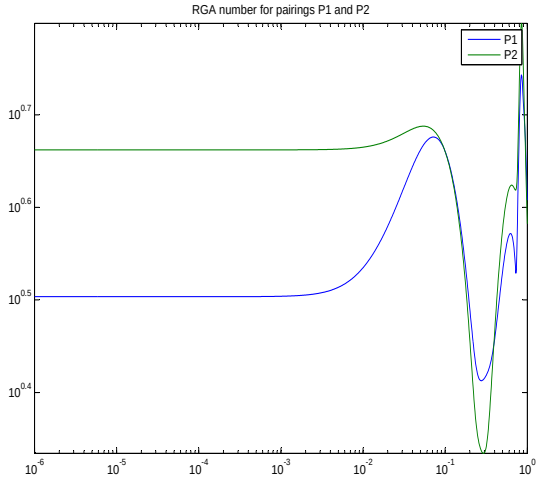

Figure 6.14: The RGA-number for pairings P1 and P2

The relative gain between the diagonal and non-diagonal elements remains constant at values of 1.3 and 0.3 for all frequencies lower than the noise band, $\omega_{noise} > 1\times10^{-2}$ Hz respectively (figure 6.15). The RGA elements converge within the noise frequencies which indicates that decentralisation is only possible at lower frequencies.

Disturbance Rejection Skogestad and Postlethwaite (2005) state that control is nec-

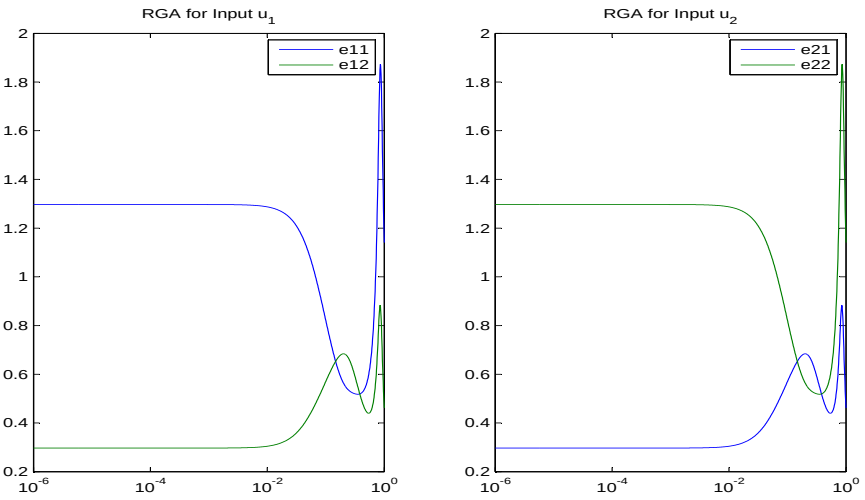

Figure 6.15: The frequency response for the RGA of pairing P_2 with diagonal elements: g_{11} = IWRatio/Power, g_{22} = Speed/Load and non-diagonal elements: g_{21} = IWRatio/Load, g_{22} = Speed/Power

essary if one of the elements in the disturbance matrix G_d is greater than 1. The frequency response of the mill feed size (figure 6.16) to the controlled variables indicates that the mill load element is greater than 1 at frequencies $\omega < 1.5 \times 10^{-4}$ and will require control.

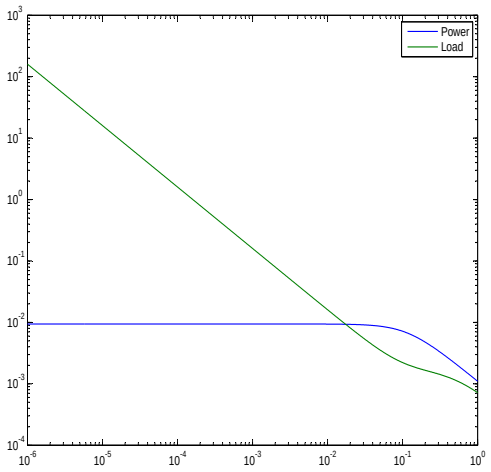

Figure 6.16: The frequency signature of the disturbance mill feed on mill power and load

6.5.2 Objective Function

The objective of this controller is to minimise the effective power usage η_{power} of the milling circuit, in units kWh/t$_{-75\mu m}$ produces, according to the steady-state objective equation 4.11. Note that for the steady-state optimisation of the primary mill, no steady-

state MV movement penalties were assigned in the objective function. As explained in section 4.4.2, both the LP and QP (equations 4.27 and 4.28) utilised by DMCPlus^{TM}, define the direction and degree of minimisation as the $SSCost$ vector. The objective of this section is to obtain the direction and magnitude of the $SSCost$ vector by modelling the effective power usage of the mill to the speed and inlet water ratio. The model of the milling parameters to the product grind would have been a better objective to pursue but could however not be established within an acceptable margin of error. The optimisation framework in subsequent sections is designed to establish this.

As in section 6.4, the 8 hour (shiftly) composite grind samples are used to calculate η_{power}. This calculation is used to model the objective function using the manipulated variables speed S, inlet-water ratio W_{rat} and mill feed rate F. A linear fit was performed where, as per the LP and QP, the $SSCost$ vector is defined by the model coefficients. During the period 1 January 2010 to 1 October 2010, when the MPC was active, 450 valid shiftly samples were obtained for modelling. The linear regression model achieved an $R^2 = 20$ % which is fairly low under normal circumstances. However, taking into account that composite average samples over an 8 hour period were used, this model was assumed good enough as a starting point for optimisation. A pure-quadratic regression was also carried out in order to increase the model validity. A root-mean-square-error equal to 1.7 kWh/t$_{-75\mu m}$ was achieved, which relative to η_{power} equates to an acceptable $RMSE_{rel}$ equal to 7 %. The two dimensional representation of the quadratic model with J relative to the MVs can be viewed in the appendix figure 11.13. Both the linear and pure-quadratic model of the effective power usage to speed and inlet water ratio are represented in figure 6.17 (feed F constant at the maximum 350 t/h).

The linear objective function obtained used for the DMCplus^{TM} controller's steady-state optimisation can thus be presented dynamically as:

$$\Delta J = \Delta\eta_{power} = 6.6 + 0.27\Delta S + 0.165\Delta W_{rat} - 0.022\Delta F \tag{6.14}$$

This implies that the objective function will be minimised with $SSCost$ parameters for mill speed, inlet water ratio and feed set to 0.27, 0.165 and -0.022 respectively. This indicates, at the very least, the optimisation direction required to increase milling efficiency $min(J)$.

The $SSCost$ parameter can be any value as per the controller's tuning requirement but the ratios between these parameters should remain within an acceptable margin of that established above, that is, $\frac{\Delta S}{\Delta W_{rat}} = \frac{0.27}{0.165} = 1.63$, $\frac{\Delta S}{\Delta F} = \frac{0.27}{-0.022} = -12.2$ and $\frac{\Delta W_{rat}}{\Delta F} = \frac{0.165}{-0.022} = -7.5$.

The speed minimisation objective is in accordance with figure 3.3a and c in section 3, where it is shown that power decreases while grind increases with a reduction in mill speed. It is however also stated in the literature that the amount of product produced, in t/h

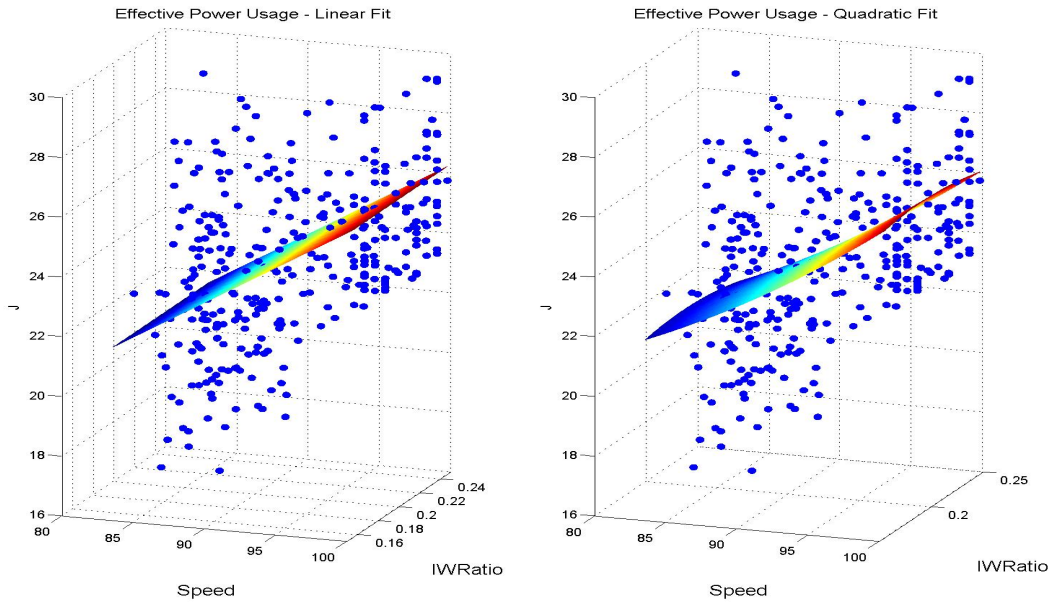

Figure 6.17: The a)linear and b) quadratic approximation of the effective power usage objective $\text{kWh/t}_{-75\mu m}$ at maximum feed $F_{max} = 350$ t/h

-75μm, is reduced as speed decreases (figure 3.3). This occurrence is however disregarded for this optimisation exercise since the plant is ore supply constrained and required to run, according the mine-plan, at a maximum of 350 t/h. *Increasing the amount of desired product produced is therefore only achievable with an increase in grind and not an increase in throughput.*

The water minimisation objective implies that the mill is operating in either the A or B-regions of figure 3.4. As indicated by the step-response models above, a water increase leads to an increase in power. A reduction in water will therefore lead to the minimisation of J if and only if the amount of desired product (the numerator) is either unaffected as found in region A or increased as in region B of figure 3.4. The quadratic model indicates that the inlet water achieved an absolute power usage minimum at a ratio of about 0.19. In the linear environment, this apparent optimum water addition ratio can be treated as a constraint which is defined by the feasible region (explained in section 4.4.2).

6.5.3 Controller Tuning

The primary mill MPC at RPMA was implemented and commissioned by the author and a BluESP representative, Dr. K. Brooks. During controller implementation, various DMCPlus tuning parameters where adjusted to achieve acceptable control both theoretically and practically. They are discussed as follows:

Steady State Tuning Three manipulated variables can be used for controlling the mill, which implies that three degrees-of-freedom are available for steady state

optimisation. Since the feed should be kept at maximum, only two degrees-of-freedom remain. The $SSCost$ parameters were tuned to regard feed maximisation as the first priority and subsequently to adhere to the direction of optimisation established in (section 6.5.2).

The final $SSCost$ vector implemented:

$$\begin{aligned} SSCost_F &= -30 \\ SSCost_{WRatio} &= 0.165 \\ SSCost_S &= 0.27 \end{aligned}$$

In a linear environment, these cost parameters together with the model gains and MV movement penalties (to be discussed later), imply that once the feed is increased to its maximum limit and a feasible solution is still possible, the speed and inlet-water ratio optimisation will commence. To determine which MV will then take precedence (speed or water minimisation), consider the following argument (Brooks commissioning notes 2010):
As per the definition of an integrator, one degree of freedom is used for the control thereof. In order to keep the mill load stable with the remaining degrees-of-freedom, the following equation must be adhered to,

$$\begin{aligned} \Delta L &= g_1 \Delta W_{rat} + g_2 \Delta S = 0 \\ \Rightarrow \Delta S &= -\frac{g_1}{g_2} \Delta W \end{aligned} \tag{6.15}$$

With $g_1 = -0.085$ and $g_2 = -0.097$, the modelled rate of change of the integrator. Taking into account the dynamic linear objective function,

$$\Delta J \approx a \Delta W_{rat} + b \Delta S \tag{6.16}$$

Substituting equation 6.15 into 6.16,

$$\begin{aligned} \Delta J &\approx a \Delta W - b \frac{g_1}{g_2} \Delta W \\ &\approx (a - 0.876b) \Delta W \end{aligned} \tag{6.17}$$

So, for the integrator to remain stable and to minimise water addition,

$$a - 0.876b > 0$$
$$a > 0.876b \tag{6.18}$$

Since $a = SSCost_{WRat} = 0.165$ and $b = SSCost_S = 0.27$, equation 6.18 is untrue. Similarly, it can also be shown that for integrator stability and speed minimisation, $a > -0.876b$. With the same cost parameters, the controller will allow speed minimisation to take preference over water minimisation. Since the speed minimum of 80 % is rarely reached in practise, water will be maximised whenever a feasible solution is available. If the mill is to be operated at an optimum water addition, the high limit should be set to the local minimum of 19 % as mentioned in section 6.5.2. Under normal operating conditions, the three degrees-of-freedom of the system will therefore be consumed by the two constrained MVs, feed and water, and one constrained CV, load at its maximum. The objective of the optimisation framework that is to follow, is to verify the optimum operating points for load and water.

Dynamic Tuning Manipulated variable movement penalties were assigned to the controller in order to stabilise the circuit. The highest movement penalty was assigned to the feed at 20 with inlet water ratio at 5 and the lowest assigned to the speed at 0.5. The high $SSCost$ and movement penalty allocated to the feed will ensure that the controller maintains the throughput at its maximum and only allows movement during upset conditions. Speed was given a low movement penalty to ensure that enough flexibility is granted to control the integrator. Water will remain at its high limit until abnormal upset conditions that require movement develop, or when speed saturates at its low limit.

6.5.4 Preliminary Controller Performance

As a preliminary indication of the controller's performance, the first month of operation (19 October to 22 November 2010) was compared to the base-case scenario in section 6.4. Similar requirements for "good" data were applied, which produced 16430 good data points at a sampling rate of 1 per minute. The following results were observed:

- The mill load standard deviation was decreased from 6.8 ton to 2.3 ton which amounts to a 66 % decrease. These plots are presented in appendix B. A load increase from a mean of 204 ton with fuzzy control to 214 ton with MPC was observed. Note that at this time it was not yet confirmed whether this exceeds the power to load peak or moved closer to the optimum grind peak discussed in the literature.

- The power deviation was also reduced from 364 kW to 219 kW ($\sim$ 40% reduction). The 2D density plot below illustrates how the load and power are more densely compacted closer to the load high limit as a direct result of the reduction in deviation.

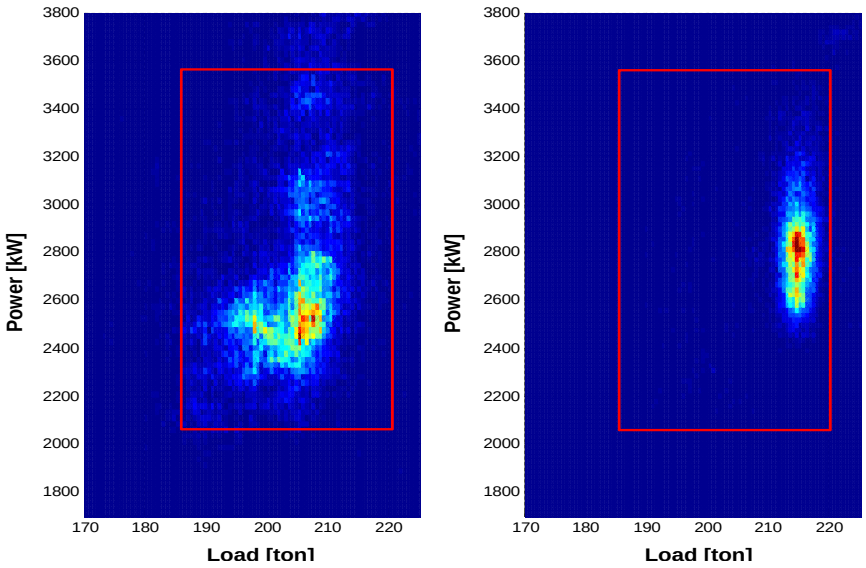

Figure 6.18: Primary mill power to load curve as a 2D histogram with controller limits (red) a) base-case (1 August to 9 September 2010) and b) first month of MPC operation (19 October to 22 November 2010)

Manipulated variable movement also changed with the inception of the MPC. Ore feed standard deviation increased by 90 % from 3.3 t/h to 6.5 t/h, which is still within acceptable limits. Inlet water ratio standard deviation increased from 0.015 to 0.016, a 6 % increase in water deviation during MPC operation. Speed movement was reduced with the implementation of online speed control from 4.4 to 3.9, which amount to a decrease of 13 %. The feed size was more variable during the month of MPC operation. The feed size deviation increased from 6.76 % to 11.9 %, close to double the amount of disturbance experienced during the first month of predictive control. In the light of the increased disturbances, the decrease in CVs and selected MVs disturbances becomes even more significant.

Hulbert (2002) and Craig and Koch (2003) warns that comparing the performance of the improved, post-project circuit to the benchmarked plant can lead to bias. The reason for this bias is due to unmeasured external factors such as ore properties that might be different for the two cases. The recommended way of removing such bias is to reducing the effect of these external factors by conducting an experiment where both the cases are utilised in a structured ON/OFF manner. This could however not be performed due to the expense and time demands of a properly designed ON/OFF experiment on an entire circuit. In order to confirm the significant reduction in variability observed in figure 6.18,

the theoretical minimum variance of the load was investigated to determine whether any change in ore properties are observed.

The power spectral density of the mill load indicates a decrease in amplitude during MPC operation at frequencies $\omega < 3 \times 10^{-4}$ (figure 6.19). The mill load appears to converge on the minimum variance approximation at lower frequencies (see figure 6.19). This concurs with the results shown in figure 6.18. The minimum variance of the load indicated very little difference between data for before and after the project. This implies that best-case control performance were similar during the two periods in question and that ore-properties can be considered similar.

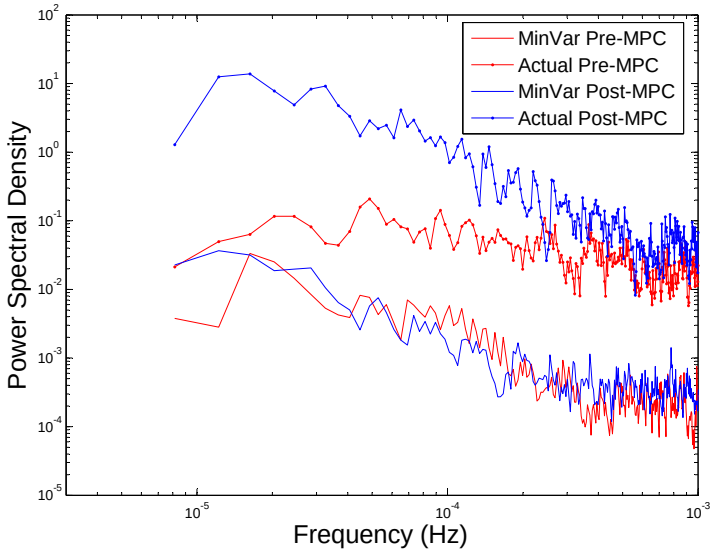

Figure 6.19: The mill load frequency comparison between pre and post MPC as well as the load's theoretical minimum variance response of the pre and post MPC

To further verify the reduction in variance, the historical standard deviation of load on a month to month basis was compared to that observed as a result of the project. A load standard deviation consistent with the 6.8 ton observed in figure 6.18 was obtained for the 10 months before the project (figure 6.20). The reduction in load standard deviation from 6.8 ton to 2.3 ton are observed for three months after commissioning the MPC.

The mill power did not indicate any significantly different behaviour after the MPC was commissioned. The frequency comparison of power can be seen in the appendix, figure 11.19. An 11 % reduction in effective power utilisation from 25.3 kWh/t$_{-75\mu m}$ to 22.4 kWh/t$_{-75\mu m}$ was observed after the MPC was switched on. The standard deviation of this metric was significantly reduced by 51 % from 6.76 kWh/t$_{-75\mu m}$ to 3.29 kWh/t$_{-75\mu m}$ with the implementation of the MPC.

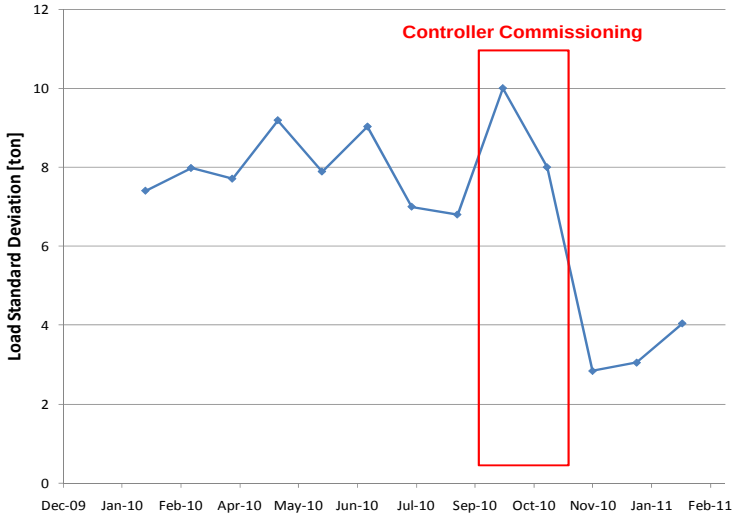

Figure 6.20: The mill load frequency comparison between pre and post MPC as well as the load's theoretical minimum variance response of the pre and post MPC

CHAPTER 7

Optimisation

7.1 Optimisation Framework

The implementation of MPC on the primary milling circuit at RPMA2 resulted in a significant reduction in variance in most of the milling parameters. As explained, the mill feed maximisation is regarded as the primary objective and mill speed minimisation as secondary. In doing this, the mill inlet water will be moved and kept at its high limit as it shares a gain and optimisation directionality with speed (considering load). The three degrees of freedom available to the system are consumed as follows:

1. Feed high limit,
2. Load high limit due to reducing speed and
3. Inlet water ratio high limit.

Since the feed high limit is dictated by mining supply, the objective of this framework is to verify the optimum operating region of the mill. This optimum region is defined for a certain throughput at the load and inlet water ratio high limits. As mentioned in section 5.2, the benefit of milling circuits is usually expressed in terms of liberation or particle size distribution of the product. The optimal operating region is thus defined as the limits conducive to the best grind. It was decided to launch a trial where the mill would be controlled at various operating regions. More specifically, the tests would include a campaign to determine the mill load to % volume relationship and two optimisation trials to achieve these objectives. They are:

1. Defining the load to percentage volume filling % vol inside the mill. The literature refers to the grindcurves as a function of the mill's volumetric filling, instead of mill load. It is therefore critical that the load measurement to filling relationship be established. Powell and Mainza (2006) suggest that a minimum of three filling measurements are necessary to determine this relationship. The filling information is

obtained by means of crash stopping the mill and measuring the chord of the charge at the feed, middle and the discharge end of the mill. The load reading associated with this filling should usually be the average of the last 10 to 20 minutes before the mill is stopped. Note that the bearing lubrication oil pressure of the RPMA mill is a function of the load. The load is thus inferred from the oil pressure. According to Powell and Mainza (2006) (figure 3.2), the load/% vol relationship will typically be non-linear.

2. *Trial 1:* Determine the grind to % vol relationship. To achieve this, the mill will be operated at three different load high limits in order to obtain the grindcurve specified in figure 3.1.

3. *Trial 2:* Determine the effect of inlet water on grind at a certain % vol. Note that this trial is aimed at expanding the response surface on the inlet water axis. Both load and inlet water limits will therefore be moved as shown in figure 7.2.

The tests were structured as follows:

1. The various operating regions, specified by the load and inlet water high limits, were tested separately. The trials were only allowed to commence once a three point load to filling relationship had been established. Note that the load to % vol was validated by conducting a mass balance around the milling circuit. The volume filling was thus calculated by integrating the accumulation inside the mill.

2. Three conditions were tested per trial. Each operating condition, defined by the respective set of limits, should be at least three standard deviations apart (see figure 7.1).

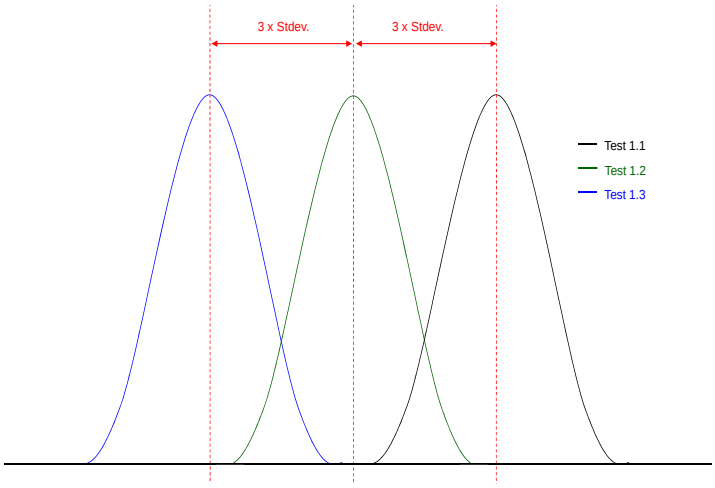

Figure 7.1: The proposed trial limits should adhere to a difference of three times the normal operating standard deviation as obtained in section 6.5.3

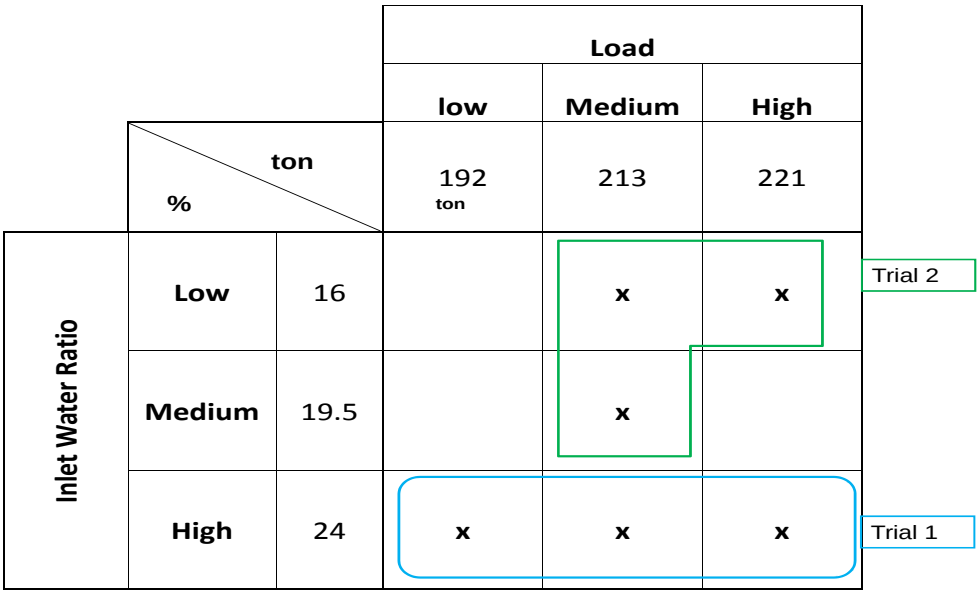

Figure 7.2: A 2-dimensional representation of the grind response surface that will be tested

3. The limits assigned to the test groups for load and inlet-water ratio can be seen in figure 7.2.

4. It was suggested that each trial continues until:

   - a statistical significance with a 95 % confidence disproving a zero-difference hypothesis between the three conditions is achieved, or
   - until a maximum of four cycles (2 days per set load or inlet water) of successful running data were collected (5 cycles $\times$ 5 samples $\times$ 3 groups samples per day = 75 grind samples or 25 samples)

5. During the trials the following conditions needed to be achieved before a sample could be considered as valid:

   (a) The coarse ore ratio must remain constant. A fixed coarse ore ratio based on silo management was suggested for the duration of each trial

   (b) Upstream conditions must remain similar if the tests were to be considered comparable. The feed size in cumulative percentage passing 45 mm was be used as an indicator of upstream stability

   (c) Trial 1: Water ratio must remain constant at a predetermined limit at a standard deviation similar to that mentioned in section 6.5.3

   (d) Trial 2: Load must remain constant at the predetermined limits for the duration of the trial at the standard deviation mentioned in section 6.5.3

6. The trials commenced on 14 February 2011 but were interrupted on 17 April 2011. The trials recommenced on 1 July 2011 and were concluded by 15 July 2011. A complete trial schedule can be found in appendix A.

7.2 Response Surface Analysis

7.2.1 Load to percentage volume filling % vol

Three mill crash stops was conducted during December 2010 and February 2011 to determine a load to % vol relationship. The % vol results obtained during these stops indicates that an exponential equation better describes the relationship than a linear model (figure 7.3). An R^2 of 97.4 % was obtain using the $Load = A - Be^{-C.\%vol}$ model. The linear model obtained a lower R^2 value of 93 %. Note that although a quadratic relationship will result in a perfect fit for the three data points, it is however not possible for the load to decrease as the volume filling increases as will be the case after the parabola's peak.

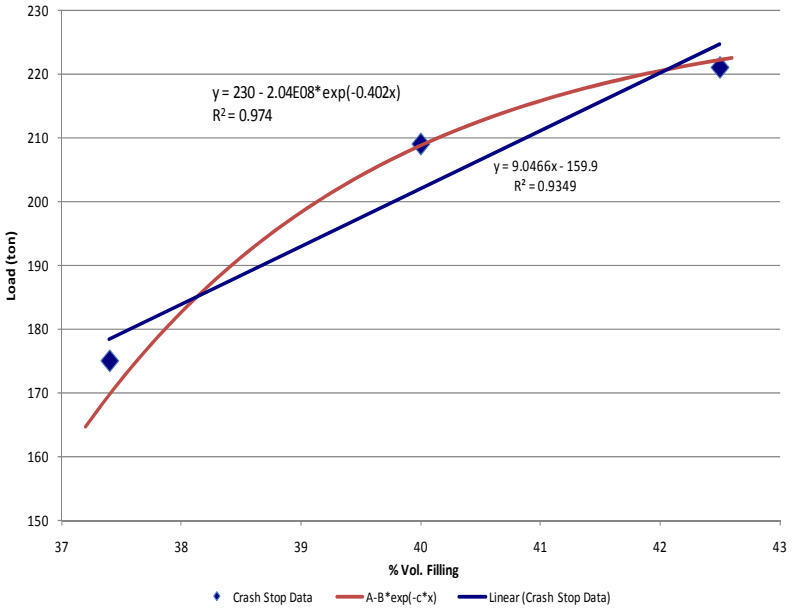

Figure 7.3: The exponential(red) and linear(blue) representation of the load to $\%vol$ relationship based on mill crash stop data

Due to the expense of a crash-stop, only three measurements were possible during the time provided. It was therefore necessary to validate the two models by means of a mass balance around the circuit with the aim of obtaining the volume inside the mill. Due to instrument inaccuracies, this method may not be the best to obtain the mill's volumetric filling. It will however provide an indication of the validity of the crash stop load/%

vol models. The mass accumulated inside the mill is obtained by constructing mass balance boundaries around the mill, classification screen and flotation feed surge tank (use figure 7.4). Note that subscript s and w indicate the solids and water fraction of the stream:

Boundary 1: Mill Assuming negligible bleed mass flow and no accumulation in discharge vessel,

$$Acc_{mill} = F + R + Iw - Md \tag{7.1}$$

with F measured by weightometer on feed conveyor belt and Iw measured by flow meter. $Md = D$ as per assumption.

Boundary 2: Classification Screen Assuming zero accumulation of the screen and no water in R,

$$R = D_S - Sc_S \tag{7.2}$$

with D_S measured by flowmeter and densitometer in stream.

Boundary 3: Rougher flotation feed surge tank Assuming perfect mixing,

$$Acc_S = Rf_S - Sc_S \tag{7.3}$$

with Acc_S measured by means of level in surge tank and densitometer in Rf and Rf_S measured by flow and densitometer. Note that $Sc = Sc_S + Sc_W$.

The derived mill load DL is then calculated by means of integration – note that one minute sampled data are used and that all flows are in m^3/h:

$$DL = \frac{1}{60} \int Acc_{mill} \tag{7.4}$$

The volume filling by means of the mass balanceV_{MB} is calculated using the in-mill density ρ_m calculation, assuming two species inside the mill, large rocks at an SG of $\rho_r = 3.6$ and pulp at a density exiting the mill ρ_p. The latter is obtained via a mass balance around the mill and discharge vessel. ρ_m is derived as follows: The total volume of the charge

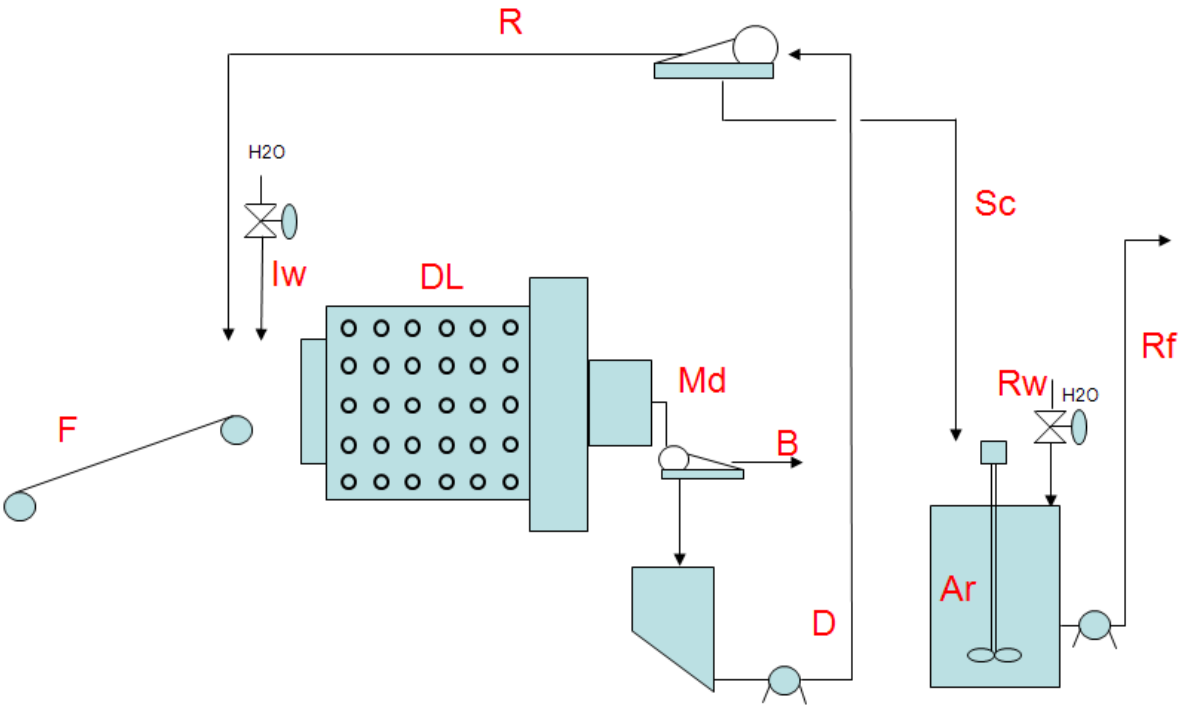

Figure 7.4: Milling circuit with streams labelled as used in the circuit mass balance

inside the mill V_m is equal to the volume of rocks V_r and pulp V_p,

$$\begin{aligned} V_m &= V_r + V_p \\ \frac{M_m}{\rho_m} &= \frac{M_s}{\rho_s} + \frac{M_p}{\rho_p} \\ \frac{1}{\rho_m} &= \frac{x_s}{\rho_s} + \frac{1 - x_s}{\rho_p} \end{aligned}$$

$$\therefore \rho_m = \frac{\rho_s \rho_p}{x_s(\rho_p - \rho_s) + \rho_s} \tag{7.5}$$

The volume of the mill by means of mass balance, calculated using the in-mill density approximation with a 40 % large rocks 60 % pulp fraction:

$$V_{MB,m} = \frac{1}{\rho_m} DL \tag{7.6}$$

The mill volume filling obtained by calculation and crash stop models was compared with data from the morning shift of 21 February 2011. Both the exponential and linear models resulted in a trend relatively close to the in-mill density approximated version of the volume, remaining within approximately 1 % of $V_{MB,m}$. Taking into consideration the high amount of variability, measurement noise and the stochastic nature of the mill, the load/% vol models based on the crash stops are considered accurate enough to be used in subsequent trials. The response surface of the mill, in terms of grind, can thus

be expressed, similarly to the literature, as % vol and inlet water ratio. However, since the load is measured continuously and is used as a CV in the controller, it was decided to continue using load rather than the derived volume. It is however, still valuable to consider that the mill is being operated within the 40 % to 45 % (or 208 ton to 225 ton) region which, according to the literature is where the mill reaches its power peak. It is also the region where a volumetric overload of the mill occurs. Note that both the medium and high load conditions for trial 1 and 2 are conducted within this region. This indicates that the trials will most likely obtain the power peak and hence the grind peak at a particular throughput.

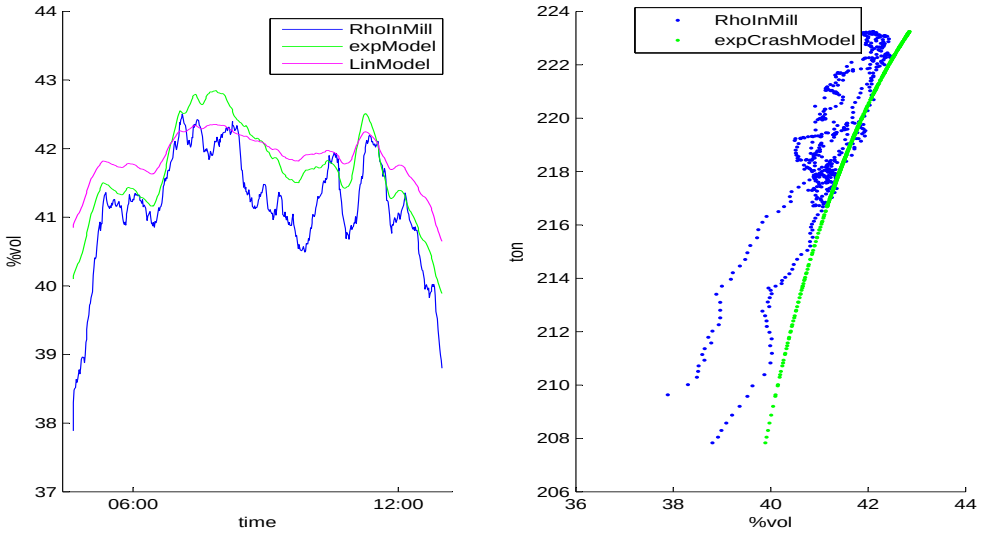

Figure 7.5: a) The mill volumetric fill based on in-mill density (blue), exponential fit(green) and linear fit (magenta) of the crash stop data. b) The load-to-% vol relationship based on in-mill density (blue) and the exponential fit (green)

7.2.2 Trial 1: Load

As mentioned before, the load high limits chosen for this trial are 221, 213 and 192 ton. The controller will however retain a safety margin of 10 % of the load limit range. The controller achieved average loads of 217.5, 210.7 and 191.1 ton at an average standard deviation of 2.5 ton for the entire trial 1. This equates to a % vol of 41.3 %, 40.2 % and 38.5 % volume filling respectively. The amount of successful samples that adhered to all trial conditions, feed at maximum 350 t/h, inlet water at maximum ratio 0.24 and similar coarse ore addition, are 23, 17 and 19 samples, respectively. The average grind obtained at these operating regions are 36.1 %, 36.9 % and 33.8 % respectively. Statistical significance with a zero-hypothesis of no difference between the average grinds was tested by means of an equal variance t-test. The zero-hypothesis between the 217.5 and the 191.1 ton as well as the 210.7 and 192 ton region was rejected with a 94 % and 96 % confidence interval

(one-tail) respectively. This magnitude is considered sufficient for the difference in grind to be significant. The confidence between the two higher load regions however produced a lower 70% (one-tail) confidence for zero-hypotheses rejection. Detailed results of these tests are shown in appendix B. The grindcurves which result from trial 1 suggest a 2nd order polynomial grind/load model:

$$G(L)|_{W_{rat}=0.24} = -0.011x^2 + 4.4x - 421.4 \tag{7.7}$$

With maximum grind obtained at $\frac{dy}{dx} = -0.022x + 4.4 = 0$ which equates to $V_{Grind,max} = 211.2$ ton mill load, or 40.3 % volume filling (see figure 7.6). The average power obtained at these operating regions also formed a parabola with maximum power of 2850 kW achieved to the left of $V_{Grind,max}$. This is contradictory to the literature, figure 3.1, where the power maximum is shown to the right of the grind peak. Due to the high standard deviation of the plot, this phenomenon can be an artifact of fitting and is not considered significant. The standard deviation of power during trial 1 averaged at 107 kW.

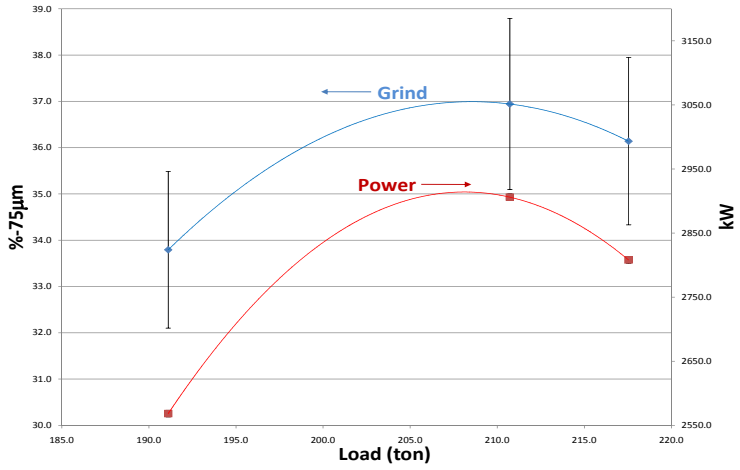

Figure 7.6: RPMA2 primary AG Mill grindcurves

7.2.3 Trial 2: Inlet Water Ratio – Response Surface

Effect of Throughput on Grind The maximum throughput was increased from 350 t/h to 370 t/h. An increased mass flowrate through the mill will result in lower residence times in the mill and hence an adverse effect on product particle size. In order to expand the response surface to include inlet water, the effect of throughput on grind must first be obtained. The method was as follows:

1. The throughput was modelled in a linear relationship to grind together with a

pure quadratic fit of load and inlet water. The starting coefficients for load were taken from the results of trial 1:

$$G = c_1 + c_2 \cdot W_{rat} + c_3 \cdot L + c_4 \cdot F + c_5 \cdot W_{rat}^2 + c_6 \cdot L^2 \tag{7.8}$$

The model produced a relatively poor fit with an R^2-value of 20 % and a mean-square-error of 0.84. The purpose of this model fit to obtain an indication of the steady-state relationship between throughput on grind to correct the samples recorded at a higher throughput. The relationship obtained: $\frac{\partial G}{\partial F} = -0.033$, that is, a 0.033 % loss in grind for every 1 t/h increase in throughput.

2. The next step was to normalise the grind data to 350 t/h using the throughput to grind relationship. The corrected versus actual grind is indicated in figure 7.7.

$$G'(L, W_{rat})\Big|_{F_0} = G(L, W_{rat})\Big|_{F} - \frac{\partial G}{\partial F}(F - F_0) \tag{7.9}$$

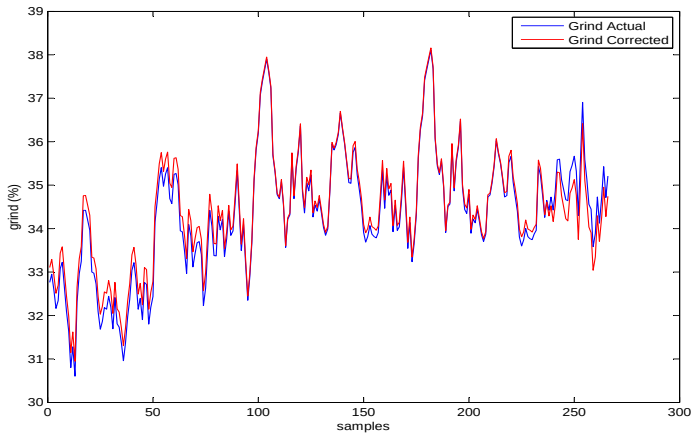

Figure 7.7: The corrected grind used to determine the response surface

The response surface of the load and inlet-water was then modelled to the corrected grind with all data normalised to a throughput of 350 t/h. The resulting model was obtained with a root-mean-square-error value of 1.06 % or 3 % relative to the mean of the grind (see figure 7.8 and 7.9). The pure-quadratic relationship of load and inlet water ratio on grind is given as follows:

$$G'(L, W_{rat}) = -0.0076 \cdot L^2 + 3.2 \cdot L + 266 \cdot W_{rat} - 592.48 \cdot W_{rat}^2 - 336.6 \tag{7.10}$$

The optimum point in terms of maximising grind, based on equation 7.10, is obtained at $\frac{\partial G}{\partial L} = 0$ and $\frac{\partial G}{\partial W_{rat}} = 0$ for load and inlet water ratio, respectively. This amounts to a load of $L_{opt} = 213$ ton and an inlet water ratio of $W_{rat} = 0.224$. It is thus concluded that

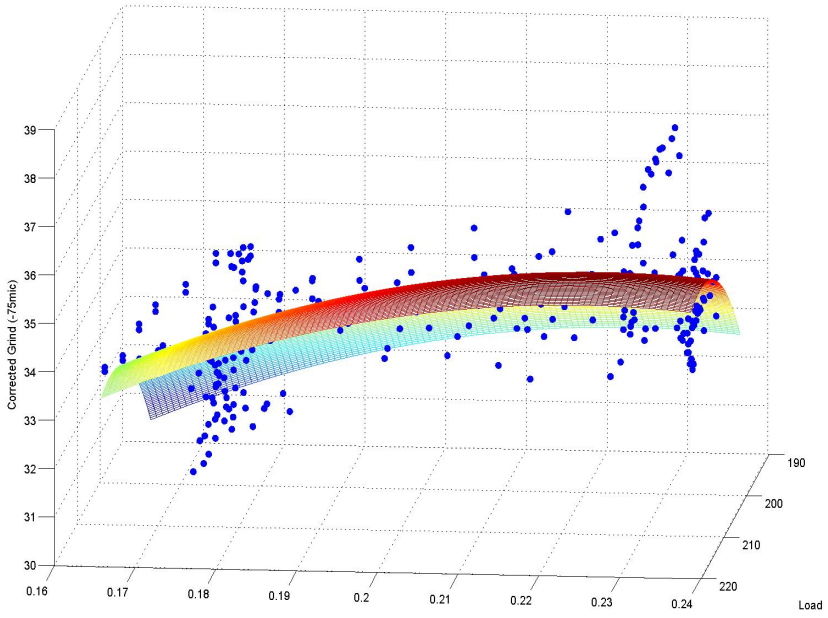

Figure 7.8: The 3-dimensional pure-quadratic response surface of load and inlet water ratio to grind

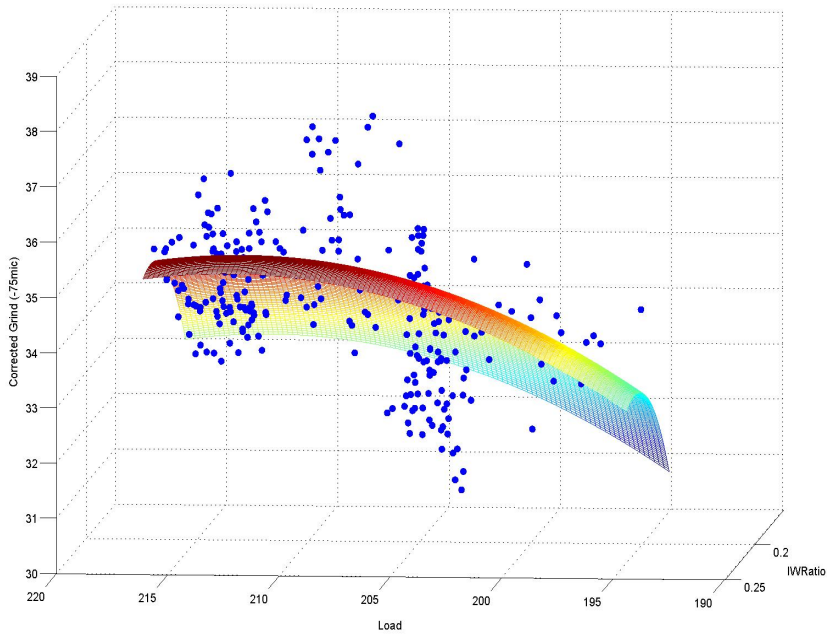

Figure 7.9: The 3-dimensional pure-quadratic response surface of load and inlet water ratio to grind

the mill will be operating at its maximum grind of 35.4 % passing -75 μm, for a specific throughput, at controller limits: L_{HI} = 216 ton and W_{rat} = 0.224. The 10 % safety margin that DMCplus^{TM} enforce on CVs are included in the load limit. It is important to note that this is only an empirical model, applicable to the primary mill and UG2 ore body of RPMA2 at a nominal feed rate of 350 t/h. Due to the seemingly high model error this optimum is not considered exact but rather an indication of the optimal operating region of the mill.

CHAPTER 8

Benefit Analysis

The purpose of this analysis is to determine the financial benefits achieved by stabilising the milling circuit at its optimum. This analysis can also be used to determine profitability of the milling circuit for future optimisation initiatives. The financial benefit of the milling circuit will be determined using the performance function method devised by Wei and Craig (2009b) as described by equations 5.7 and 5.8 in section 5.2.2.

8.1 Performance Functions

Profit Function The economic performance of comminution circuits is obtained by relating product grind to the performance of the downstream circuit (section 5.2). The economic consequence in terms of profit is thus defined by the effect of primary grind on PGM recovery in the flotation circuit. Due to numerous factors influencing the final PGM recovery of a concentrator, it was not possible to extract a representative model of the primary mill's product size to overall plant performance alone. The method used to obtain the effect of primary grind on flotation recovery is explained as follows:

1. The potential recovery to grind relationship for RPMA2 UG2 ore was obtained from laboratory test work (figure 8.1). Note that this grind represents the final grind and hence the final plant recovery by assuming perfect flotation operation. The test work does not include particle size distributions that cause the drop-off in recovery at finer grinds as mentioned in the literature (figure 5.4). The RPMA2 circuit however, achieves a final grind which is lower than 80 % passing 75 μm (coarser than that achieved in the laboratory test). It is therefore assumed that the recovery-grind relationship is linear within the operating region and that the circuit will not achieve grinds that will cause the recovery to decrease as the particles gets finer.

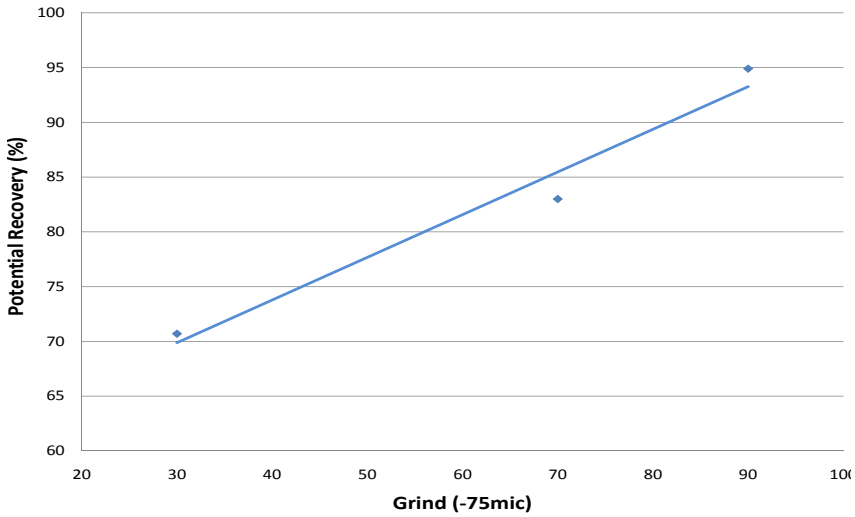

Figure 8.1: Potential PGM recovery at a specific grind measured as % passing 75 μm

2. The next step is to obtain a model between primary and final grind. As with recovery, modelling this relationship is difficult due to the large amount of variation of the measured grind (shiftly composite samples). Measured grind variation is mainly a result of sampling error, process variation and unmeasured variables (ore properties). A relationship was obtained by modelling the filtered versions of the two sets of grind data (see figure 11.22). A linear model was used which resulted in an RMSE of 1.5 % passing 75 μm (see figure 11.23) with the following model coefficients:

   - slope 0.87,
   - constant 35.8 % passing 75 μm

   The RMSE of the model relates to 20 % of the range of the filtered final grind and is therefore considered a poor model (figure 11.23). Due to the model quality, the relationship between primary and final grind remains an assumption rather than a proven fact.

3. The effect of primary grind G(L,IW) on potential recovery PR can then be deduced by means of convolution (figure 11.24 in appendix):

$$PR = 0.134 \cdot G(L, W_{rat}) + 79.61 \tag{8.1}$$

   with model boundaries:

$$185 < L < 230$$
$$0.13 < W_{rat} < 0.26$$

   $G(L, W_{rat})$ as obtained from the optimisation framework described by equa-

tion 7.10. The profit PF in terms of the main process variables are thus defined as:

$$Pr(L, W_{rat}) = \alpha \cdot PR \tag{8.2}$$

with $\alpha = \alpha_1 \cdot F \cdot HG$.
α_1 is equal to the monetary value of a gram of PGMs in the final concentrate at a certain grade c_i. F represents the amount of ore treated by the mill in ton per unit time and HG the head grade in g/t.

Cost Function As the purpose of this financial benefit model is to provide a metric to compare various optimisation or control strategies, only the operating cost will be included in the cost PF. Fixed costs are considered constant. Energy and grinding media are the two highest operating cost factors associated with comminution. As the RPMA2 primary mill is a fully autogenous mill, the economic effect of cost is defined only by the energy consumption of the mill. Note that the cost of liners and the performance of the discharge sump was not included in the scope of this benefit analysis and is considered negligible. The cost function is defined as follows:

$$C(L, W_{rat}) = -\beta \cdot P(L, W_{rat}) \tag{8.3}$$

Where β represents the cost of power in \$/kWh and,

$$P(L, W_{rat}) = \frac{\mathrm{d}P}{\mathrm{d}L} L + \frac{\mathrm{d}P}{\mathrm{d}W_{rat}} W_{rat} \tag{8.4}$$

The effect of load on power P is described by the parabola obtained during trial 1 with $\frac{\mathrm{d}P}{\mathrm{d}L} = -2.39L + 497.4$ kW/ton (see figure 7.6). The inlet water ratio to power relationship is obtained from the linear step-response model where the steady-state gain represents $\frac{\mathrm{d}P}{\mathrm{d}W_{rat}} = 43$ kW.

Overall Performance Function Equations 5.6 and 5.7 state the overall financial performance of the milling circuit can be defined as (note that the Ψ in these equations are represented as the potential nett profit PNP):

$$PNP = \alpha \cdot PR(L, W_{rat}) f(L, W_{rat}) + \beta \cdot P(L, W_{rat}) f(L, W_{rat}) \tag{8.5}$$

With $PR(L, W_{rat})$ described in terms of grind by equation 8.1 and $P(L, W_{rat})$ by equation 8.4. The probability density function PDF of the grind is defined by the PDF of the load and inlet water ratio which relationship was found to be quadratic (section 7.2). This differs from the literature where the financial impact of load is described as a piece-wise performance function.

8.2 Comparing Financial Performance

One of the main objectives of this dissertation is to determine the financial benefit of stabilising and optimising the primary milling circuit. The potential net profit PNP performance function (equation 8.5) indicates that only load and inlet water ratio are necessary to determine financial impact. Considering that the recovery of the subsequent processes in the value chain are about 98 %, any losses in PGM recovery due to sub-optimal milling performance will be considered as a loss of final refined metal. Comparing financial performance in terms of minimising PGM losses in the concentrator, α_1 is considered a function of basket price of refined PGMs, less the operating cost to treat the additional recovered material in the subsequent smelting and refining processes. These cost are confidential. For the purpose of this dissertation, α_1 was assumed to be \$1500 per ounce of PGM. The price of power supplied to the mill is about \$0.1/kWh. β is thus equal to \$876/kWa. Note that at a throughput of 210 kton per month and given the undisclosed PGM head-grade of RPMA, $\alpha \approx 10^5\beta$. The highest financial benefit is achieved at the maximum grind and hence potential recovery.

The financial benefit is derived by considering the impact of load and inlet water ratio separately:

Financial Benefit - Load As mentioned in sections 6.4 and 6.5.3, the standard deviation of the load was reduced from 6.8 ton to 2.3 ton with the implementation of the MPC. The financial impact of this project in terms of load is estimated by comparing the following three scenarios at the optimum $W_{rat} = 0.224$:

1. The benchmarked plant with load at a mean of 204 ton and standard deviation of 6.8 ton .
2. The benchmarked stability at the optimum load, a mean of 213 ton and at deviation of 6.8 ton.
3. MPC's performance at the optimum load, a mean 213 ton and a deviation of 2.3 ton.

A grind increase of 0.56 % passing 75 μm or a potential recovery increase of 0.1 % from 87.2 % to 87.3 % was observed by moving the load mean from 204 ton to the optimum 213 ton (comparing scenarios 1 and 2). A further 0.35 % passing 75 μm grind or 0.05 % PR increase was observed when reducing the load variance around the optimum from 6.8 ton to 2.3 ton (comparing scenarios 2 and 3). As the power peak is left of the grind peak on the grind curves, power draw was decreased moving towards the optimum load and recorded at 2885 kW, 2840 kW and 2830 kW for scenarios 1, 2 and 3 respectively. Figure 8.2 illustrates how the financial impact manifests by reducing the operating region of the mill and then moving it higher up

on the PNP surface. The PNP increase was calculated as $24.3 million per annum by moving to the optimum point and increased by a further $15.0 million per annum increase after reducing variance at the optimum. This equates to a financial benefit of $39.3 million per annum.

In order to interpret the benefits analysis plots in figures 8.2, 8.3 and 8.4, it is important to note the following:

- Due to the high amount of noise in the data, the correlations presented in these plots could not be considered exact. The distributions of the parameters power, potential recovery and grind were thus assumed to be independent.
- The contour of the various scenarios on all the power to potential recovery plots, represents the 80 % confidence interval of the relative distribution.
- A one standard deviation distribution of the exact model value is presented as a dotted line in the colour of the respected scenario on the power to recovery contour plot.

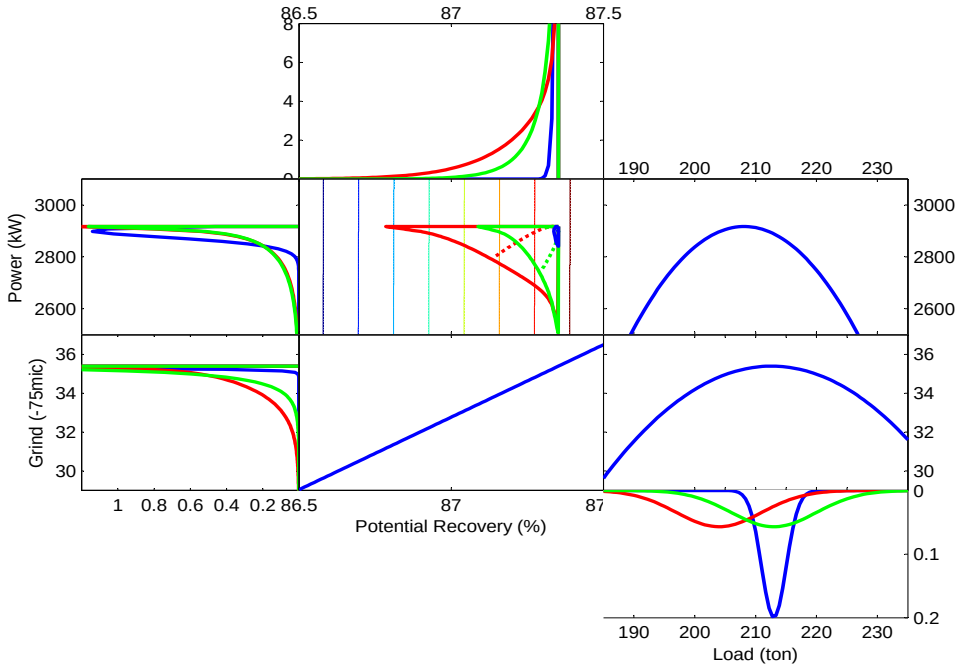

Figure 8.2: Comparing the potential financial benefit of the a) benchmarked plant (red), b) benchmarked controller performance at the optimum load (green) and c) the performance of the MPC at the load optimum (blue). The contours on power-recovery represents the 80 % confidence intervals

Financial Benefit - Inlet Water Ratio Since no significant difference in water ratio variability was observed (W_{rat} standard deviation difference of 0.001 is considered negligible), the financial benefits for water will be estimated by investigating two scenarios both at the optimum load of 213 ton:

1. At the benchmarked inlet water ratio mean of 0.178,
2. the optimum inlet water ratio, $W_{rat} = 0.224$

A grind increase of 1.3 % passing 75 μm from 34.0 % to 35.3 % was observed by increasing the inlet water to the optimum. This results in a PR increase of 0.17 % from 87.17 % to 87.33 % and an increase on the PNP curve as illustrated in figure 8.3. The resulting financial benefit of a 0.17 % increase in PR was estimated at an increase of $53.8 million per annum.

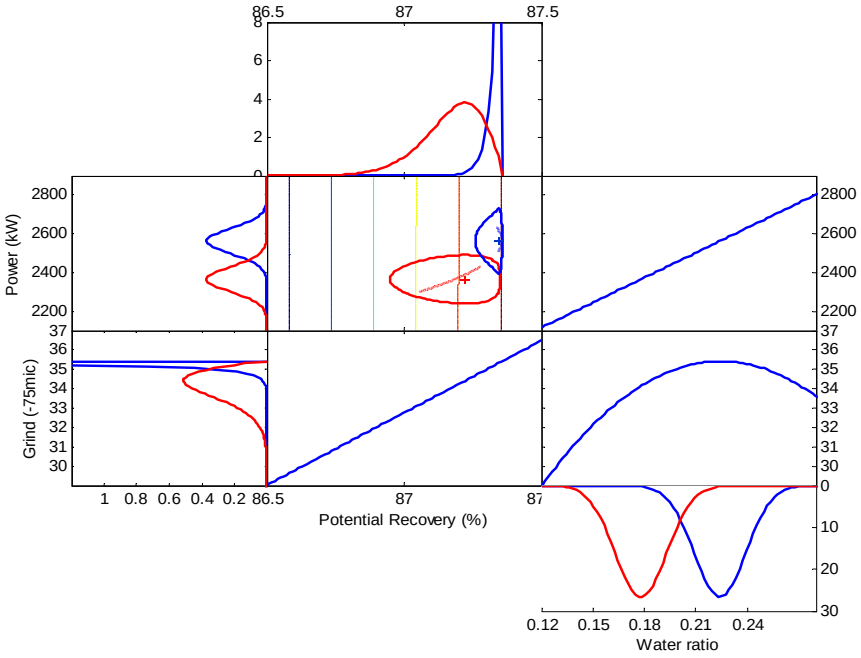

Figure 8.3: Comparing the potential financial benefit of the a) benchmarked plant (red) and b) MPC at the inlet water ratio optimum (blue). The contours on power-recovery represents the 80 % confidence intervals

The total grind increase observed by moving the load and water ratio mean to 213 ton and 0.224 respectively and stabilising load at a standard deviation of 2.3 ton was calculated at 2.2 % passing 75 μm. This equates to a potential recovery increase of 0.31 %. By assuming the price of PGMs in the final concentrate is $1500 per ounce, a total potential nett profit increase of $93.1 million per annum is made possible by this AG milling optimisation project.

8.3 Power Crisis Scenario

All of the above results were obtained at the current price of power which is negligible when compared to the benefit of increased recovery. A scenario where the price of power

is increased to a point where $\alpha \approx 10^3\beta$ is simulated. The objective of this section is to determine the financial impact of such an increase in cost and to obtain a revised optimum point in load and inlet water. The load region conducive to minimum power usage and hence maximum financial benefit is obtained at the highest load possible (demonstrated in figure 8.4). Considering that a 230 ton load is a physical constraint to the mill, a mean of 225 ton will ensure that this limitation falls outside the 98 % confidence interval. The optimum inlet water ratio is obtained at the lowest possible value, that is, just above the point where transport through the mill and production rate (area C in figure 3.4) stops.

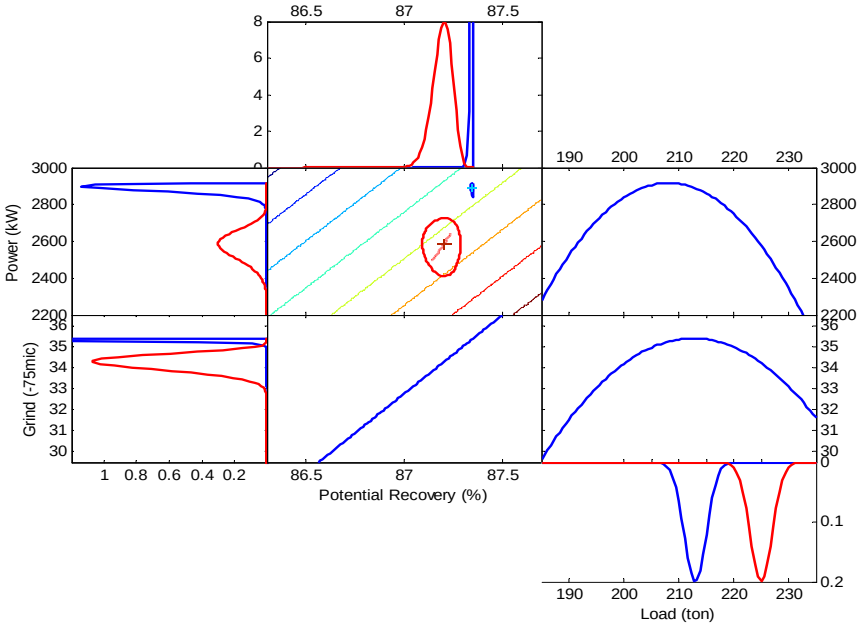

Figure 8.4: Comparing operating regions for load during a power crisis where $\alpha = 10^3\beta$. The contours on power-recovery represents the 80 % confidence intervals

CHAPTER 9

Conclusions and Recommendations

9.1 Modelling

A dimensional analysis was conducted on the AG mill using only measured parameters reported in the literature as having an effect on the system. The results showed that:

- the power draw of the mill is correlated to the speed and load of the mill,
- the uncorrelated inputs satisfied Buckingham's theorem which indicates that a complete subset of dimensionless groups was present
- the behaviour of the mill can be explained by the inputs used in the dimensional analysis

The dimensional analysis provided the platform to launch a step test campaign from which the dynamic step-response models were derived. The step-response models reported that the circuit has a 60 min time to steady state and that the load is an integrator. Inlet water ratio and mill feed rate have the highest scaled effect on power while speed showed the most significant effect on load

9.2 Control

A model predictive controller that utilises the step-response models was implemented and commissioned. The objective function of the controller was designed to minimise effective power utilisation. To do this, the controller will move the MVs, in the following way, until its three degrees of freedom are saturated (in order of importance):

1. maximise throughput within the ore supply limits
2. minimise mill speed
3. minimise inlet water ratio

The controller managed to improve the circuit stability by reducing the standard deviation of the mill load and power by 66 % and 40 % respectively. The load frequency spectrum indicates that the load converges on its theoretical minimum variance benchmark without increasing MV movement. The controller managed to reduce the average of its online objective function, effective power utilisation by 11 %.

9.3 Optimisation

A test campaign to obtain the mill's grindcurves was conducted and completed. The test results enabled the construction of the primary mill's load to percentage volume filling, power to load, grind to load and grind to inlet water relationships. At a maximum throughput of 350 t/h, as dictated by the ore supply, a maximum grind of 35.4 % passing -75 μm is achieved at a load of 213 ton and an inlet water ratio of 0.224.

9.4 Benefit Analysis

The total potential financial impact of this AG mill optimisation project was estimated at $93.1 million. This was achieved by:

- moving the load from an average of 204 ton to 213 ton ($24.3 million)
- stabilising the load at the optimum grind by reducing the standard deviation from 6.8 ton to 2.3 ton ($15.0 million)
- moving the inlet water ratio average from 0.178 to 0.224 ($53.8 million)

9.5 Recommendations

The following issues were identified as possible areas of improvement on this dissertation:

- Expand the dimensional analysis to include variables not measured online, for example, Bond's work index, in-mill viscosity and various mineralogical characteristics of the ore body (mineral components, grain size)
- Conduct an error analysis on all the models presented in the investigation. This will help to better define the confidence of the resulting economic benefit.
- The relationship between secondary and primary grind proved to be a weakest link in the argument for economic benefit. Further investigation should be conducted to better define this relationship. Such an investigation should include better modelling techniques, data filtering to exclude data during sub-optimal plant performance.

Adding additional key performance indicators such as secondary milling efficiency should improve this model.

- Investigate the effect of load and inlet water ratio on the wear of the primary mill's liners. The aim of this will to include this seemingly major cost in the economic assessment of the process.

CHAPTER 10

Appendix A

This appendix is reserved for additional material use during the literature study (sections 2, 3, 4 and 5)

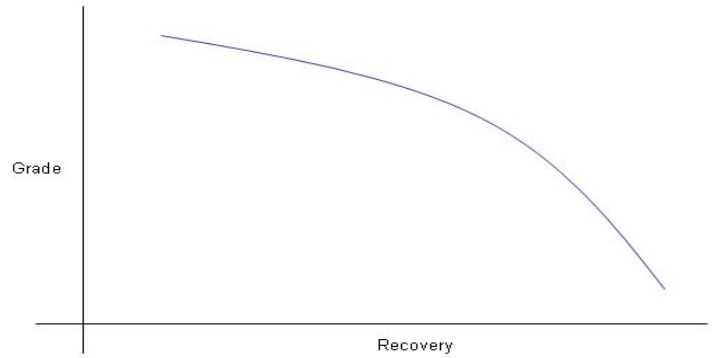

Figure 10.1: The typical grade recovery curve (Hayes, 2003):68.

10.1 Regulatory Control

10.1.1 Description

A typical industrial plant is controlled in a hierarchical structure divided into the supervisory/advanced control layer and the regulatory/base control layer (Skogestad and Postlethwaite, 2005). The supervisory layer contains the optimisation algorithm that provides a setpoint SP to the regulatory control which is then tasked to have the process variable PV track this value by actuating a control output OP. The proportional-integral-derivative PID is the most commonly used regulatory control algorithm in industry since its inception in 1940 (Marlin, 2000). The block diagram of a feedback control system, as discussed in Luyben (1990), Marlin (2000), Skogestad and Postlethwaite (2005), can be seen in figure 10.2.

As its name suggests, the PID loop consists of proportional, integral and derivative elements. The fist mode of action is proportional to the difference between process y

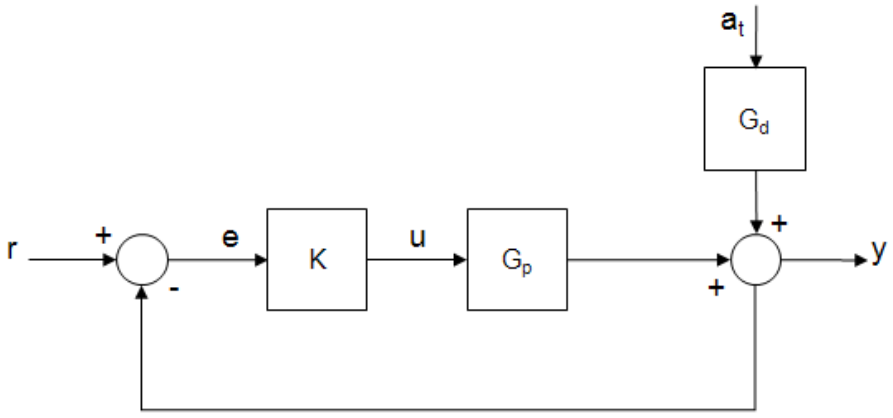

Figure 10.2: A block diagram of a typical SISO feedback control system

value and reference r. As this error e increases, so does the movement of the manipulated variable u increase. The proportional mode or controller gain K_c is hence in units [u]/[y]. Since proportional action decreases with e, it does not provide zero offset between y and r. The next element provides MV movement until the steady-state magnitude of the error is reduced to zero. Controller action is faster for a given e as the integral time τ_i is reduced. The derivative element of the controller keeps track of the velocity of y movement. If e is almost zero but y starts to move away from r, fast MV movement is justified and generated by the derivative mode of the controller. Derivative mode compensates for process lag and is used in systems where tight dynamic response is necessary. The Laplace domain representation of the PID controller is given as follows. Note that this ideal form is not physically realisable:

$$K(s) = K_c \left(1 + \frac{1}{\tau_i s} + \tau_d s\right) \tag{10.1}$$

10.1.2 Advantages

1. The controller is simple to understand and easy to maintain and tune
2. Due to the fact that the PID algorithm was developed decades ago, its resource intensity in today's digital environment is fairly low
3. Very well suited for single-input single-output SISO systems without dead-time

10.1.3 Disadvantages

1. The PID algorithm is not suited for a multi-variable environment
2. It struggles in controller circuits with extended dead-times

3. Not suited for non-linear systems

10.2 Fuzzy Logic/Expert System Control

10.2.1 Description

Fuzzy logic was introduced in the 1960's by Lofti Zadeh as a way to translate non-statistical, linguistic statements into precise mathematical language (v Lith, 2002; Johnston, 1998; Scheffer, 2001). The objective of this technology is to distill and translate the human operator's experience into deterministic control rules. The fuzzy logic method provides a framework for the characterisation and capture of human expert knowledge and decision making. Fuzzy logic can also be described as a reasoning method based on Boolean logic that defines a certain process state and direction. The controller consists of a sequence of statements that connect a set of process beliefs to a crisp control action. The process beliefs are called the antecedent while the action is known as the consequent. The statements that connect them are rules usually of the form IF-THEN. This structure, as illustrated in figure 10.3, forms the basis of the fuzzy controller.

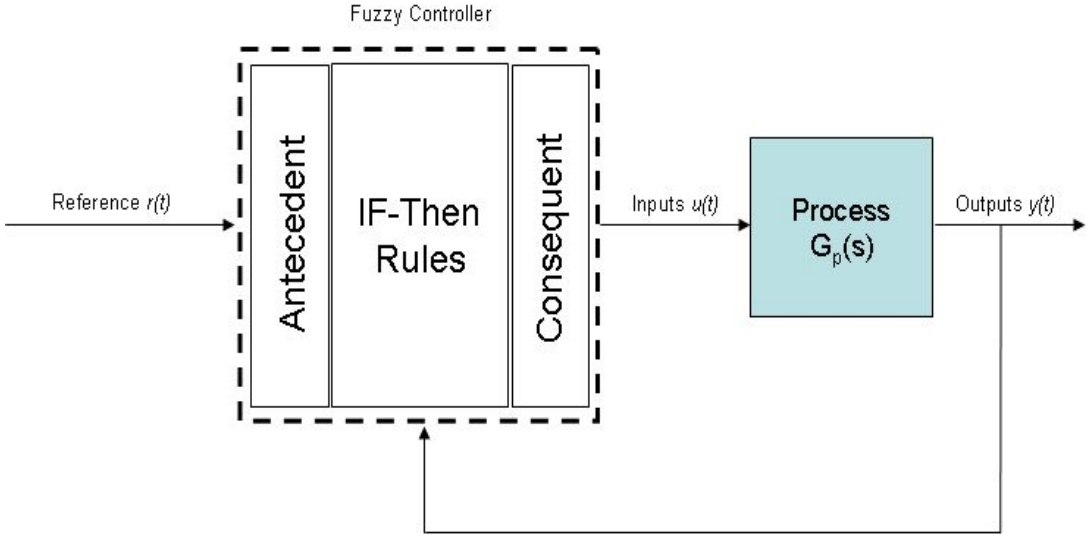

Figure 10.3: A block diagram of the basic fuzzy logic controller

Antecedents The antecedents are presented as a series of fuzzy membership functions MF that translate process conditions into concepts such as power high, load increasing or sump level decelerating. These membership functions describe a concept in the form of a belief value (a degree of membership) between 0 and 1. The form of these mathematical translations is normally given as a series of trapezoids, sigmoid or triangles (shown in figure 10.4). For the example in figure 10.4, the belief or degree of membership B_n passed onto the rule set for the parameter μ_1 with a normalised

value of 0.65 will be as follows;
for $\mu_1 = 0.60$, B_1 (LOW) = 0, B_2 (OK) = 0.75 and B_3 (HIGH) = 0.25.

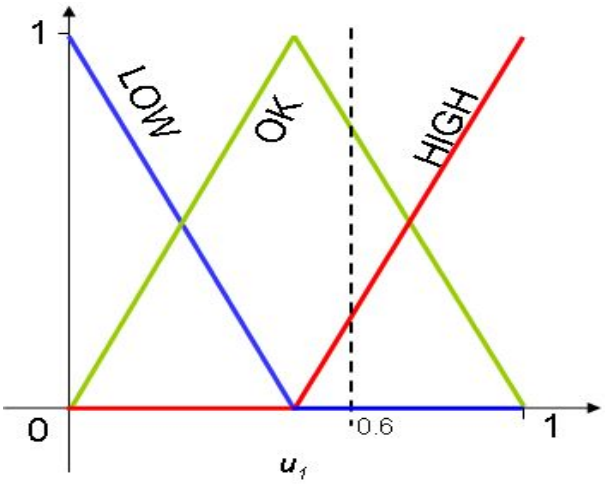

Figure 10.4: Example of a fuzzy membership function for parameter u_1

Consequent The rules that describe the linguistic knowledge are formulated to encompass all the possible permutations of every fuzzy membership of all the parameters taking part in the controller. The number of rules for a system with two input parameters (μ_1, μ_2), each with 3 members will therefore be 9. v Lith (2002) mentions that Linguistic Models (LMs) are the most common form of fuzzy rules and are formulated as follows:
For two antecedent parameters μ_1 and μ_2, the appropriate action (y) is assigned based on IF-THEN rules,

$$\textbf{IF } \tau_i \text{ is A } \textbf{AND } \tau_{i+1} \text{ is B } \textbf{THEN } y \text{ is } D_i$$

The process of extracting a crisp control move or output from a series of fuzzy sets and rules is also known as defuzzyfication. This output is formulated from the influence of the different rules in the LM. Each of these permutations (or rules), together with a the fuzzy degree of membership, is assigned to a specific defuzzy member D_i. This describes the degree of activation or the degree of firing (DOF) of the rule. For fuzzy members B_i and C_i for parameters μ_1 and μ_2 at values x_1 and x_2 respectively, the DOF for rule i is calculated as follows:

$$\tau_i = B_i(x_1) * C_i(x_2) \tag{10.2}$$

The output fuzzy set (F_i) for a specific rule is then determined by the rule's defuzzy sets $(D_i(\text{y}))$ and the DOF.

$$F_i(y) = \tau_i \wedge D_i(y) \tag{10.3}$$

Note that the defuzzy members are similar to the fuzzy members presented in figure 10.4 but for the following differences:

- Fuzzy members reference a process condition or direction while defuzzy sets refer to the output or action (manipulated parameters) of the process. Examples of defuzzy members are valve-opening decrease, pump-output increase or flow-rate no-action.
- Where the input to a fuzzy set is a crisp value and the output is a belief, the defuzzy receives a belief value and outputs a crisp absolute value

Note that several rules can be assigned to one defuzzy member. The inferred fuzzy sets are then aggregated to the final fuzzy set $F(y)$ by using only the members with maximum in $F_i(y)$.

$$F(y) = \vee_{i=1}^{n} F_i(y)) \tag{10.4}$$

Defuzzification that concludes an absolute, crisp control action y from the finalised fuzzy set F(y) can then commence by making use the Centre of Area (COA) method.

$$y^{COA} = \frac{\int y\mu \mathrm{d}y}{\int \mu \mathrm{d}y} \tag{10.5}$$

In the example presented in figure 10.5, fuzzy set F(y) was concluded with rules 1, 2 and 3 concluding the largest DOF for the respective defuzzy set $D_i(y)$ with members decrease (DEC), no-action(N-A) and increase(INC). The example demonstrates a controller with triangular defuzzies at peaks y = -5, 0 and 5 for members DEC, N-A and INC respectively. The F(y) fuzzy set $D_{DEC}(-5) = 0.2$, $D_{N-A}(0) = 0.4$ and $D_{INC}(-5) = 0.65$ will hence conclude an action of 1.2.

10.2.2 Advantages

1. The method makes use of existing process knowledge which makes an application easier to implement (Johnston, 1998)
2. High degree of robustness
3. Due to its simplicity and robustness, Fuzzy logic is very well equipped for non-linear, non-stationary systems with a high amount of unmeasured disturbance (Scheffer, 2001)
4. The method is independent of any process model and avoids cumbersome trail-and-error calculations associated with the empirical control examples

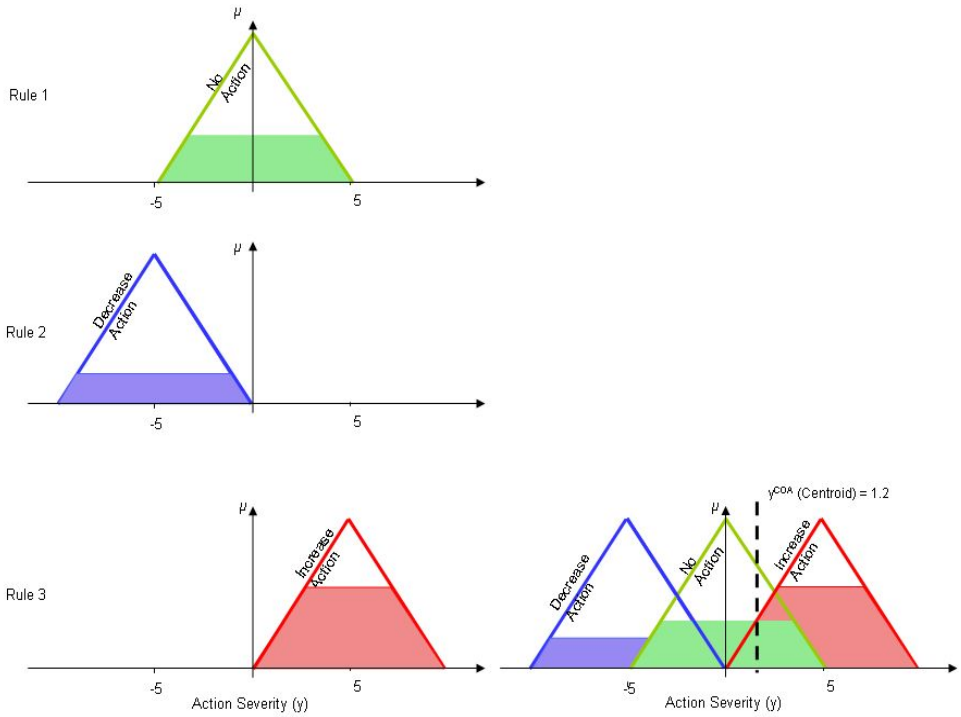

Figure 10.5: Example of a centroid (COA) calculation for parameter u_1

5. It is also effective for control lacking a describing function with vague, complex relationships.

10.2.3 Disadvantages

1. Due to the large number of rules, element weights, fuzzy and de-fuzzy members, the tuning and maintenance of such controllers can become complex and intensive.

2. As larger controllers can potentially result in an extreme high number of rules, the algorithm is usually limited to smaller applications

10.3 Fourier Transforms

Jean Baptiste Joseph Fourier claimed that any continuous signal can be described by the sum of a series of sinusoidal waves (Smith, 2002). The Fourier transform represents a family of mathematical techniques enabling the user to decompose signals into a series of sine and cosine functions. The Discrete Fourier Transform DFT is probably the most widely known member of this family that decomposes any discrete input signal into two output signals (a real and an imaginary part) containing the amplitudes at the respective frequencies. The DFT decomposes a discrete, continuous time domain signal $X[]$ with N samples into two parts, a real $ReX[]$ (cosine amplitudes) and an imaginary $ImX[]$ (sine amplitudes) part.

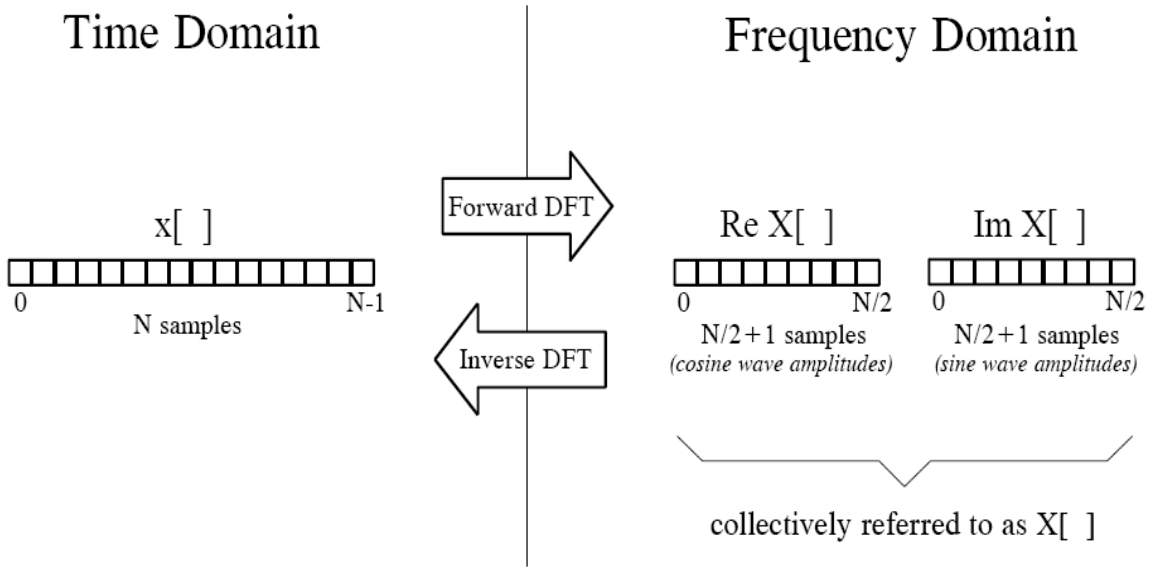

Figure 10.6: Decomposition of a time domain signal $X[]$ with N samples to two frequency domain parts $Re[X]$ and $Im[X]$ each with $N/2+1$ parts (Smith, 2002):147

This decomposition from the time domain to the frequency domain is done by defining a series of sinusoids or basis functions:

$$c_k[i] = \cos\left(\frac{2\pi ki}{N}\right), \quad s_k[i] = \sin\left(\frac{2\pi ki}{N}\right) \tag{10.6}$$

where $c_k[]$ and $s_k[]$ represent the cosine and sine wave amplitude held in $ReX[k]$ and $ImX[k]$ respectively. The parameter k equals the number of complete cycles that occur over the entire time domain with N amount of samples.

The next step to obtain samples in the frequency domain is to correlate the input time domain signal with each basis function. This leads to the formulation of the formalised analysis equation:

$$\begin{aligned} ReX[k] &= \sum_{i=0}^{N-1} x[i] cos\left(\frac{2\pi ki}{N}\right) \\ ImX[k] &= \sum_{i=0}^{N-1} x[i] sin\left(\frac{2\pi ki}{N}\right) \end{aligned} \tag{10.7}$$

To convert these basis functions' sinusoidal amplitudes Y into power spectral density Φ one needs to multiply by the complex conjugate of the sinusoidal amplitudes at a certain

bandwidth ω and divide by the number of samples N.

$$\Phi = \frac{1}{N} Y(\omega) Y^{\star}(\omega) \tag{10.8}$$

Bandwidth is defined by a frequency range of dividing lines between the samples in the frequency domain (see figure 10.7). For a frequency domain signal of 16 samples, 17 bandwidth ranges are defined; 2 with bandwidth $1/N$ and 15 of bandwidth $2/N$.

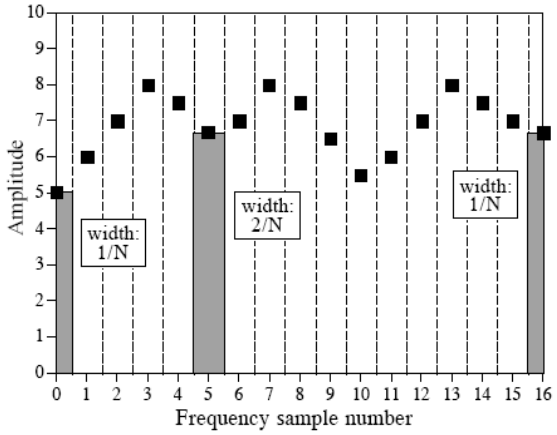

Figure 10.7: Bandwidth of frequency expressed as a fraction of the total bandwidth (Smith, 2002):156

Note that frequency can be represented in terms of:

- *fractions* $f = \frac{k}{N}$ (or samples - as shown in figure 10.7),
- the *natural frequency* $\omega = 2\pi f$ or,
- the *analog frequency*.

The analog frequency uses the sampling frequency of an application and presents the frequency in terms of real world meaning (Hz or samples per second).

CHAPTER 11

Appendix B

This appendix is reserved for additional material use during sections 6, 7 and 8

P_2	P_2	P_3	P_4	P_5	P_6
P_3	1.00	0.32	0.21	-0.01	-0.01
P_4	0.32	1.00	0.25	0.43	0.18
P_5	0.21	0.25	1.00	0.20	0.08
P_6	-0.01	0.43	0.20	1.00	-0.05
P_6	-0.01	0.18	0.08	-0.05	1.00

Figure 11.1: Correlation coefficients of the milling variables listed in table 6.1 but with power removed

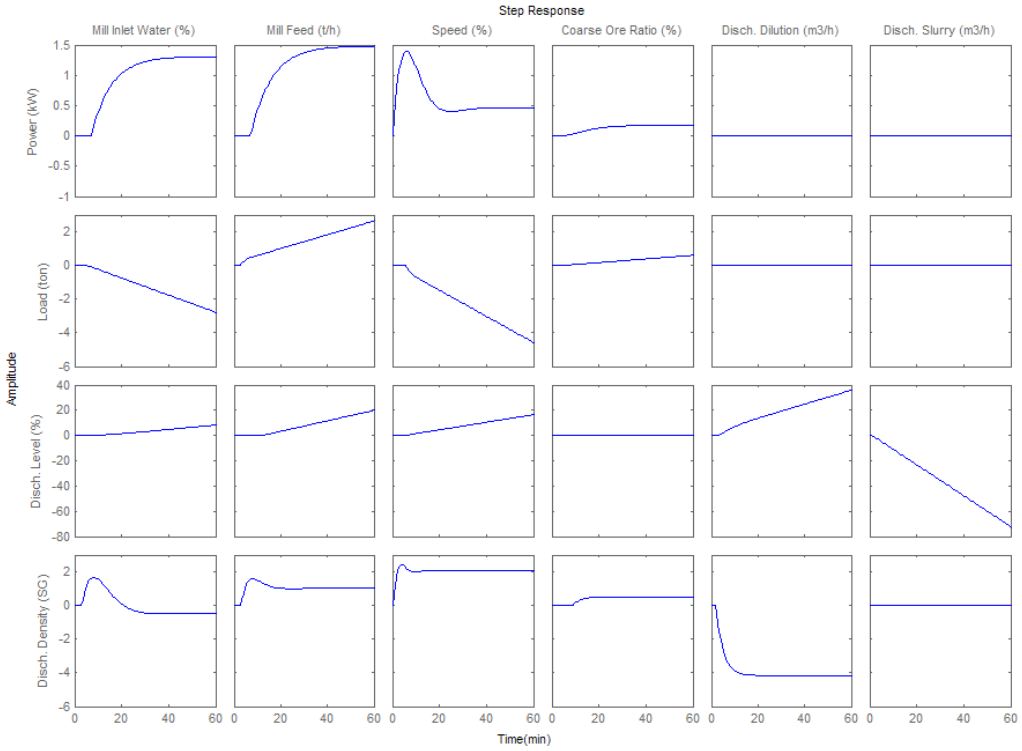

Figure 11.2: The scaled DMCplus^{TM} response matrix for the RPMA2 mill and discharge sump obtained from the September 2010 step campaign

	Time Constant (min)					Dead-time (min)				
	IWRatio	Feed	Speed	CORatio	FeedSize	IWRatio	Feed	Speed	CORatio	FeedSize
Power	8.5	9	20	42	8.5	7	7	0	4	4
Load	1	1	1	1	2	4.4	4	6	4	4

	Damped Coefficient					Lead Constant				
	IWRatio	Feed	Speed	CORatio	FeedSize	IWRatio	Feed	Speed	CORatio	FeedSize
Power	0	0	0.3	0.3	0	0	0	25	0	0
Load	0	0	0	0	0	0	8.5	6	0	0

Figure 11.3: The dynamic constants for the primary mill's step-models – obtained from the step campaign and DMCplus

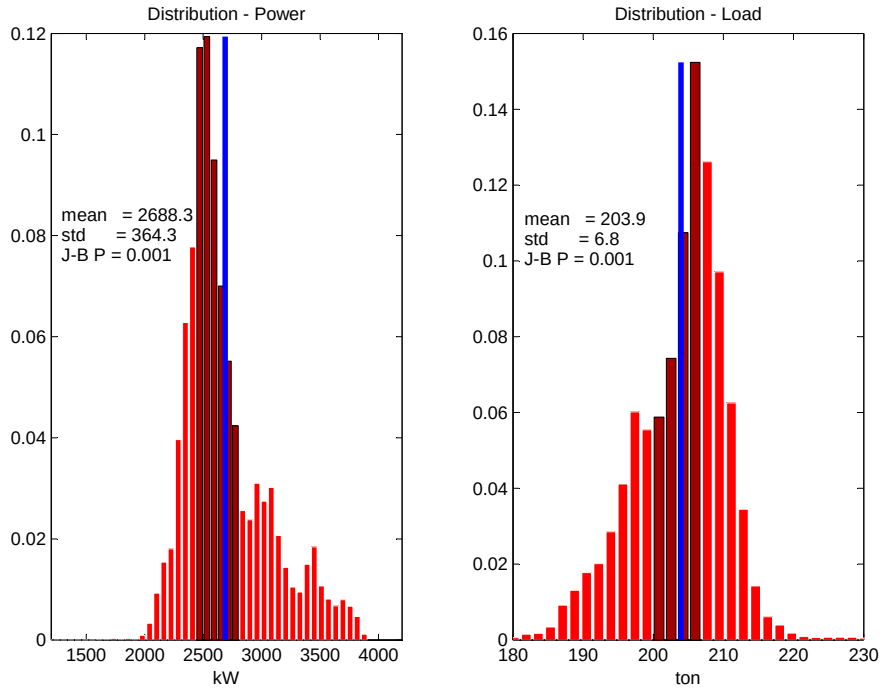

Figure 11.4: Distribution plot of the primary mill controlled variables a)power kW and b)load ton – 1 August 2010 to 9 September 2010

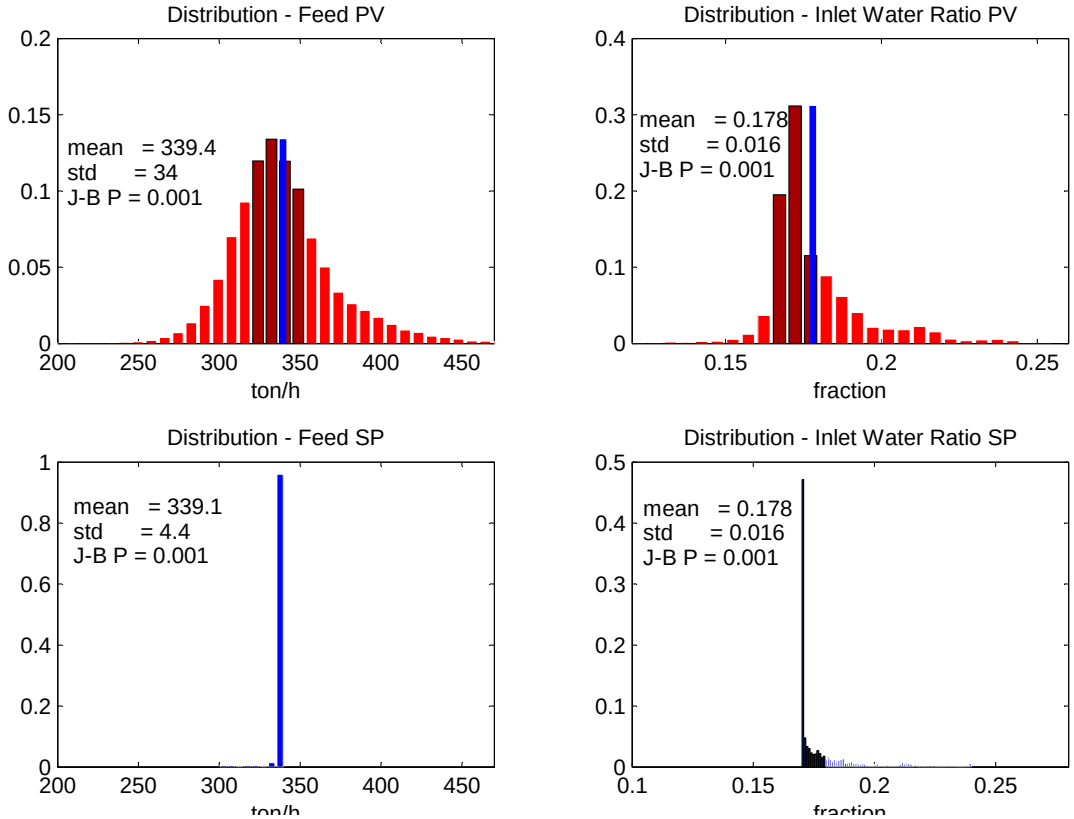

Figure 11.5: The distribution plot of the primary mill manipulated variables a+c)mill feed t/h and b+d)inlet water ratio – 1 August 2010 to 9 September 2010

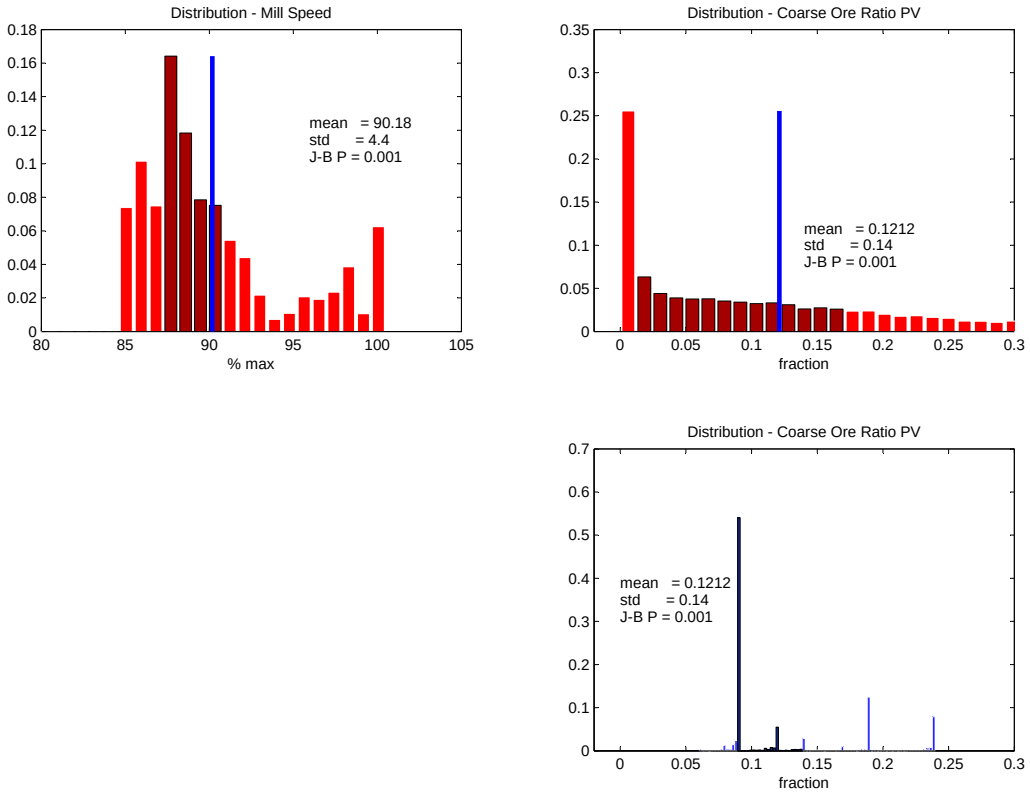

Figure 11.6: The distribution plot of the primary mill manipulated variables a)mill speed % maximum speed and b+d)coarse ore ratio – 1 August 2010 to 9 September 2010

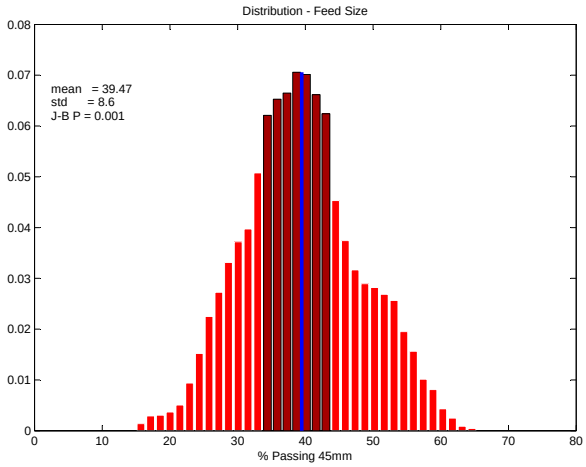

Figure 11.7: The distribution plot of the primary mill disturbance variable feed size %passing 45 mm – 1 August 2010 to 9 September 2010

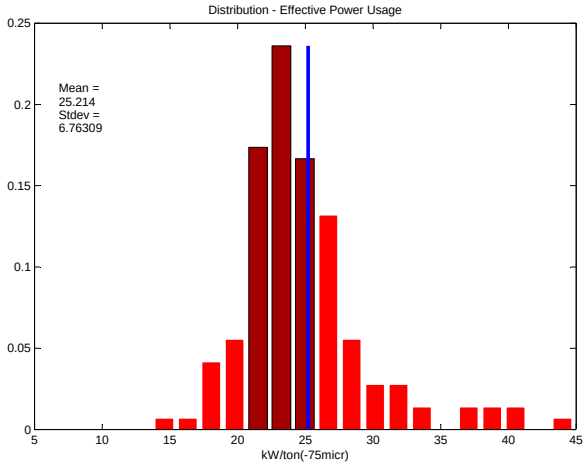

Figure 11.8: The distribution plot of the primary mill's effective power usage kWh/t-75μ m – 1 August 2010 to 9 September 2010

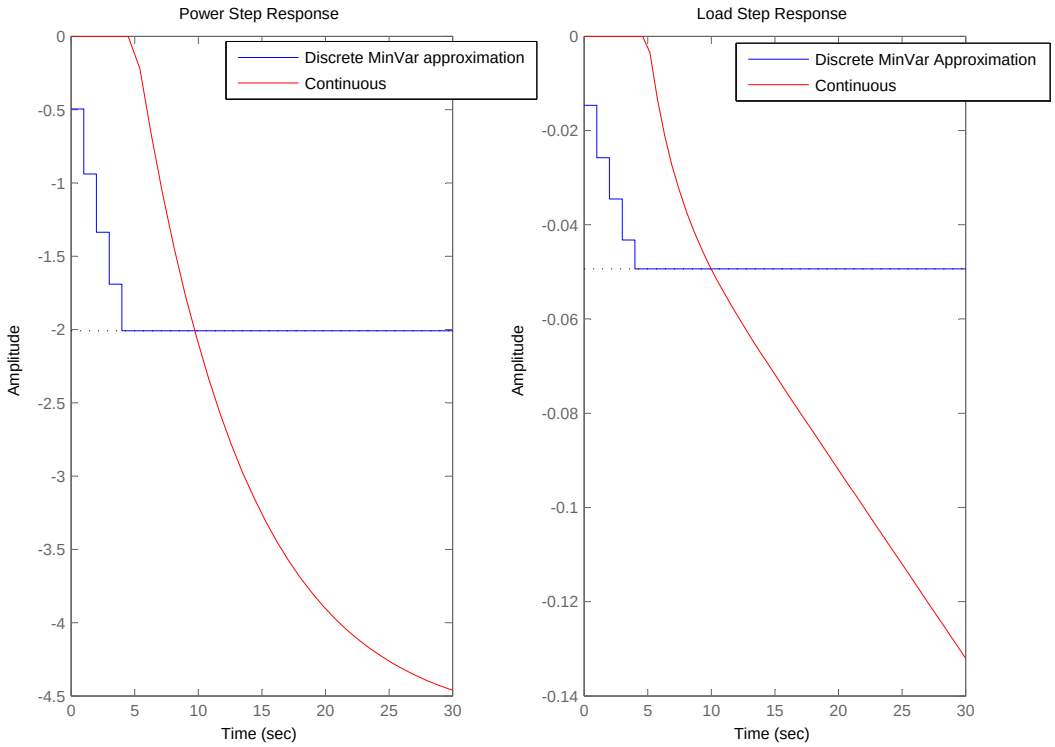

Figure 11.9: Discreet minimum variance approximation and actual model of the feed size to a)power and b)load

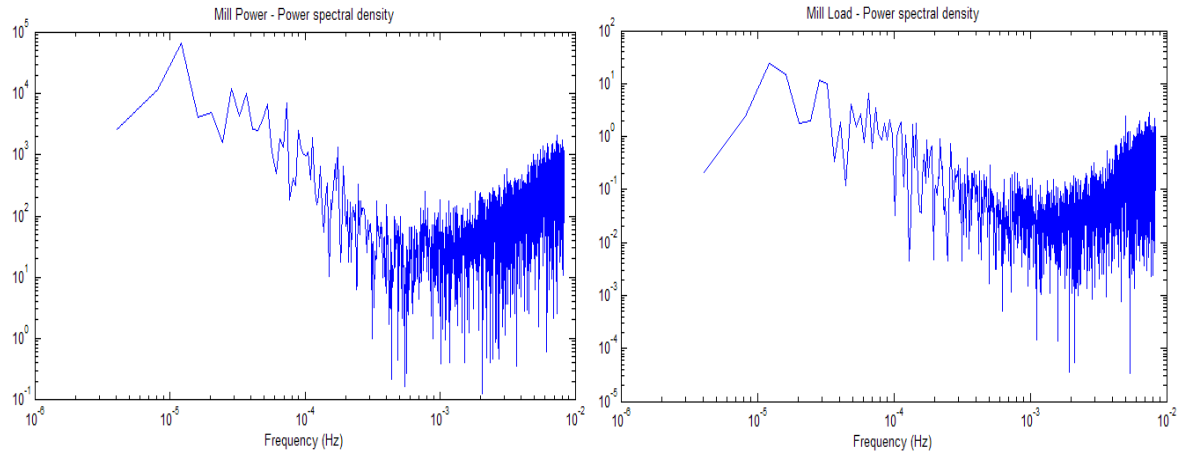

Figure 11.10: Power spectral density PSD plot of the primary mill controlled variables a)power kW and b)load ton – 1 August 2010 to 9 September 2010

Table 11.1: Tabular representation of the RPMA2 primary mill response matrix in the Laplace domain

	MIW Ratio(%)	Feed (t/h)	Speed(%)	CO Ratio(%)
Power(kW)	$\frac{43.7e^{-7s}}{8.5s+1}$	$\frac{2.97e^{-7s}}{9s+1}$	$\frac{11.42(25s+1)}{20s^26s+1}$	$\frac{2.97e^{-7s}}{9s+1}$
Load(ton)	$\frac{-0.085e^{-4.4s}}{s(s+1)}$	$\frac{-0.0041(8.5s+1)e^{-3s}}{s(s+1)}$	$\frac{-0.097(6s+1)e^{-6s}}{s(s+1)}$	$\frac{-1.81e^{-3s}}{s(s+1)}$

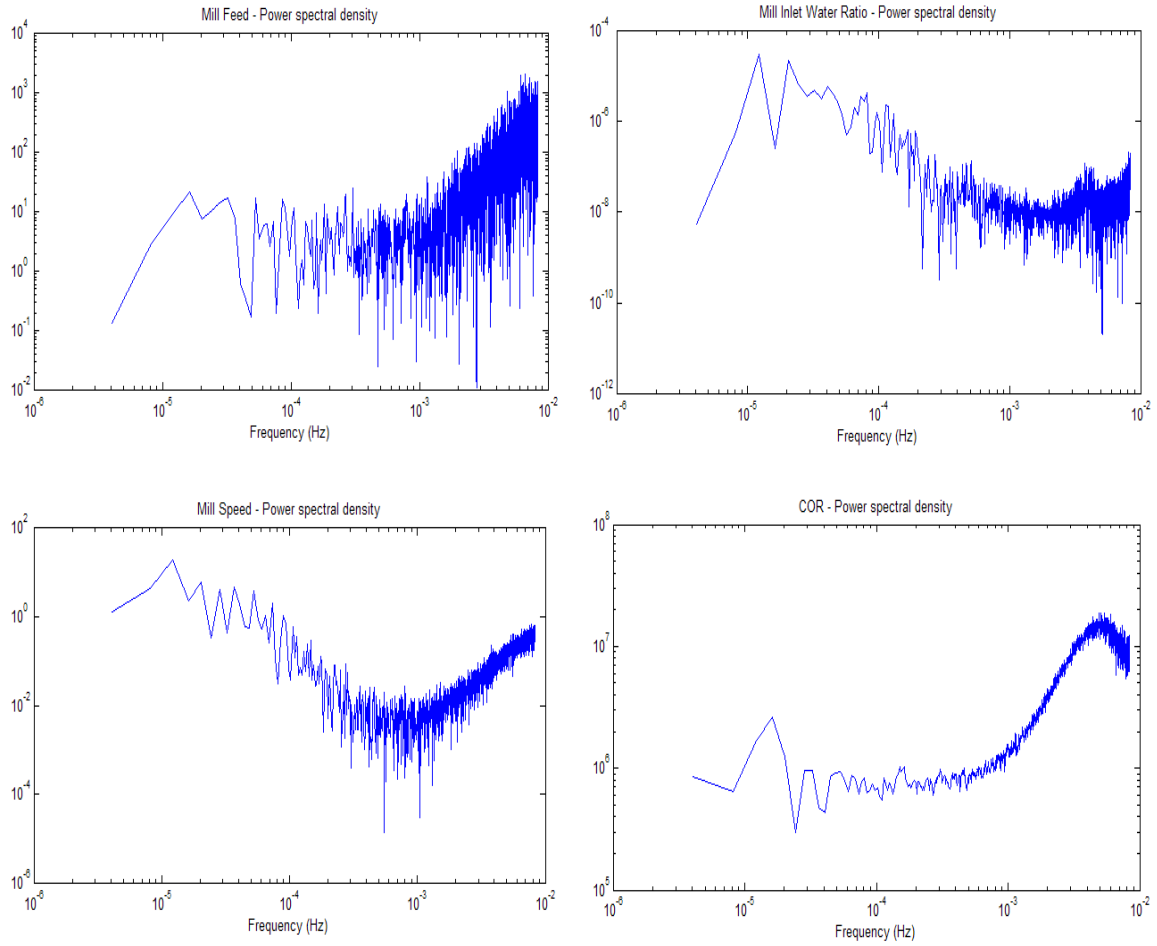

Figure 11.11: Power spectral density PSD plot of the primary mill manipulated variables a)mill feed t/h, b)inlet water ratio c)mill speed % maximum speed and d)coarse ore ratio – 1 August 2010 to 9 September 2010

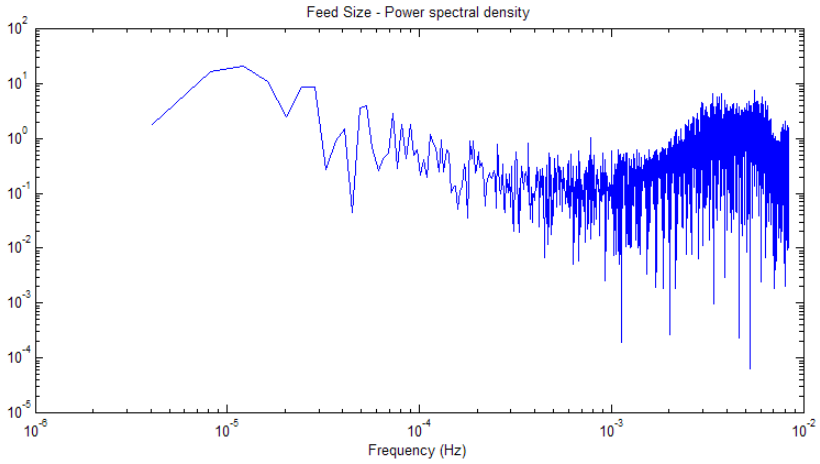

Figure 11.12: Power spectral density PSD plot of the primary mill's measured disturbance variable feed size % -45 mm – 1 August 2010 to 9 September 2010

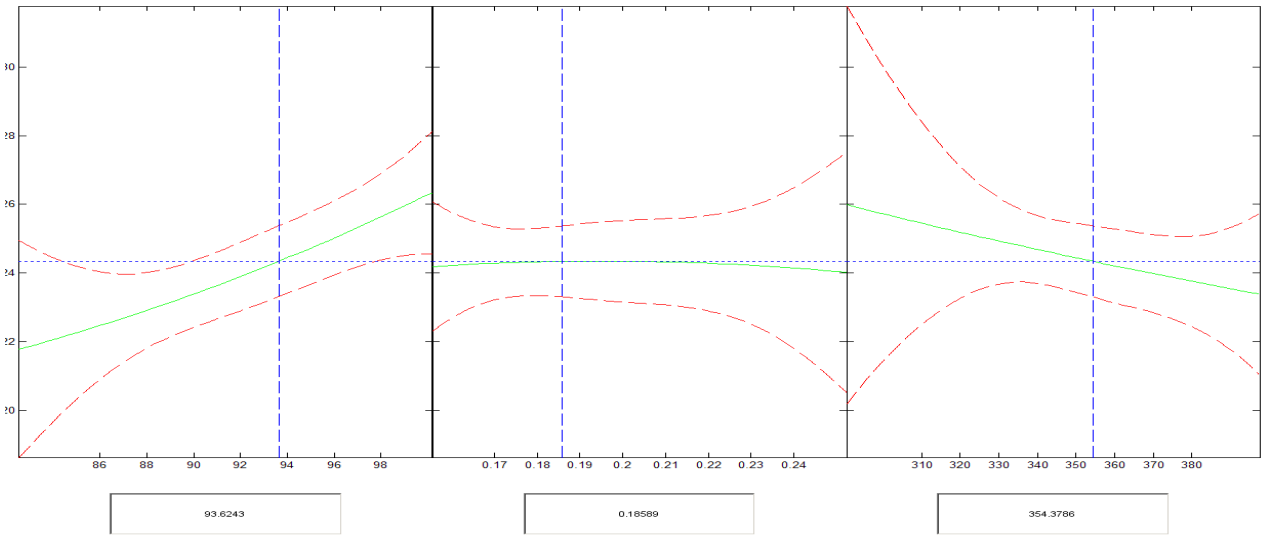

Figure 11.13: The pure-quadratic fit of the effective power usage objective kW/t$_{-75\mu m}$ and the mill manipulated variables

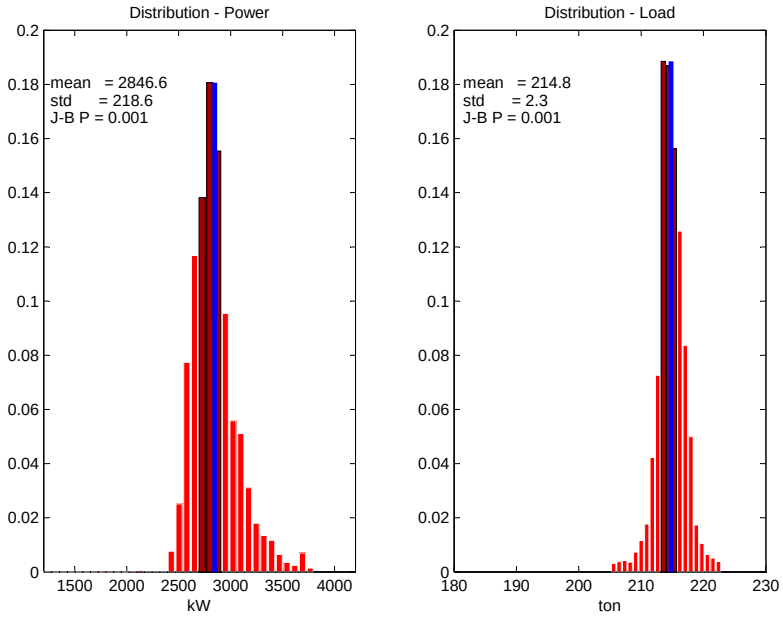

Figure 11.14: The distribution plot of the primary mill controlled variables a)power kW and b)load ton – 19 October 2010 to 22 November 2010

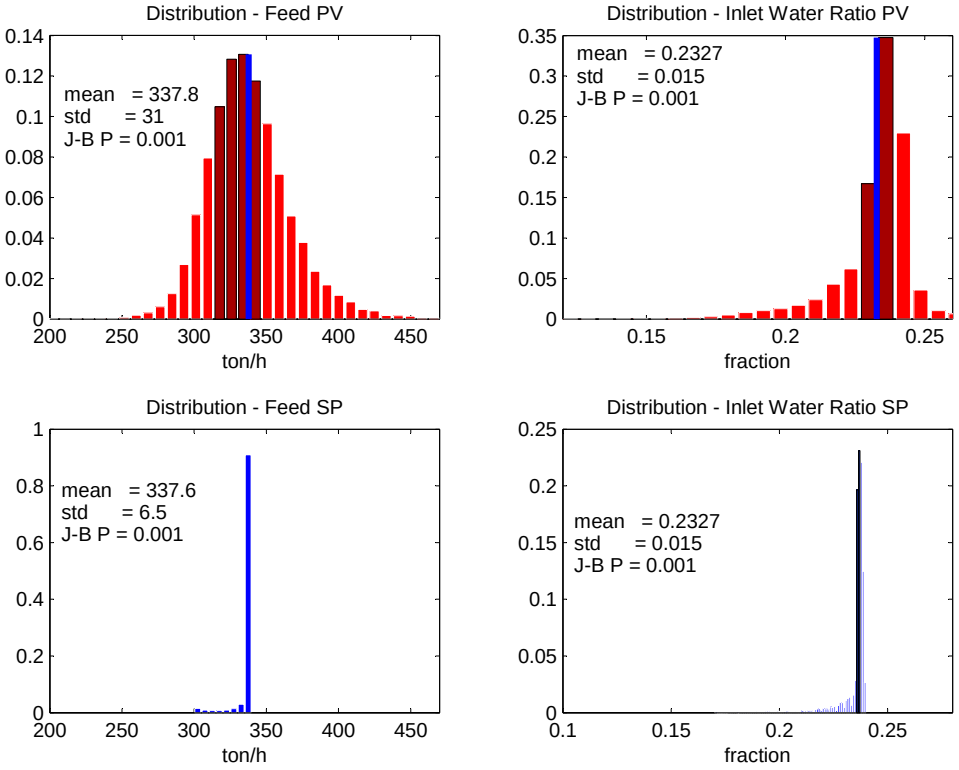

Figure 11.15: The distribution plot of the primary mill manipulated variables a+c)mill feed t/h, b+d)inlet water ratio – 19 October 2010 to 22 November 2010

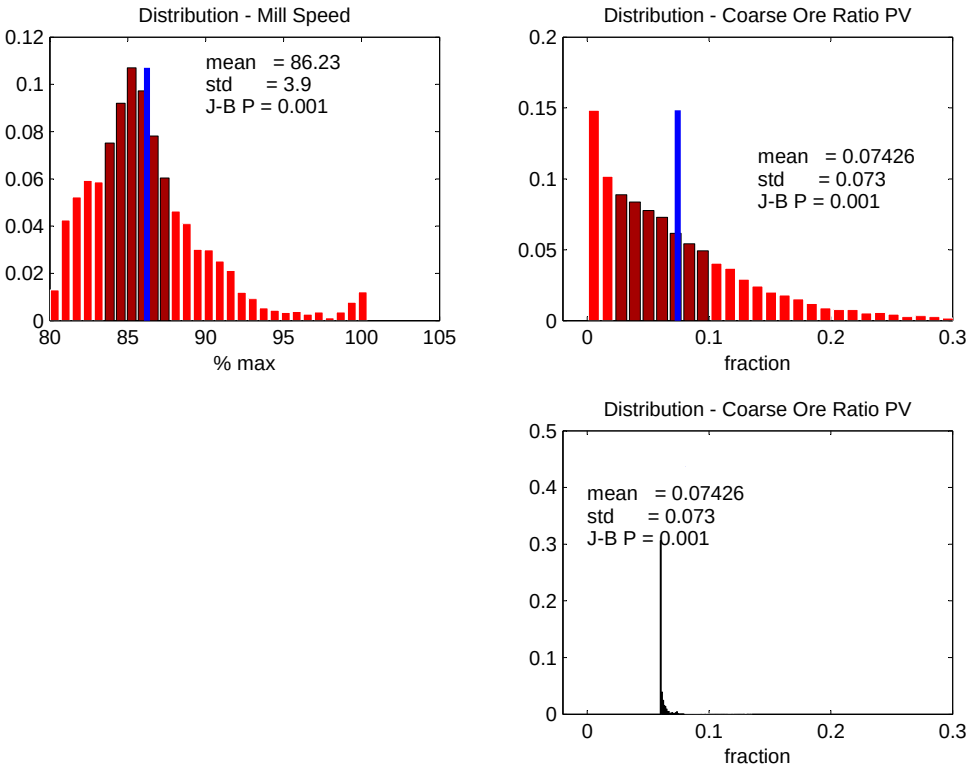

Figure 11.16: The distribution plot of the primary mill manipulated variables a)mill speed % maximum speed and b+d)coarse ore ratio – 19 October 2010 to 22 November 2010

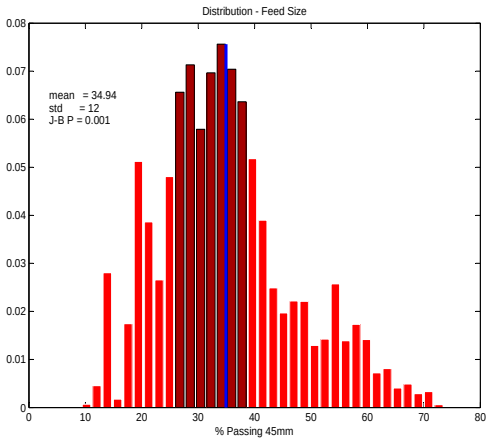

Figure 11.17: The distribution plot of the primary mill disturbance variable feed size %passing 45 mm – 19 October 2010 to 22 November 2010

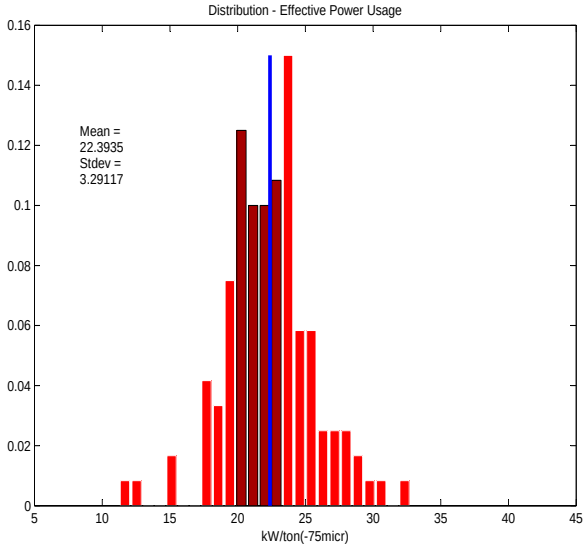

Figure 11.18: The distribution plot of the primary mill's effective power usage kWh/t-75μ m – 19 October 2010 to 22 November 2010

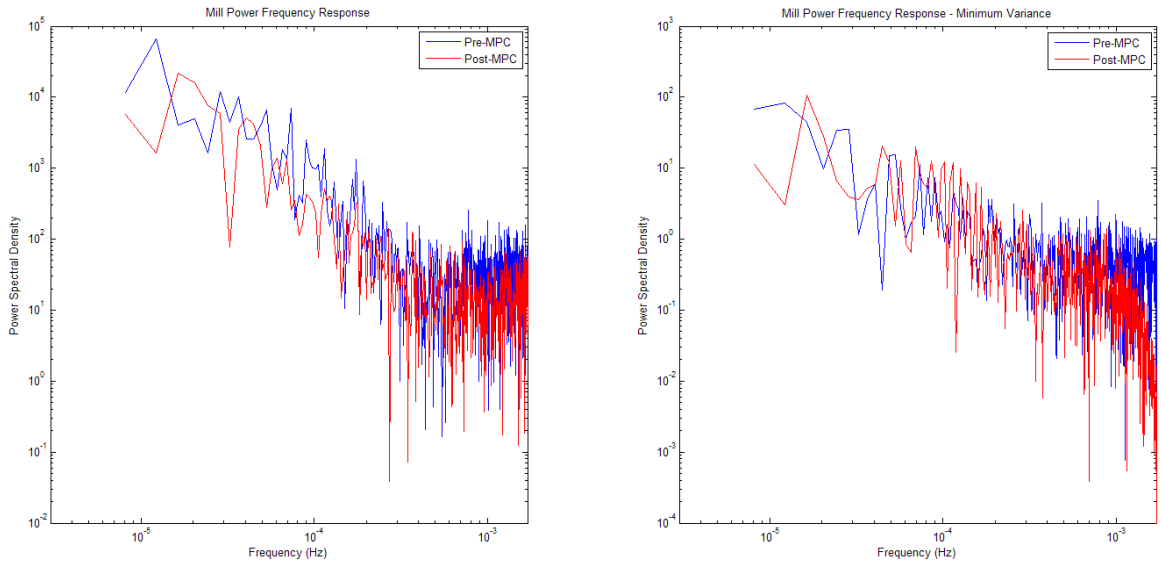

Figure 11.19: The mill power frequency comparison between a)pre and post MPC as well as the b)power's theoretical minimum variance response for the pre and post MPC

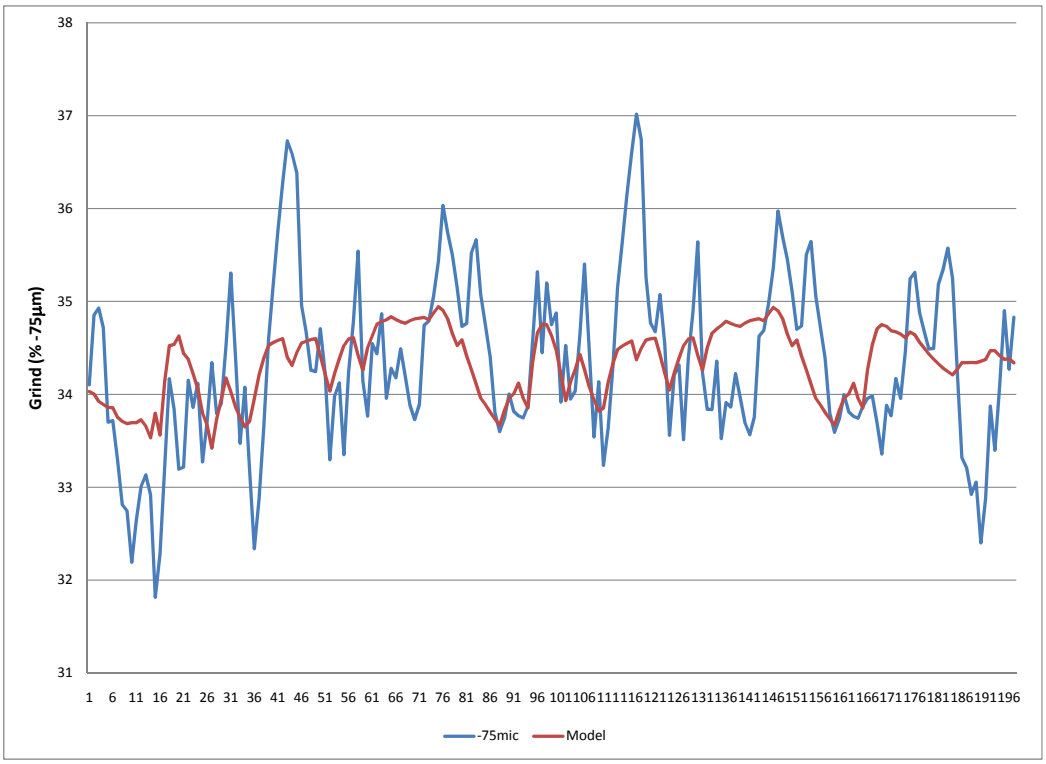

Figure 11.20: Grind model: pure-quadratic mill load and inlet water ratio with linear throughput. Model stats: $R^2 = 20\%$, mean-sum-errors 0.84 %

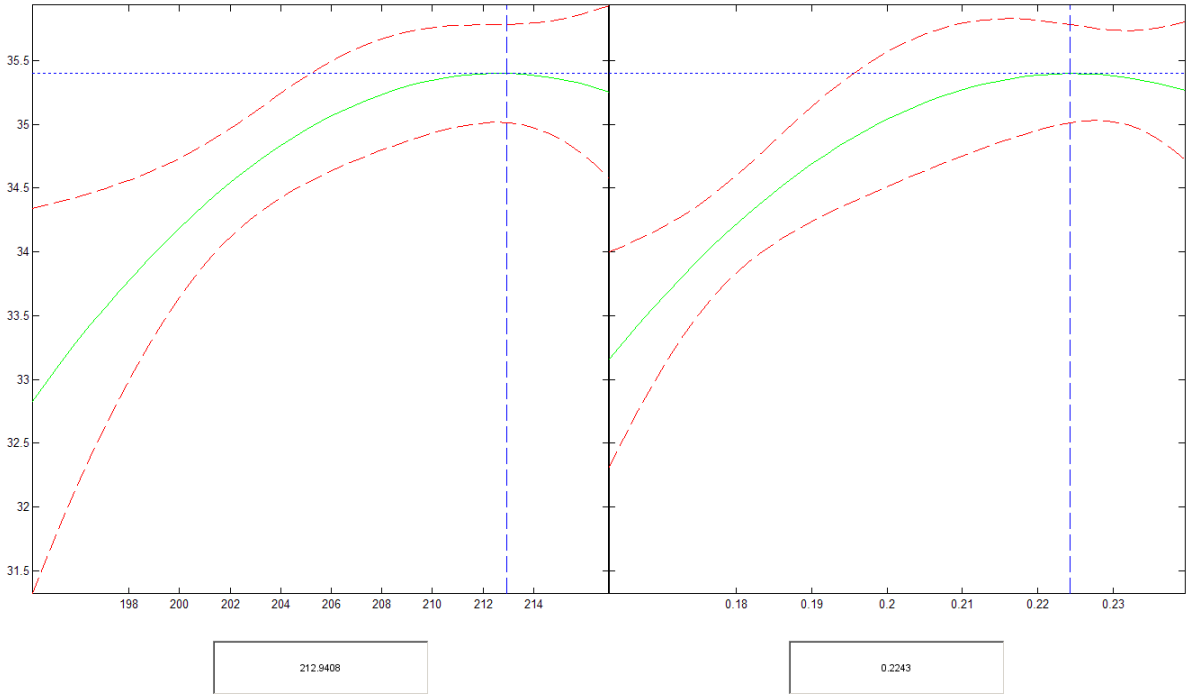

Figure 11.21: The pure-quadratic response surface of a)load and b)inlet water ratio to grind. Model stats: Root-mean-square-error 1.06 % or 3 % relative to the mean of the grind

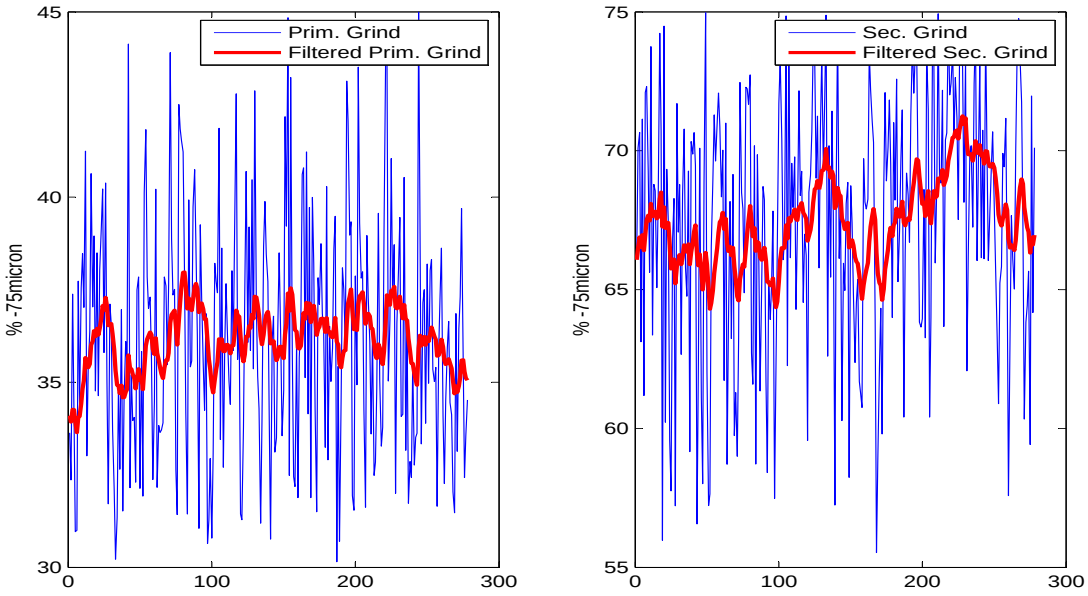

Figure 11.22: The raw and filtered signals of the a)primary and b)secondary grind. Exponential filters with constants $\alpha = 0.9$ for both grinds

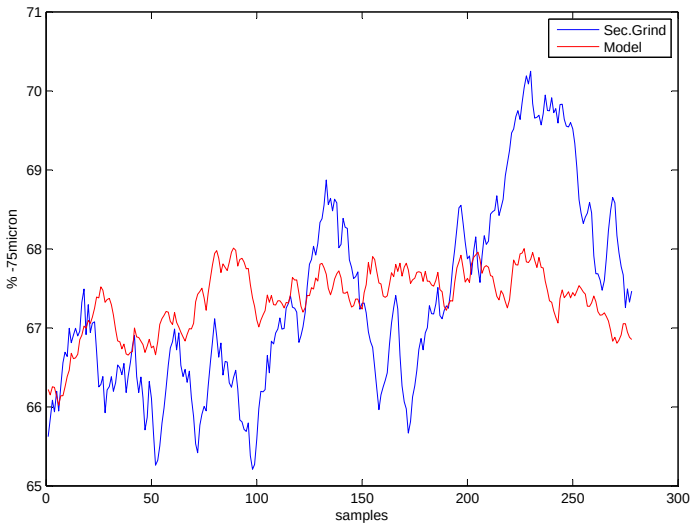

Figure 11.23: The final grind of RPMA2 with its model using only the primary grind. Model stats: $rmse$ – 0.74 % passing 75 μ m

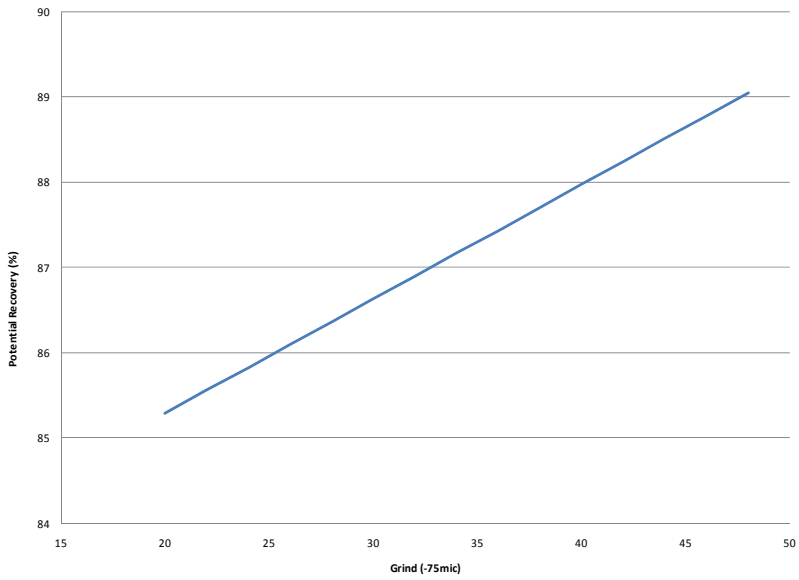

Figure 11.24: Potential PGM recovery at a specific primary milling product grind measured as % passing 75 μ m

Day nr	Shift nr	Date	Weekday	Internal Load Hi (MPC Hi)	Inlet Ratio Hi
1	1	02/14/2011 06:00	Monday	221	24
	2	02/14/2011 14:00	Monday	221	24
	3	02/14/2011 22:00	Monday	221	24
2	4	02/15/2011 06:00	Tuesday	221	24
	5	02/15/2011 14:00	Tuesday	221	24
	6	02/15/2011 22:00	Tuesday	213.5	24
3	7	02/16/2011 06:00	Wednesday	213.5	24
	8	02/16/2011 14:00	Wednesday	213.5	24
	9	02/16/2011 22:00	Wednesday	213.5	24
4	10	02/17/2011 06:00	Thursday	213.5	24
	11	02/17/2011 14:00	Thursday	192	24
	12	02/17/2011 22:00	Thursday	192	24
5	13	02/18/2011 06:00	Friday	192	24
	14	02/18/2011 14:00	Friday	192	24
	15	02/18/2011 22:00	Friday	192	24
6	16	02/19/2011 06:00	Saturday	221	24
	17	02/19/2011 14:00	Saturday	221	24
	18	02/19/2011 22:00	Saturday	221	24
7	19	02/20/2011 06:00	Sunday	221	24
	20	02/20/2011 14:00	Sunday	221	24
	21	02/20/2011 22:00	Sunday	213.5	24
8	22	02/21/2011 06:00	Monday	213.5	24
	23	02/21/2011 14:00	Monday	213.5	24
	24	02/21/2011 22:00	Monday	213.5	24
9	25	02/22/2011 06:00	Tuesday	213.5	24
	26	02/22/2011 14:00	Tuesday	192	24
	27	02/22/2011 22:00	Tuesday	192	24
10	28	02/23/2011 06:00	Wednesday	192	24
	29	02/23/2011 14:00	Wednesday	192	24
	30	02/23/2011 22:00	Wednesday	192	24
11	31	02/24/2011 06:00	Thursday	221	24
	32	02/24/2011 14:00	Thursday	221	24
	33	02/24/2011 22:00	Thursday	221	24
12	34	02/25/2011 06:00	Friday	221	24
	35	02/25/2011 14:00	Friday	221	24
	36	02/25/2011 22:00	Friday	213.5	24
13	37	02/26/2011 06:00	Saturday	213.5	24
	38	02/26/2011 14:00	Saturday	213.5	24
	39	02/26/2011 22:00	Saturday	213.5	24
14	40	02/27/2011 06:00	Sunday	213.5	24
	41	02/27/2011 14:00	Sunday	192	24
	42	02/27/2011 22:00	Sunday	192	24
15	43	02/28/2011 06:00	Monday	192	24
	44	02/28/2011 14:00	Monday	192	24
	45	02/28/2011 22:00	Monday	192	24
16	46	03/01/2011 06:00	Tuesday	221	24
	47	03/01/2011 14:00	Tuesday	221	24
	48	03/01/2011 22:00	Tuesday	221	24
17	49	03/02/2011 06:00	Wednesday	221	24
	50	03/02/2011 14:00	Wednesday	221	24
	51	03/02/2011 22:00	Wednesday	213.5	24
18	52	03/03/2011 06:00	Thursday	213.5	24
	53	03/03/2011 14:00	Thursday	213.5	24
	54	03/03/2011 22:00	Thursday	213.5	24
19	55	03/04/2011 06:00	Friday	213.5	24
	56	03/04/2011 14:00	Friday	192	24
	57	03/04/2011 22:00	Friday	192	24
20	58	03/05/2011 06:00	Saturday	192	24
	59	03/05/2011 14:00	Saturday	192	24
	60	03/05/2011 22:00	Saturday	192	24
21	61	03/06/2011 06:00	Sunday	221	24
	62	03/06/2011 14:00	Sunday	221	24
	63	03/06/2011 22:00	Sunday	221	24
22	64	03/07/2011 06:00	Monday	221	24
	65	03/07/2011 14:00	Monday	221	24
	66	03/07/2011 22:00	Monday	213.5	24
23	67	03/08/2011 06:00	Tuesday	213.5	24
	68	03/08/2011 14:00	Tuesday	213.5	24
	69	03/08/2011 22:00	Tuesday	213.5	24
24	70	03/09/2011 06:00	Wednesday	213.5	24
	71	03/09/2011 14:00	Wednesday	192	24
	72	03/09/2011 22:00	Wednesday	192	24
25	73	03/10/2011 06:00	Thursday	192	24
	74	03/10/2011 14:00	Thursday	192	24
	75	03/10/2011 22:00	Thursday	192	24
26	76	03/11/2011 06:00	Friday	221	24
	77	03/11/2011 14:00	Friday	221	24
	78	03/11/2011 22:00	Friday	221	24
27	79	03/12/2011 06:00	Saturday	221	24
	80	03/12/2011 14:00	Saturday	221	24
	81	03/12/2011 22:00	Saturday	213.5	24
28	82	03/13/2011 06:00	Sunday	213.5	24
	83	03/13/2011 14:00	Sunday	213.5	24
	84	03/13/2011 22:00	Sunday	213.5	24
29	85	03/14/2011 06:00	Monday	213.5	24
	86	03/14/2011 14:00	Monday	221	24
	87	03/14/2011 22:00	Monday	221	24
30	88	03/15/2011 06:00	Tuesday	221	24
	89	03/15/2011 14:00	Tuesday	221	24
	90	03/15/2011 22:00	Tuesday	221	24
31	91	03/16/2011 06:00	Wednesday	221	24
	92	03/16/2011 14:00	Wednesday	221	24
	93	03/16/2011 22:00	Wednesday	221	24
32	94	03/17/2011 06:00	Thursday	221	24
	95	03/17/2011 14:00	Thursday	221	24
	96	03/17/2011 22:00	Thursday	213.5	24
33	97	03/18/2011 06:00	Friday	213.5	24
	98	03/18/2011 14:00	Friday	213.5	24
	99	03/18/2011 22:00	Friday	213.5	24
34	100	03/19/2011 06:00	Saturday	213.5	24
	101	03/19/2011 14:00	Saturday	221	24
	102	03/19/2011 22:00	Saturday	221	24
35	103	03/20/2011 06:00	Sunday	221	24
	104	03/20/2011 14:00	Sunday	221	24
	105	03/20/2011 22:00	Sunday	221	24
36	106	03/21/2011 06:00	Monday	213.5	24
	107	03/21/2011 14:00	Monday	213.5	24
	108	03/21/2011 22:00	Monday	213.5	24
37	109	03/22/2011 06:00	Tuesday	213.5	24
	110	03/22/2011 14:00	Tuesday	213.5	24

Figure 11.25: Trial 1 schedule: Load tests – 14 February 2011 to 22 March 2011

Day nr	Shift nr	Date	Weekday	Internal Load Hi (MPC Hi)	Inlet Ratio Hi
1	1	03/29/2011 06:00	Tuesday	213.5	19.5
	2	03/29/2011 14:00	Tuesday	213.5	19.5
	3	03/29/2011 22:00	Tuesday	213.5	19.5
2	4	03/30/2011 06:00	Wednesday	213.5	19.5
	5	03/30/2011 14:00	Wednesday	213.5	19.5
	6	03/30/2011 22:00	Wednesday	213.5	19.5
3	7	03/31/2011 06:00	Thursday	213.5	16
	8	03/31/2011 14:00	Thursday	213.5	16
	9	03/31/2011 22:00	Thursday	213.5	16
4	7	04/01/2011 06:00	Friday	213.5	16
	8	04/01/2011 14:00	Friday	213.5	16
	9	04/01/2011 22:00	Friday	213.5	16
5	10	04/02/2011 06:00	Saturday	213.5	16
	11	04/02/2011 14:00	Saturday	213.5	16
	12	04/02/2011 22:00	Saturday	221	16
6	13	04/03/2011 06:00	Sunday	221	16
	14	04/03/2011 14:00	Sunday	221	16
	15	04/03/2011 22:00	Sunday	221	16
7	16	04/04/2011 06:00	Monday	221	16
	17	04/04/2011 14:00	Monday	213.5	19.5
	18	04/04/2011 22:00	Monday	213.5	19.5
8	19	04/05/2011 06:00	Tuesday	213.5	19.5
	20	04/05/2011 14:00	Tuesday	213.5	19.5
	21	04/05/2011 22:00	Tuesday	213.5	19.5
9	22	04/06/2011 06:00	Wednesday	213.5	16
	23	04/06/2011 14:00	Wednesday	213.5	16
	24	04/06/2011 22:00	Wednesday	213.5	16
10	25	04/07/2011 06:00	Thursday	213.5	16
	26	04/07/2011 14:00	Thursday	213.5	16
	27	04/07/2011 22:00	Thursday	221	16
11	28	04/08/2011 06:00	Friday	221	16
	29	04/08/2011 14:00	Friday	221	16
	30	04/08/2011 22:00	Friday	221	16
12	31	04/09/2011 06:00	Saturday	221	16
	32	04/09/2011 14:00	Saturday	213.5	19.5
	33	04/09/2011 22:00	Saturday	213.5	19.5
13	34	04/10/2011 06:00	Sunday	213.5	19.5
	35	04/10/2011 14:00	Sunday	213.5	19.5
	36	04/10/2011 22:00	Sunday	213.5	19.5
14	37	04/11/2011 06:00	Monday	213.5	16
	38	04/11/2011 14:00	Monday	213.5	16
	39	04/11/2011 22:00	Monday	213.5	16
15	40	04/12/2011 06:00	Tuesday	213.5	16
	41	04/12/2011 14:00	Tuesday	213.5	16
	42	04/12/2011 22:00	Tuesday	221	16
16	43	04/13/2011 06:00	Wednesday	221	16
	44	04/13/2011 14:00	Wednesday	221	16
	45	04/13/2011 22:00	Wednesday	221	16
17	46	04/14/2011 06:00	Thursday	221	16
	47	04/14/2011 14:00	Thursday	213.5	19.5
	48	04/14/2011 22:00	Thursday	213.5	19.5
18	49	04/15/2011 06:00	Friday	213.5	19.5
	50	04/15/2011 14:00	Friday	213.5	19.5
	51	04/15/2011 22:00	Friday	213.5	19.5
19	52	04/16/2011 06:00	Saturday	213.5	16
	53	04/16/2011 14:00	Saturday	213.5	16
	54	04/16/2011 22:00	Saturday	213.5	16
20	55	04/17/2011 06:00	Sunday	213.5	16
	56	04/17/2011 14:00	Sunday	213.5	16
	57	04/17/2011 22:00	Sunday	221	16
21	58	07/01/2011 06:00	Monday	221	16
	59	07/01/2011 14:00	Monday	221	16
	60	07/01/2011 22:00	Monday	221	16
22	61	07/02/2011 06:00	Tuesday	221	16
	62	07/02/2011 14:00	Tuesday	213.5	19.5
	63	07/02/2011 22:00	Tuesday	213.5	19.5
23	64	07/03/2011 06:00	Wednesday	213.5	19.5
	65	07/03/2011 14:00	Wednesday	213.5	19.5
	66	07/03/2011 22:00	Wednesday	213.5	19.5
24	67	07/04/2011 06:00	Thursday	213.5	16
	68	07/04/2011 14:00	Thursday	213.5	16
	69	07/04/2011 22:00	Thursday	213.5	16
25	70	07/05/2011 06:00	Friday	213.5	16
	71	07/05/2011 14:00	Friday	213.5	16
	72	07/05/2011 22:00	Friday	221	16
26	73	07/06/2011 06:00	Saturday	221	16
	74	07/06/2011 14:00	Saturday	221	16
	75	07/06/2011 22:00	Saturday	221	16
27	76	07/07/2011 06:00	Sunday	221	16
	77	07/07/2011 14:00	Sunday	213.5	19.5
	78	07/07/2011 22:00	Sunday	213.5	19.5
28	79	07/08/2011 06:00	Monday	213.5	19.5
	80	07/08/2011 14:00	Monday	213.5	19.5
	81	07/08/2011 22:00	Monday	213.5	19.5
29	82	07/09/2011 06:00	Tuesday	213.5	16
	83	07/09/2011 14:00	Tuesday	213.5	16
	84	07/09/2011 22:00	Tuesday	213.5	16
30	85	07/10/2011 06:00	Wednesday	213.5	16
	86	07/10/2011 14:00	Wednesday	213.5	16
	87	07/10/2011 22:00	Wednesday	221	16
31	88	07/11/2011 06:00	Thursday	221	16
	89	07/11/2011 14:00	Thursday	221	16
	90	07/11/2011 22:00	Thursday	221	16
32	91	07/12/2011 06:00	Friday	213.5	19.5
	92	07/12/2011 14:00	Friday	213.5	19.5
	93	07/12/2011 22:00	Friday	213.5	19.5
33	94	07/13/2011 06:00	Saturday	213.5	19.5
	95	07/13/2011 14:00	Saturday	213.5	19.5
	96	07/13/2011 22:00	Saturday	213.5	16
34	97	07/14/2011 06:00	Sunday	213.5	16
	98	07/14/2011 14:00	Sunday	213.5	16
	99	07/14/2011 22:00	Sunday	213.5	16
35	100	07/15/2011 06:00	Monday	213.5	16
	101	07/15/2011 14:00	Monday	221	16
	102	07/15/2011 22:00	Monday	221	16
36	103	07/16/2011 06:00	Tuesday	221	16
	104	07/16/2011 14:00	Tuesday	221	16

Figure 11.26: Trial 2 schedule: Inlet Water ratio tests – 29 March 2011 to 17 April 2011 and 01 July 2011 to 16 July 2011

t-Test: Two-Sample Assuming Equal Variances

	Vol - 38.5%	*Vol - 40.2%*
Mean	33.79	36.94
Variance	27.32	27.35
Observations	19	17
Pooled Variance	27.34	
Hypothesized Mean Difference	0	
df	34	
t Stat	-1.80	
P(T<=t) one-tail	0.04	0.96
t Critical one-tail	1.69	
P(T<=t) two-tail	0.08	0.92
t Critical two-tail	2.03	

	Vol - 38.5%	*Vol - 41.3%*
Mean	33.79	36.14
Variance	27.32	20.58
Observations	19	23
Pooled Variance	23.62	
Hypothesized Mean Difference	0	
df	40	
t Stat	-1.56	
P(T<=t) one-tail	0.06	0.94
t Critical one-tail	1.68	
P(T<=t) two-tail	0.13	0.87
t Critical two-tail	2.02	

	Vol - 40.2%	*Vol - 41.3%*
Mean	36.94	36.14
Variance	27.35	20.58
Observations	17	23
Pooled Variance	23.43	
Hypothesized Mean Difference	0	
df	38	
t Stat	0.52	
P(T<=t) one-tail	0.30	0.70
t Critical one-tail	1.69	
P(T<=t) two-tail	0.61	0.39
t Critical two-tail	2.02	

Figure 11.27: Trial 1 results: Two sample T-test assuming equal variance of the % vol comparison with statistical significance indicated by the green blocks

BIBLIOGRAPHY

AspenTech (2000), "AspenTech pty. ltd. DMCplus course notes," .

Barnes, A and Newall, A (March 2006), "Spinel removal from PGM smelting furnaces," *South African Institute of Mining an Metallurgy*, South African Pyrometallurgy 2006, 77–88.

Bascur, O (August 1991), "Integrated grinding/flotation controls and management," *Proceedings of the Copper 91 - Cobre 91*, 2, 411–427.

Bauer, M and Craig, IK (January 2008), "Economic assessment of advanced process control - a survey and framework," *Journal of Process Control*, 18 (1), 2–18, ISSN 0959-1524, doi:10.1016/j.jprocont.2007.05.007, URL `http://www.sciencedirect.com/science/article/B6V4N-4P90398-1/2/999116b4acb08a4223187c9e2aed7f85`.

Camacho, EF and Bordons, CA (April 2007), *Model Predictive Control*, 2nd edition, Springer, ISBN 1852336943.

Cawthorn, RG (December 1999), "The platinum and palladium resources of the bushveld complex," *South African Journal of Science*, pages 481–489.

Craig, I and Koch, I (January 2003), "Experimental design for the economic performance evaluation of industrial controllers," *Control Engineering Practice*, 11 (1), 57–66, ISSN 0967-0661, doi:10.1016/S0967-0661(02)00094-1, URL `http://www.sciencedirect.com/science/article/pii/S0967066102000941`.

Craig, IK, Hulbert, DG, Metzner, G and Moult, SP (December 1992), "Extended particle-size control of an industrial run-of-mine milling circuit," *Powder Technology*, 73 (3), 203–210, ISSN 0032-5910, doi:10.1016/0032-5910(92)85027-S, URL `http://www.sciencedirect.com/science/article/B6TH9-440YWCT-CT/2/7b2e7f1c8aab556b8b258604d357753f`.

Edwards, R and Vien, A (1999), "Application of a model based size-recovery methodology," *Canadian Institute fo Mining*, pages 147 – 159.

Fuerstenau, DW, Kapur, PC and Velamakanni, B (February 1990), "A multi-torque model for the effects of dispersants and slurry viscosity on ball milling," *International Journal of Mineral Processing*, 28 (1-2), 81–98, ISSN 0301-7516, doi:10.1016/0301-7516(90)90028-W, URL `http://www.sciencedirect.com/science/article/pii/030175169090028W`.

Giordano, FR, Weir, MD and Fox, WP (July 2009), *A First Course in Mathematical Modeling*, 003rd edition, Brooks Cole, ISBN 0534384285.

Hayes, P (2003), *Process Principles in Minerals and Materials Production*, 3rd edition, Hayes Publishing Co, ISBN 0958919739.

Hodouin, D, Jms-Jounela, SL, Carvalho, MT and Bergh, L (September 2001), "State of the art and challenges in mineral processing control," *Control Engineering Practice*, 9 (9), 995–1005, ISSN 0967-0661, doi:10.1016/S0967-0661(01)00088-0, URL `http://www.sciencedirect.com/science/article/B6V2H-43VYY2C-7/2/8150af3b79424ed7b76f79575adf2312`.

Hugo, A (July 2003), "Performance assessment of controllers applied to integrating processes," URL `http://www.freepatentsonline.com/6594593.html`.

Hulbert, D (2002), "Evaluation of the economic benefit of milling circuit control," *Proceedings of the 15th IFAC Triennial World Congress. Elsevier Science Barcalona, Spain.*

Johnston, R (1998), "Fuzzy logic for high performance control," *Applied Technology Laboratory.*

Jollie, D (2009), "Platinum 2009," Technical report, Johnson Mattey.

Klimpel, RR (1983), "Slurry rheology influence on the performance of mineral/coal grinding circuits. part II," *Minerals Engineering*, 35, 21 – 26.

Luyben, WLM (June 1990), *Process Modeling, Simulation and Control for Chemical Engineers*, 2nd edition, McGraw-Hill, ISBN 0071007938.

Mainza, A and Powell, M (2006), "Rom ball mills - a comparison with ag/sag milling," in "SAG conference 2006 - Part 3," volume 2, pages 314 –325, CIM, University of British Columbia.

Marlin, T (July 2000), *Process Control*, 2nd edition, McGraw-Hill Inc.,US, ISBN 0071163573.

Martin, GD, Turpin, LE and Cline, RP (June 1991), "Estimating control function benefits," *Hydrocarbon Processing*, pages 68 – 73.

Morell, S and Kojovic, T (1996), "The influence of slurry transport on the power draw of autogenous and semiautogenous mills," *Proc SAG '96, Vancouver,*, pages pp 373–389,.

Napier-Munn, T, Morell, S, Morrison, R and Kojovic, T (1999), *Mineral Comminution Circuits - Their Operation and Optimization*, second edition edition, Julius Kruttschnitt Mineral Research Centre, The University of Queensland.

Nel, E, Valenta, M and Naude, N (July 2005), "Influence of open circuit regrind milling on UG-2 ore composition and mineralogy at impala's UG-2 concentrator," *Minerals Engineering*, 18 (8), 785–790, ISSN 0892-6875, doi:10.1016/j.mineng.2005.01.031, URL `http://www.sciencedirect.com/science/article/B6VDR-4G94HT5-5/2/8458edb1432e24608fe965da513a10e1`.

Platinum, AA (2006), "Anglo american platinum limited annual report," Technical report, Anglo American Platinum.

Powell, M and Mainza, A (December 2006), "Extended grinding curves are essential to the comparison of milling performance," *Minerals Engineering*, 19 (15), 1487–1494, ISSN 0892-6875, doi:10.1016/j.mineng.2006.08.004, URL `http://www.sciencedirect.com/science/article/B6VDR-4M3RP3B-1/2/8ff6988fa1c3dcf5f978d656fe2359c2`.

Powell, MS, Morrell, S and Latchireddi, S (October 2001), "Developments in the understanding of south african style SAG mills," *Minerals Engineering*, 14 (10), 1143–1153, ISSN 0892-6875, doi:10.1016/S0892-6875(01)00132-7, URL `http://www.sciencedirect.com/science/article/B6VDR-44RRFMW-2/2/a9e863375f673d106ff95462b35e2119`.

Priestley, M (August 1971), "Time-dependent spectral analysis and its application in prediction and control," *Journal of Sound and Vibration*, 17 (4), 517–534, ISSN 0022-460X, doi:10.1016/0022-460X(71)90064-2, URL `http://www.sciencedirect.com/science/article/pii/0022460X71900642`.

SAIMM (1987), *The extractive metallurgy of gold in South Africa*, English, South African Institute of Mining and Metallurgy, (Johannesburg), ISBN TN'760'E98'2001, URL `http://openlibrary.org/b/OL20768001M/extractive_metallurgy_of_gold_in_South_Africa`.

Scheffer, E (2001), "Bridging the gap between fuzzy logic and mathematical modeling," *University of the Witwatersrand*.

Seborg, D, Edgar, T and Mellichamp, D (2004), *Process Dynamics and Control*, 2nd edition, John Wiley & Sons Inc., ISBN 0471000779.

Shackleton, N, Malysiak, V and O'Connor, C (December 2007), "Surface characteristics and flotation behaviour of platinum and palladium arsenides," *International Journal of Mineral Processing*, 85 (1-3), 25–40, ISSN 0301-7516, doi:10.1016/j.minpro.2007.08.002, URL `http://www.sciencedirect.com/science/article/B6VBN-4PF6B6M-1/2/45810de2ac7e591a8bdb978221182a04`.

Skogestad, S and Postlethwaite, I (October 2005), *Multivariable Feedback Control: Analysis and Design*, 2nd edition, Wiley-Interscience, ISBN 0470011688.

Smith, S (2002), *The Scientist and Engineer's Guide to Digital Signal Processing*, California Technical Publishing.

Snyman, JA (2005), *Practical mathematical optimization: an introduction to basic optimization theory and classical and new gradient-based algorithms*, Springer, ISBN 9780387243481.

Sosa-Blanco, C, Hodouin, D, Bazin, C, Lara-Valenzuela, C and Salazar, J (September 2000), "Economic optimisation of a flotation plant through grinding circuit tuning," *Minerals Engineering*, 13 (10-11), 999–1018, ISSN 0892-6875, doi:10.1016/S0892-6875(00)00086-8, URL `http://www.sciencedirect.com/science/article/B6VDR-417NH4R-2/2/720d0e26b7bbbf3419891444abfd55f7`.

Steyn, C, Brooks, K, de Villiers, PGR, Muller, D and Humphries, G (August 2010), "A holistic approach to control and optimization of an industrial run-of-mine ball milling circuit," in J Gorden, editor, "IFAC MMM conference 2010," pages 137–141.

v Lith (2002), *Issues in Hybrid Fuzzy - First Principles*, Ph.D. thesis, University of Twente, Faculty of Chemical Technology.

van der Westhuizen, APP and Powell, MS (2006), "Milling curves as a tool for characterising sag mill performance," in "SAG conference 2006 - Part 2," University of British Columbia, Dept of Mining and Mineral Process Engineering.

Vishnubhotla, A, Engineering, UoADoC and Materials (1997), *Frequency and time-domain techniques for control loop performance assessment*, University of Alberta.

Wei, D and Craig, IK (August 2009a), "Economic performance assessment of two ROM ore milling circuit controllers," *Minerals Engineering*, 22 (9-10), 826–839, ISSN 0892-6875, doi:10.1016/j.mineng.2009.02.013, URL `http://www.sciencedirect.com/science/article/B6VDR-4VYW690-2/2/21e28f427788921f681c6d987df7aeab`.

Wei, D and Craig, IK (February 2009b), "Grinding mill circuits – a survey of control and economic concerns," *International Journal of Mineral Processing*, 90 (1-4), 56–66, ISSN

0301-7516, doi:10.1016/j.minpro.2008.10.009, URL `http://www.sciencedirect.com/science/article/B6VBN-4TX33TC-2/2/34f02b64bbbee854d1a4dd23b86b60d8`.

Wesseldijk, QI, Reuter, MA, Bradshaw, DJ and Harris, PJ (October 1999), "The flotation behaviour of chromite with respect to the beneficiation of UG2 ore," *Minerals Engineering*, 12 (10), 1177–1184, ISSN 0892-6875, doi:10.1016/S0892-6875(99)00104-1, URL `http://www.sciencedirect.com/science/article/B6VDR-3XSK0X4-3/2/d6424151be491b268cc17d51086b5589`.

Wills, BA (January 1992), *Mineral Processing Technology, Fifth Edition: An Introduction to the Practical Aspects of Ore Treatment and Mineral Recovery*, 5th edition, Pergamon, ISBN 0080418724.